Physics Reports 1174 (2026) 1–66

Contents lists available at ScienceDirect

Physics Reports

journal homepage: www.elsevier.com/locate/physrep

Review article

Evolution of methods for assessing fMRI-based functional networks: From classical pairwise connectivity to higher-order interactions

Semen A. Kurkin [a,c], Alexander N. Pisarchik [b,*], Larisa A. Mayorova [c], Alexander E. Hramov [a,c]

[a] Research Institute of Applied Artificial Intelligence and Digital Solution, Plekhanov Russian University of Economics, Stremyanny per. 36, 117997 Moscow, Russia
[b] Center for Biomedical Technology, Universidad Politécnica de Madrid, Campus Montegancedo, 28223 Pozuelo de Alarcón, Spain
[c] Federal Research and Clinical Center of Intensive Care Medicine and Rehabilitology, Lytkino, 777, 141534 Solnechnogorsk, Russia

ARTICLE INFO

Article history:
Received 11 December 2025
Received in revised form 29 January 2026
Accepted 16 February 2026

Editor: Massimo Vergassola

Keywords:
fMRI
Higher-order interactions (HOIs)
Functional brain networks
Pairwise connectivity
Hypergraphs
Simplicial complexes
Topological data analysis (TDA)
Partial information decomposition (PID)
Synergy
Redundancy
Multivariate connectivity
Neurological disorders
Network neuroscience
Brain connectivity

ABSTRACT

The analysis of functional magnetic resonance imaging (fMRI) data has been fundamentally shaped by network science, which models the brain as a graph of nodes (regions) and edges (pairwise interactions). This pairwise functional connectivity approach has revealed key principles of brain organization but rests on a reductionist assumption: that all interactions are dyadic. This paradigm is inherently limited, as it cannot capture polyadic dependencies or emergent collective phenomena where the interaction between two nodes is modulated by the state of others. Such higher-order interactions (HOIs) are hypothesized to be crucial for complex cognitive functions like multi-sensory integration and decision-making. This review synthesizes the rapid evolution of methods for assessing HOIs in fMRI-based functional networks. We begin by defining HOIs and introducing the mathematical frameworks of hypergraphs and simplicial complexes, which formally represent interactions among groups of brain regions. We then provide a comprehensive overview of the methodologies for detecting and quantifying HOIs, categorizing them into three major families: (1) multivariate statistical models that disentangle direct from indirect effects; (2) information-theoretic measures, such as Partial Information Decomposition and O-information, which quantify the synergistic and redundant information shared among multiple regions; and (3) machine learning techniques, including sparse regression and graph neural networks, that learn complex HOIs directly from data. We critically examine the application of these methods in neuroscience, highlighting growing evidence that HOIs provide a more sensitive and mechanistically informative view of brain function in health and disease. They have proven superior to pairwise connectivity in classifying neurological and psychiatric disorders – including Alzheimer's disease, autism spectrum disorder, and schizophrenia – and in revealing the brain's dynamic, integrative processes underlying cognition. Finally, we address the significant methodological challenges facing the field, such as distinguishing genuine HOIs from lower-order effects and the computational complexity of analysis, and outline future directions, including the integration of multimodal data and the translation of HOIs into clinical biomarkers.

* Corresponding author.
E-mail address: alexander.pisarchik@upm.es (A.N. Pisarchik).

https://doi.org/10.1016/j.physrep.2026.02.004

Contents

1. Introduction

Understanding how the brain is organized remains one of the central challenges in contemporary science, spanning physics, biology, nonlinear dynamics, and information theory. The quest to decipher the brain's functional architecture has evolved dramatically over the past several decades, driven by advances in both neuroimaging technology and analytical methodologies. This evolution reflects a broader trajectory in the study of complex systems—from reductionist approaches focused on isolated components to integrative frameworks that capture collective behavior.

1.1. Historical perspective: From classical signal analysis to network neuroscience

The modern study of brain connectivity has its roots in classical signal processing and time series analysis developed in the mid-twentieth century. Norbert Wiener's foundational work on cybernetics and the statistical theory of communication [1] established the mathematical framework for analyzing correlated signals, introducing concepts such as cross-correlation and coherence that remain central to neuroimaging analysis today. These tools were originally developed for engineering applications but found natural application in the analysis of electrophysiological recordings.

The introduction of power spectral analysis to neuroscience, pioneered by researchers studying electroencephalography (EEG) in the 1950s and 1960s [2–4], marked a crucial turning point. By decomposing neural signals into their frequency components, investigators could characterize oscillatory brain activity and identify spectral signatures associated with different cognitive states. Cross-spectral analysis extended these methods to examine frequency-specific correlations between brain regions, laying the groundwork for modern connectivity analysis [5].

The concept of functional connectivity – statistical dependencies between spatially distinct neurophysiological events – was formalized in the 1990s following the development of functional magnetic resonance imaging (fMRI) [6,7]. Biswal and colleagues' seminal demonstration that spontaneous low-frequency fluctuations in the blood oxygenation level-dependent (BOLD) signal exhibit coherent patterns across the brain [6] opened a new era of connectivity research. This discovery revealed that the brain maintains organized functional networks even in the absence of explicit task demands, fundamentally reshaping our understanding of neural organization.

1.2. The pairwise paradigm: Foundations and limitations

Network science has provided a powerful framework for studying the brain's complex wiring patterns [8,9]. Viewing the brain as a network – with regions represented as nodes and their interactions as edges – has reshaped neuroscience. Studies of functional connectivity, usually measured through temporal correlations in neuroimaging data such as fMRI, have shifted the focus from isolated brain regions to the topology of the entire system. This approach has highlighted several key principles of brain organization: the economical small-world architecture that balances segregation and integration [10,11]; the rich-club organization that supports efficient communication among central hubs [12]; and the dynamic modular communities that reconfigure to enable flexible cognitive processes [13]. These graph-theoretical perspectives have revealed important links between network topology and brain function, development, aging, and the pathophysiology of disorders including schizophrenia, major depressive disorder, and Alzheimer's disease.

Classical correlation-based approaches, including Pearson correlation, partial correlation, and coherence analysis, have been instrumental in characterizing pairwise functional connectivity [14,15]. Partial correlation methods, which attempt to isolate direct relationships by controlling for the influence of other variables, represent an important refinement [16]. However, even these advanced pairwise measures cannot fully disentangle complex multivariate dependencies. Granger causality [17] and its extensions to neuroimaging [18,19] have provided tools for inferring directional influences, yet these methods fundamentally operate within a pairwise framework, examining how one time series predicts another.

Despite its transformative impact, the standard network model rests on a crucial, yet often implicit, reductionist assumption: that all functional interactions are pairwise. This paradigm has made it possible to identify universal organizational principles, such as hierarchical modularity, the presence of hubs, and scale-invariant topology, which are common to a wide variety of complex networks, from social to technological. The success of this approach has been confirmed by thousands of studies linking network organization features to individual differences in behavior, cognitive abilities, and clinical conditions. This framework presupposes that the relationship between any two brain regions is independent of the context provided by the rest of the network.

Although this simplification has been methodologically necessary and heuristically valuable, it imposes a fundamental limitation. It cannot account for polyadic dependencies or emergent collective phenomena in which the interaction between two nodes is explicitly modulated by the state of a third, or of an entire group. For instance, the functional coupling between the hippocampus and prefrontal cortex during memory retrieval may be contingent on the co-activation

of the amygdala—an interaction that is intrinsically triadic and cannot be decomposed without residual information. Recent theoretical and methodological advances have begun to formalize such triadic interactions, demonstrating that one node can regulate the interaction between two others in ways that are not reducible to pairwise relationships [20]. Fundamental processes such as overtone convergence in the auditory system, multisensory integration in associative areas of the cortex, or the binding mechanism in visual perception are inherently high-order. They require the simultaneous coordinated participation of multiple distributed nodes, whose joint activity creates a new quality—a percept or cognitive act. These higher-order interactions (HOIs) are hypothesized to be the building blocks of complex cognitive functions like decision-making, conscious perception, and multi-sensory integration, where information from multiple sources is combined in a nonlinear, context-dependent manner.

1.3. The imperative for higher-order analysis

The imperative to move beyond this pairwise constraint is not merely a technical refinement, but a conceptual necessity for advancing a mechanistic theory of brain dynamics. The importance of studying HOIs is multifaceted.

First, from a theoretical perspective, systems with multi-body interactions, as studied in statistical physics and complex systems theory [21–23], exhibit rich phenomenology, including new phases of matter, enhanced synchronization, and resilience to perturbation, that is absent in their pairwise counterparts. The brain, as a biological system operating near a critical point [24], likely leverages these same principles for computation.

Second, from a computational perspective, HOIs constitute a more powerful and expressive substrate for information processing than purely pairwise models. They are a fundamental necessity for performing non-linear operations, such as exclusive-OR (XOR) logic, that are foundational to complex cognition yet intractable for any linear system confined to dyadic connections. This computational principle is vividly illustrated by the architecture of modern artificial deep neural networks; for instance, the transformative power of transformers stems directly from their self-attention mechanism, which inherently captures complex, context-dependent interactions among multiple elements. It is therefore a compelling neurobiological hypothesis that the brain has evolved to implement analogous, but far more energy-efficient, mechanisms for nonlinear information integration. Consequently, the search for HOIs in neural systems transcends the mere identification of novel statistical dependencies in data. It represents a fundamental quest to uncover the core computational primitives – the basic building blocks of non-linear integration – that underlie cognition itself.

Third, from a clinical perspective, the breakdown of sophisticated neural integration may be a core biomarker of neurological and psychiatric diseases. A framework capable of quantifying these higher-order dysfunctions could yield earlier and more precise diagnostics, moving beyond the observation that a network is "disrupted" to identifying how its integrative capacity has been impaired.

1.4. Scope and organization of this review

Thus, the key question facing modern neuroscience is this: how can we quantitatively define, measure, and interpret these multi-component interactions in order to move from a static map of connections to a dynamic model of their context-dependent cooperation? This review aims to provide a comprehensive synthesis of the emerging field of HOIs in brain networks and their growing importance for neuroscience. We begin by defining the concept of HOIs and clarifying how they differ from traditional pairwise descriptions of functional connectivity. We then introduce the principal modeling frameworks, ranging from graph-theoretic representations to hypergraphs and simplicial complexes, which allow the description of interactions among groups of brain regions rather than only pairs. The discussion then turns to the methodologies available for detecting and quantifying HOIs in neuroimaging data, including multivariate statistical approaches, information-theoretic measures, graph-theoretical tools, and machine learning techniques designed to capture complex and nonlinear dependencies. Despite growing enthusiasm, the field faces serious methodological challenges, including the problem of distinguishing true HOIs from indirect pair effects, the computational complexity of higher-order analysis, and the need to develop new statistical models and visualization tools.

In this review, we also provide a critical assessment of these limitations and outline ways to overcome them. Building on these methods, we review evidence for the biological and cognitive significance of HOIs, highlighting their role in normal brain function, their alterations in neurological and psychiatric disorders, and their relevance across development and aging. The final sections address the challenges and limitations of current approaches and outline future directions for the field, with an emphasis on methodological advances, integration of multimodal data, translation to clinical applications, and the potential for large-scale, real-time analyses.

2. Higher-order interactions in brain networks

The study of brain function through the lens of network science has yielded profound insights into its complex organization. Traditionally, these efforts have focused on pairwise interactions between brain regions, typically derived from electroencephalography (EEG), magnetoencephalography (MEG), functional near-infrared spectroscopy (fNIRS), or fMRI data. However, a growing body of evidence suggests that the rich tapestry of neural dynamics and cognitive functions arises from interactions that transcend simple dyads, involving coordinated activity among groups of three or more brain

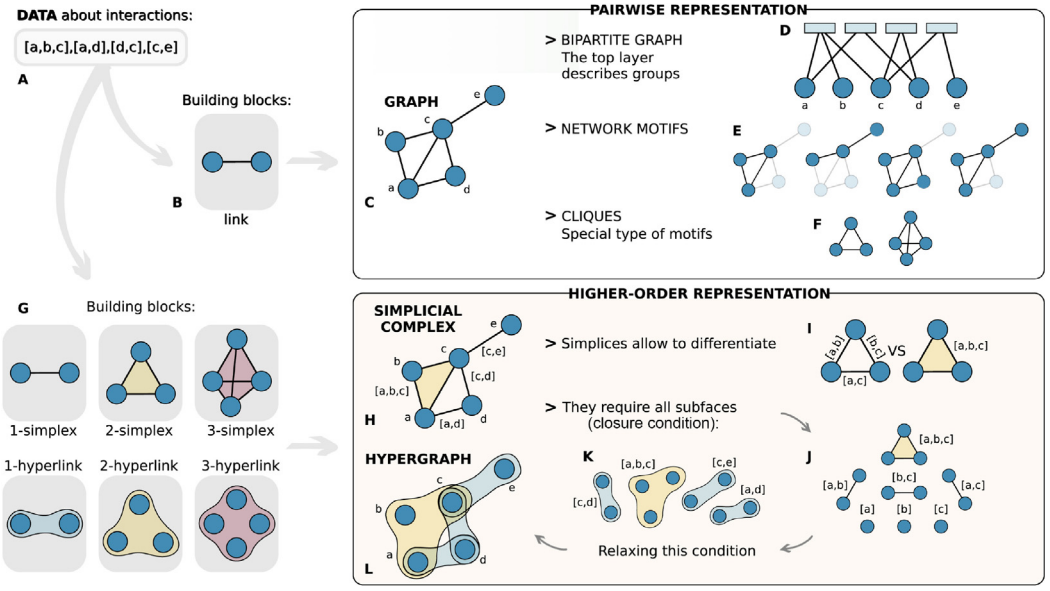

Fig. 1. Representations of higher-order interactions. A set of interactions of heterogeneous order (A) can be represented using only pairwise interactions (B). Using only low-order blocks, the set of interactions can be described in the simplest way by using a graph (C). Alternatively, interactions can be encoded as nodes in one layer of a bipartite graph, where the other layer contains the interaction vertices (D). Other examples of high-order coordinated patterns can be encoded using motifs, small subgraphs with specific connectivity structures (E). Cliques are a fundamental motif, identified as the densest subgraphs and often regarded as the essential building blocks of complex networks (F). All these representations discard information that was present in the original interaction data (A). A solution is to consider explicitly higher-order building blocks, in the form of simplices and hyperedges (G). Collection of simplices form simplicial complexes (H), which allow to discriminate between genuine higher-order interactions and – even complex – sums of low-order ones (I). Unfortunately, simplicial complexes, given a simplex, require the presence of all possible subsimplices—closure condition (J), which can be too strong an assumption in some systems. Relaxing this condition effectively implies moving from simplices to hyperedges (K), which are the most general – and less constrained – representation of higher-order interactions (L).
Source: Adapted from [21]; licensed under a Creative Commons Attribution 4.0 International license.

regions. These are termed higher-order interactions (HOIs). Capturing and analyzing HOIs necessitates a shift from classical graph theory to more sophisticated mathematical frameworks, primarily hypergraphs and simplicial complexes. This section delves into the conceptual and mathematical foundations of HOIs, their representation in brain network models derived from neuroimaging data, and their emerging biological and cognitive relevance.

2.1. Defining higher-order interactions

The concept of interaction in complex systems, particularly in the brain, extends beyond simple pairwise relationships. Many neural processes and cognitive functions are thought to emerge from the collective, synergistic activity of multiple brain regions. Understanding these phenomena requires a formal definition of interactions that can encompass these group activities.

2.1.1. Mathematical and conceptual definitions

Conceptually, HOIs refer to dependencies or influences among a group of three or more elements (e.g., brain regions, neurons) that cannot be trivially decomposed into a sum or simple aggregation of interactions between pairs of elements within that group [21,25,26]. For instance, consider three brain regions. Their simultaneous co-activation might represent a unique functional state or computation that is qualitatively different from, or quantitatively more than, the sum of their individual pairwise co-activations. This irreducibility is the hallmark of a true HOI.

Formally, a k-body interaction involves k distinct entities. In the mathematical frameworks used to represent HOIs, this translates to specific structures (see Fig. 1):

- A k-body interaction can be represented by a $(k-1)$-dimensional **simplex**.
- A k-body interaction can also be represented by a **hyperedge or hyperlink** of cardinality k.

Simplices are fundamental building blocks of simplicial complexes [27]. A d-dimensional simplex, denoted as σ, is formally defined as a set of $(d+1)$ interacting nodes: $\sigma = [v_0, v_1, \ldots, v_d]$. Geometrically, a 0-simplex is a node (vertex), a 1-simplex is an edge (link) connecting two nodes, a 2-simplex is a triangle (representing a three-body interaction), and a 3-simplex is a tetrahedron (representing a four-body interaction), and so forth. Any subset of the nodes forming a simplex

σ also forms a simplex, called a face of σ. If τ is a face of σ, then $\tau \subset \sigma$. For example, a 2-simplex $[v_0, v_1, v_2]$ has three 1-simplex faces ($[v_0, v_1]$, $[v_0, v_2]$, $[v_1, v_2]$) and three 0-simplex faces ($[v_0]$, $[v_1]$, $[v_2]$).

Hyperedges are the fundamental units of hypergraphs [21,25,26]. A hyperedge e is simply a subset of the set of nodes V, $e \subseteq V$, representing a many-body interaction among the nodes it contains: $e = [v_0, v_1, \ldots, v_k]$. The cardinality of this hyperedge is $(k + 1)$, indicating an $(k + 1)$-body interaction.

It is important to maintain clarity in terminology when discussing these structures. A d-simplex, involving $(d+1)$ nodes, represents a $(d + 1)$-body interaction. A hyperedge of cardinality k involves k nodes and represents a k-body interaction. Thus, a k-body interaction corresponds to a $(k - 1)$-dimensional simplex. This review will adhere to these definitions.

2.1.2. Differences between pairwise and higher-order interactions in brain networks

Traditional graph theory, which models brain networks as collections of nodes (brain regions) and edges (pairwise functional connectivity derived from neuroimaging data), inherently simplifies the complex landscape of neural dynamics [28–32]. Such pairwise models, for example, cannot distinguish between two scenarios: one in which three brain regions (A, B, and C) are all correlated because they are driven by a common external input and one in which these three regions engage in a synergistic three-way interaction, resulting in collective behavior that is greater than the sum of their individual activities.

Many cognitive functions are thought to emerge from the precisely coordinated activity of distributed ensembles of brain regions, suggesting that interactions often extend beyond simple dyads [28,32]. For instance, the simultaneous activation of multiple regions identified in an fMRI study might signify a higher-order functional assembly or a computational process that is not adequately captured by merely summing pairwise correlations. An illustrative example is the contrast between three regions A, B, and C being connected by edges [A,B], [B,C], and [A,C] in a graph, versus these three regions forming a 2-simplex or a hyperedge [A,B,C]. The latter explicitly represents a distinct functional unit or process involving all three simultaneously.

The critical distinction lies in the concept of emergent functional properties. While pairwise functional connectivity measures the statistical dependency between the time series of two regions, e.g., EEG or Blood Oxygenation Level Dependent (BOLD) signals from fMRI, HOIs aim to capture synergistic effects where the whole is greater than the sum of its parts [31,33]. If regions A, B, and C are all strongly driven by a common input, their signals will naturally be correlated pairwise. However, an additional, irreducible interaction might occur only when all three are active together. This is a true HOI. Methods such as the generalized Ising model [21,34] or data-driven approaches [35] attempt to disentangle these true HOIs from effects explainable by lower-order interactions. Therefore, HOI analysis in neuroimaging data seeks to identify these emergent group interactions, which could correspond to more complex cognitive computations or integrated functional units. Overlooking HOIs may lead to an incomplete or even misleading understanding of brain function [32].

2.1.3. Hypergraphs and simplicial complexes as frameworks for HOIs

To formally represent and analyze HOIs, network science has turned to two primary mathematical structures: hypergraphs and simplicial complexes (see Fig. 1) [21,25,26].

Hypergraphs are defined by a pair $G = (V, E_H)$, where V is a set of nodes and E_H is a set of hyperedges, with each hyperedge being a non-empty subset of V [26]. A key property of hypergraphs is that hyperedges are not required to be *subset-closed*. Unlike in a graph, where an edge between multiple nodes implies edges between all their pairs, a hyperedge containing vertices v_0, v_1, v_2 does not automatically imply the existence of hyperedges for its subsets, like $[v_0, v_1]$. This makes hypergraphs suitable for modeling systems where a group interaction is specific and does not necessarily mean that all its sub-groups also interact in a similar, significant manner. For example, a cognitive task might require three brain regions to activate together as a single, coordinated ensemble. However, outside of this specific trio, any pair of these regions may not show strong coordination when operating independently.

Simplicial complexes, denoted K, are collections of simplices that adhere to a crucial "simplex condition" or "closure under inclusion of faces": if a simplex σ is in K, and τ is any face of σ (i.e., $\tau \subset \sigma$), then τ must also be in K [26]. Geometrically, a simplicial complex can be visualized as a collection of points, edges, triangles, tetrahedra, and their higher-dimensional counterparts (polyhedra) that are "glued" together along their common faces. This closure property makes simplicial complexes naturally endowed with rich topological structure, which is a significant advantage for analytical purposes. They are particularly appropriate when it is assumed that if a group of brain regions is strongly co-active, then subsets of that group are also likely to be co-active to some degree, or at least their pairwise interactions are considered relevant components of the higher-order structure [28]. When considering brain data, especially fMRI, simplicial complexes are often favored due to the natural applicability of powerful tools from Topological Data Analysis (TDA), such as persistent homology [21,26].

The "simplex condition" inherent in simplicial complexes is a strong modeling assumption with significant implications for interpreting HOIs in neuroimaging data. If a set of k brain regions forms a $(k - 1)$-simplex (e.g., representing a k-body interaction based on mutual co-activation above a certain threshold), the simplex condition mandates that all its (m)-node subsets (for $m < k$) also form simplices (i.e., $(m - 1)$-simplices). For instance, if fMRI data show that regions A, B, and C form a strongly co-activated group, we can model this as a 2-simplex. A key property of this model is that it inherently includes all its subset interactions. Therefore, by representing the trio as a simplex, the framework automatically defines

the pairwise connections [A,B], [A,C], and [B,C] as significant components of the structure (1-simplices). This might be neurobiologically plausible if robust three-way co-activation relies on underlying strong pairwise functional links.

However, if the three-way interaction is purely emergent and does not depend on individually significant strong pairwise links (e.g., pairwise links are weak, but their specific combination yields a strong HOI), then the simplicial complex representation might impose a hierarchical structure not fully supported by the data at all scales. A hypergraph representation would allow for the hyperedge [A,B,C] without necessarily requiring the constituent pairwise hyperedges. Consequently, when interpreting results from simplicial complex analysis of neuroimaging data, such as Betti numbers indicating topological "holes", it is crucial to remember that these features are defined relative to this inherent closure property. A topological "hole" in a simplicial complex of brain activity might signify a different neurobiological phenomenon than a "gap" in a less constrained hypergraph representation. The choice of representation thus influences the types of biological questions that can be addressed and the interpretation of the findings.

2.2. Brain network models based on HOIs

The application of HOI frameworks to neuroimaging data involves specific methods for constructing network models that go beyond pairwise connections. These models can be static, capturing average HOI patterns, or dynamic, reflecting the time-varying nature of brain function [15]. Furthermore, multilayer approaches can integrate HOIs across different conditions, frequency bands, or data modalities.

Pairwise functional connectivity (FC) networks are typically constructed by defining regions of interest (ROIs) from anatomical atlases or functional parcellations, extracting their mean BOLD fMRI time series, calculating a measure of statistical dependence (e.g., Pearson correlation, coherence) between all pairs of ROI time series, and often thresholding the resulting correlation matrix to create an adjacency matrix representing the graph [29,30,36]. While this approach has been foundational in network neuroscience, it captures only a fraction of the complex interdependencies that likely underpin brain activity [28,33]. Many sophisticated brain functions are believed to arise from synergistic interactions among multiple regions, patterns that are not fully described by an aggregation of pairwise links.

2.2.1. From graph theory to higher-order representations of functional networks

Standard graph metrics such as degree, clustering coefficient, path length, and modularity, while informative for pairwise networks, offer limited insight into the nature and structure of group interactions [29,30,36]. For example, a high clustering coefficient in a graph indicates the presence of many triangles formed by pairwise links, but it does not distinguish whether these triangles represent true three-way interactions (i.e., 2-simplices or "filled" triangles) or are merely collections of dyadic connections. Moving to higher-order representations allows for a more nuanced characterization.

To address this limitation, recent advances have turned to higher-order representations of functional networks, which explicitly model multi-node interactions (see Table 1). These approaches provide a more nuanced characterization of functional brain organization, enabling the detection of group-level dependencies that are invisible to traditional graph-based analyses. Below, we discuss several primary frameworks for constructing static HOI representations from fMRI data based on simplicial complexes or hypergraphs. These models aim to capture time-averaged patterns of multi-region interactions, offering a snapshot of the brain's functional architecture.

Clique complex construction. A widely used method for building simplicial complexes from fMRI data is the clique complex approach, which proceeds as follows (see Fig. 2):

1. Calculating a pairwise functional connectivity matrix (e.g., Pearson correlation between BOLD time series of N ROIs). This matrix encodes pairwise functional connectivity, where each entry quantifies the linear dependence between two ROIs.
2. Thresholding the connectivity matrix at a specific correlation value ϵ to obtain an unweighted graph $G_\epsilon = (V, E_\epsilon)$, where an edge exists if the correlation exceeds ϵ. Threshold selection is critical: too low introduces spurious edges, while too high may fragment the network.
3. Identifying all cliques in G_ϵ. A k-clique is a fully connected subgraph where all k nodes are connected to each other.
4. Simplicial Complex Formation. Each $(k+1)$-clique in G_ϵ is represented as a k-simplex in the clique complex $X(G_\epsilon)$. For example, a 3-clique (a triangle of edges) becomes a 2-simplex (a filled triangle). The mathematical definition is as follows: Given a graph $G = (V, E)$, its clique complex $X(G)$ is the simplicial complex whose simplices are the vertex sets of all cliques in G.

Weighted simplicial complexes. While binary thresholding simplifies analysis, it discards valuable connectivity strength information. Weighted simplicial complexes address this by preserving edge weights. A common strategy is to assign the minimum weight of its constituent edges to each simplex, which is a conservative estimate ensuring all pairwise connections are strong. Alternatively, more sophisticated weight propagation methods can be employed, such as averaging or product-based schemes.

Table 1
Comparison of pairwise, hypergraph, and simplicial complex representations for brain networks [37].

Feature	Pairwise (Graph)	Hypergraph	Simplicial complex
Basic Unit	Edge (connects 2 nodes)	Hyperedge (connects $\geq$2 nodes)	Simplex (d-simplex connects $d+1$ nodes)
Interaction Order Represented	Dyadic (2-body) only	Polyadic (any k-body, $k \geq 2$)	Polyadic (any k-body, $k \geq 1$)
Closure Property (Subset Inclusion)	Not applicable (edges are minimal)	No (a hyperedge does not imply its sub-hyperedges exist)	Yes (a simplex implies all its faces exist)
Primary Topological Tools	Graph theory metrics (degree, clustering, paths)	Emerging hypergraph theory, some TDA	Algebraic Topology, TDA (Homology, Persistent Homology, Higher-Order Laplacians, Q-analysis)
Suitability for fMRI Co-activation	Captures pairwise correlations	Flexible for specific group co-activations without assuming sub-group links	Captures hierarchical co-activation patterns; well-suited for TDA of correlation-based structures
Example Brain Application (fMRI-based)	Standard functional connectivity networks from ROI correlations	Modeling specific multi-region functional synergies where sub-synergies are not assumed	Clique complexes from correlation matrices; persistent homology of evolving functional connectivity

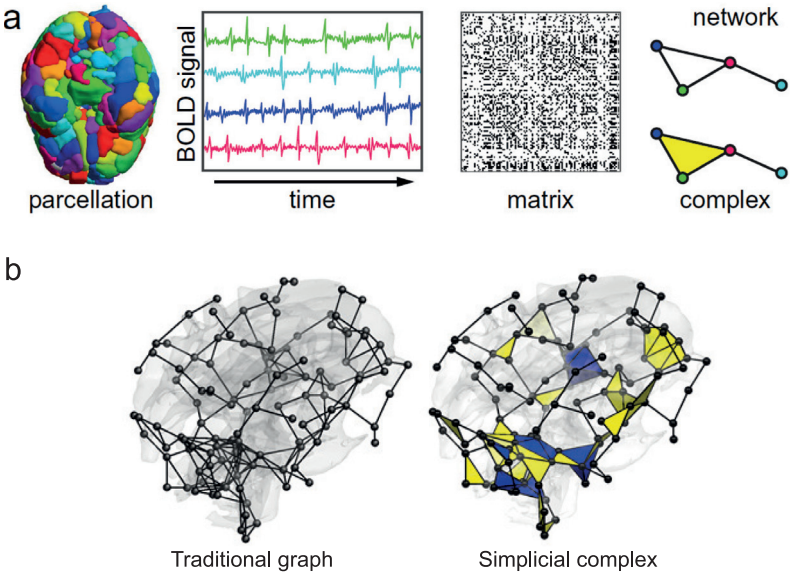

Fig. 2. Clique Complex Construction. (a) Correlation or coherence matrices between regional BOLD time series can be encoded as a type of simplicial complex called a clique complex, formed by taking every complete (all-to-all) subgraph in a binarized functional connectivity matrix to be a simplex. Adapted from [28]. (b) The traditional graph representation (left) and the simplicial complex representation (right) of a brain network: 2-simplices (yellow triangles) show the connectivity of three regions while 3-simplices (blue tetrahedrons) show the connectivity of four regions. Standard graph data structure cannot encode such complex connectivity patterns directly without additional models. Based on data from [28,38].

Hypergraphs from fMRI. Hypergraph construction from fMRI data offers more flexibility as it does not require the strict subset closure property of simplicial complexes. Common strategies include:

1) *Distance-based methods.* Here, ROIs are defined as nodes. Hyperedges are formed by grouping ROIs that are "close" in some feature space [39,40]. The features can be derived from fMRI time series (e.g., activity profiles, connectivity profiles).

   - *k-Nearest Neighbors (k-NN):* For each ROI, its k nearest neighbors in the chosen feature space (e.g., based on Euclidean distance of their correlation vectors with all other ROIs) form a hyperedge [41].

- *Clustering-based:* Clustering algorithms (e.g., k-means, hierarchical clustering) are applied to ROI features. Each resulting cluster of ROIs forms a hyperedge [42,43]. If features are derived from patterns of co-activation, this method directly captures groups of co-activating regions as hyperedges [44].

Distance-based methods are often considered simple and efficient in various applications. However, they are limited by an inability to accurately measure distances between paired vertices in a given feature space due to noise and data outliers. Hyperparameters significantly impact the hypergraph's structure and, consequently, the performance of hypergraph learning when the nearest-neighbor-based strategy is employed. Currently, there is no general principle available to guide the selection of hyperparameters. Additionally, identifying the k nearest neighbors of each center vertex is computationally expensive for large-scale data. A key limitation of the clustering-based approach is the sensitivity of the resulting hypergraph to the pre-defined number of clusters [40].

2) *Representation-based methods.* Hyperedges are defined based on how well a group of ROIs can reconstruct or represent another ROI's activity or features (e.g., via sparse coding or regression techniques) [39,40]. Representation-based methods are more flexible and adaptive than distance-based methods. They are particularly suitable for datasets with clear clustering structures in lower-dimensional feature spaces. However, representation-based methods are vulnerable to data noise and outliers, which is a major drawback. Additionally, if the center vertex is represented by all vertices except itself, the computational cost increases. Conversely, if the center vertex is represented only by its nearest neighbors, the resulting hypergraph may not accurately capture the correlation among samples in the entire data distribution [40].
3) *Multi-hyperedge Binary Masking.* In machine learning applications, hyperedge structures can be learned from data rather than predefined. For example, in disease classification tasks, a neural network might optimize binary masks to identify hyperedges that best discriminate between groups [39].

2.2.2. Mathematical tools for characterizing HOI structures

Once a HOI representation (simplicial complex or hypergraph) is constructed, various mathematical tools can be employed for its characterization. We will briefly discuss the most important ones.

Incidence and adjacency representations. The following approaches describe HOIs in terms of matrices or tensors.

- *Incidence Matrix B_k for Simplicial Complexes.* Let K be an oriented simplicial complex. The orientation can be chosen arbitrarily and it is only needed in order to perform computations coherently. For simplicity and without loss of generality, we will use the orientation induced by the ordering of the vertex labels. The incidence matrix, B_k, encodes the boundary relationships between k-simplices and $(k-1)$-simplices in K (see Fig. 3D). The rows correspond to $(k-1)$-simplices and the columns correspond to k-simplices. The entry $B_k(\tau,\sigma)$ indicates the incidence between $\tau \in K_{k-1}$ and $\sigma \in K_k$ as follows [26]:

$$B_k(\tau,\sigma) = \begin{cases} +1 & \text{if } \tau \text{ is a face of } \sigma \text{ with consistent orientation,} \\ -1 & \text{if } \tau \text{ is a face of } \sigma \text{ with opposite orientation,} \\ 0 & \text{otherwise.} \end{cases}$$

  Thus, the incidence matrix relates k-simplices to their $(k-1)$-dimensional faces.
- *Incidence Matrix I for Hypergraphs.* For a hypergraph with N nodes and M hyperedges, the $N \times M$ incidence matrix I has entries $I_{i\alpha} = 1$ if node i is part of hyperedge α, and 0 otherwise (Fig. 3A) [21].
- *Adjacency Tensor $a^{[k]}$ for Pure k-Simplicial Complexes.* For a pure k-simplicial complex (all maximal simplices have dimension k), the $(k+1)$-order tensor $a^{[k]}$ has elements $a^{[k]}_{\alpha} = 1$ if the k-simplex α exists in the simplicial complex, and 0 otherwise (Fig. 3H). This tensor is symmetric under permutation of indices within α [21,26].
- *Adjacency Hypermatrix $A^{[k]}$ for k-uniform Hypergraphs.* For a hypergraph where all hyperedges have cardinality k, the k-order hypermatrix $A^{[k]}$ has elements $A^{[k]}_{i_1,\ldots,i_k} = 1$ if the hyperedge $\{i_1,\ldots,i_k\}$ exists, and 0 otherwise (Fig. 3G) [21].

Topological Data Analysis (TDA). TDA provides a suite of tools to quantify the shape and structure of data, particularly well-suited for simplicial complexes. These tools include:

- *Simplicial Homology:* provides a rigorous mathematical framework for characterizing the topological structure of HOIs in brain networks represented as simplicial complexes [21,27]. At its core, this approach leverages algebraic topology to quantify the multi-dimensional connectivity patterns through homology groups, which capture essential topological features such as connected components, cycles, and voids across different dimensions [26]. The power of this method lies in its ability to compute topological invariants, particularly the Betti numbers, which reveal the organization of neural interactions beyond pairwise connections. By constructing chain complexes connected by boundary operators and examining the resulting homology groups, simplicial homology transforms the geometric structure of neural assemblies into computable algebraic signatures. This formalism enables researchers to detect and compare the persistence of functionally relevant higher-order network motifs across different cognitive states or clinical conditions, offering a principled way to bridge the gap between local neural interactions and global brain function. Key concepts and characteristics of simplicial homology include:

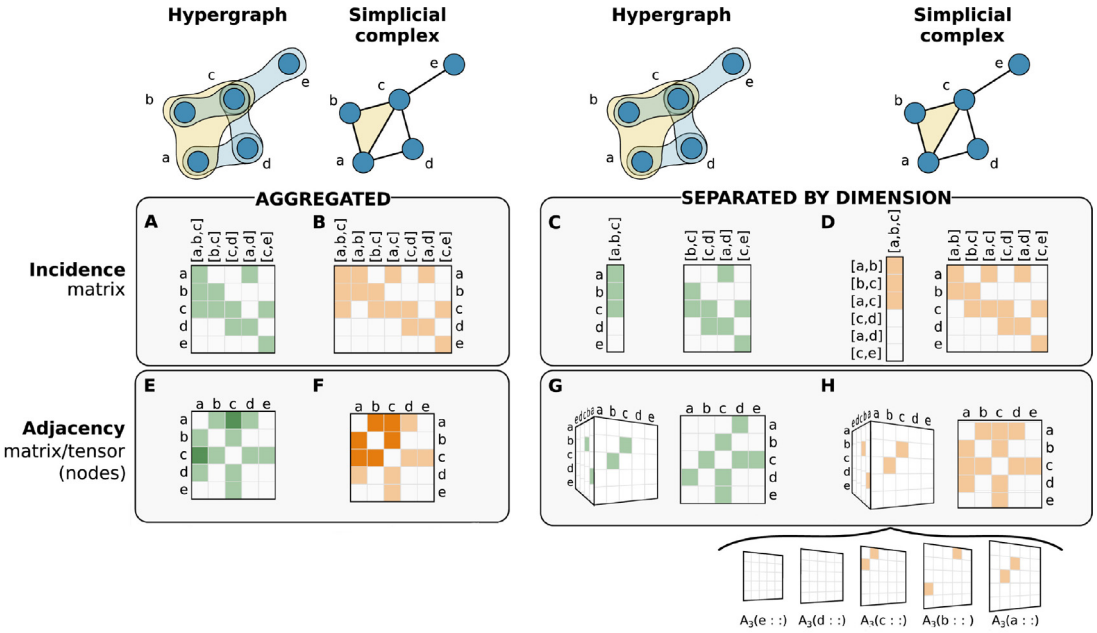

Fig. 3. Incidence matrices and adjacency hypermatrices/tensors for simplicial complexes and hypergraphs. Visualization of incidence matrices and adjacency matrices that can be used to represent the structure of HOIs. There are two types of matrices: (A–D) incidence matrices relating nodes and edges, and (E–H) adjacency matrices relating nodes to nodes via edges. Furthermore, one can consider edges aggregated by dimensions (left panels) or only subsets of edges of the same dimension, obtaining a collection of matrices, one for each of the different sizes of hyperedges present in the HOIs (right panels).
Source: Adapted from [21]; licensed under a Creative Commons Attribution 4.0 International license.

- *Chain Groups $C_k(K)$:* Vector spaces whose bases are the k-simplices of the simplicial complex K. In other words, the chain group $C_k(K)$ is like a collection of all possible "shapes" one can build using the k-dimensional pieces (simplices) of the simplicial complex K. These shapes can be added together and scaled like vectors, forming a vector space where the basis elements are the individual k-simplices themselves. For instance, if K is a triangle (a 2D simplex), then: $C_0(K)$ is all formal combinations of its vertices (0-simplices), $C_1(K)$ is all formal combinations of its edges (1-simplices), $C_2(K)$ is all formal combinations of the triangle itself (2-simplex). Thus, chain groups provide a flexible algebraic framework to "assemble" shapes from the basic building blocks of the simplicial complex.
- *Boundary Operator* $\partial_k : C_k(K) \to C_{k-1}(K)$. For an oriented k-simplex $\sigma = [v_0, v_1, \ldots, v_k]$, its boundary $\partial_k\sigma$ is a formal sum of its $(k-1)$-faces:

$$\partial_k([v_0, \ldots, v_k]) = \sum_{p=0}^{k} (-1)^p [v_0, \ldots, \hat{v}_p, \ldots, v_k], \tag{1}$$

  where $\hat{v}_p$ denotes the omission of vertex v_p. The boundary operator actually maps each k-simplex to its $(k-1)$-dimensional faces. In other words, the boundary operator ∂_k takes a k-dimensional shape (simplex) and returns its $(k-1)$-dimensional "edges" in a structured way (with signs accounting for orientation). For instance, the boundary of a triangle $[v_0, v_1, v_2]$ is the alternating sum of its three edges:

$$\partial_2[v_0, v_1, v_2] = [v_1, v_2] - [v_0, v_2] + [v_0, v_1].$$

  Note that the incidence matrix, B_k, represents the boundary operator in matrix form. The boundary operator ∂_k has the fundamental topological and algebraic property $\partial_k\partial_{k+1} = 0$ which is usually indicated by saying that *the boundary of the boundary is null*. This implies that the image of ∂_{k+1} (boundaries) is a subspace of the kernel of ∂_k (cycles). Thus, boundaries are "closed"—they have no boundary themselves. In homology, we study *cycles* (shapes with no boundary) modulo *boundaries* (shapes that are boundaries) for this reason.
- *k-th Homology Group* $H_k(K) = \ker\partial_k/\mathrm{im}\partial_{k+1}$. Elements of $H_k(K)$ are equivalence classes of k-cycles that are not boundaries of $(k+1)$-chains, representing k-dimensional "holes" or "voids" in the complex. In other words, these are cycles that cannot be filled in, i.e., they are not boundaries of anything in K. $H_0(K)$ counts how many separate pieces the complex has; $H_1(K)$ detects 1D holes, such as a missing triangle in a mesh; $H_2(K)$ detects enclosed cavities.

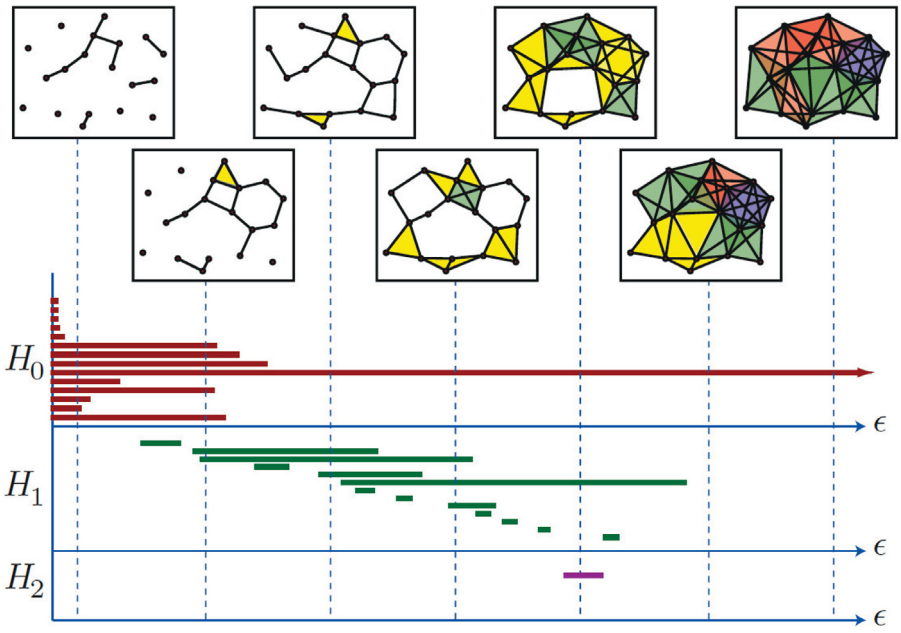

Fig. 4. An example of a topological filtration and its corresponding persistent homology barcode. The barcode depicts the birth and death of topological features across scales: H_0 (connected components), H_1 (cycles), and H_2 (2-dimensional cavities) of the simplicial complex.
Source: Reproduced from [50] by permission from Robert Ghrist.

- *Betti Numbers* $\beta_k = rank(H_k(K))$. These are key topological invariants. The dimension of the homology group H_k is called the kth Betti number and it represents a way to classify the k-dimensional topology of HOIs. Specifically, β_0 is the number of connected components, β_1 is the number of independent 1-dimensional cycles (loops or tunnels), β_2 is the number of independent 2-dimensional voids (cavities enclosed by triangles), and so on.
- *Euler Characteristic* $\xi(K)$. For any simplicial complex K, the Euler characteristic is defined as the alternating sum $\xi = \sum_{k=0}^{D}(-1)^k f_k$, where f_k is the number of k-simplices present in the simplicial complex, and D is the maximal dimension of a simplex in K [45].

- *Persistent homology:* a cornerstone of TDA, provides a multiscale framework to quantify the stability and significance of HOIs in brain networks [21,38]. Developed in the early 2000s [46], persistent homology revolutionized TDA by enabling the computation of homology across a filtration—a nested sequence of simplicial complexes that progressively approximate the data space [47]. At its core, persistent homology tracks the evolution of homological features (e.g., connected components, cycles, cavities) as the simplicial complex grows [26,48]. The persistence of a feature – its lifespan across scales in the filtration – serves as a proxy for its structural or functional relevance. While longer persistence typically indicates importance, interpretation depends critically on the filtration design (e.g., thresholding fMRI correlation matrices at varying threshold) [49]. This technique is uniquely powerful for analyzing weighted functional connectivity data, such as fMRI correlation matrices, as it: 1) identifies multiscale HOIs by distinguishing robust topological signatures from noise; 2) encodes dynamics through birth–death scales of features, and 3) generalizes beyond graphs to capture higher-dimensional interactions (e.g., k-dimensional cavities). Persistent homology bridges algebraic topology and neuroscience, offering a principled approach to unraveling the hierarchical organization of brain networks. Key concepts and characteristics include:

  - *Filtration.* A filtration is a sequence of nested simplicial complexes $K_0 \subseteq K_1 \subseteq \ldots \subseteq K_m$, typically generated by varying a threshold parameter ϵ applied to the edge weights of an initial weighted graph (from which simplicial complexes are built at each step). For fMRI, ϵ is often the correlation strength. As ϵ decreases (or increases, depending on the convention), more edges (and consequently, more higher-order simplices in the complex) are added.
  - *Persistence Diagram/Barcode.* This visualization tracks the "birth" (appearance) and "death" (disappearance or merging) of topological features (quantified by Betti numbers) across the filtration. Birth and death occur at specific ϵ values. Features that persist over a long range of ϵ values (long bars in a barcode, or points far from the diagonal in a persistence diagram) are considered robust and significant, while short-lived features are often attributed to noise (see Fig. 4).

- *Higher-Order Laplacians (Combinatorial Laplacians).*
The graph Laplacian is a fundamental operator that plays a key role in processing relational data. It describes the diffusion of information from one node to another through links. The graph Laplacian matrix can be written as follows:

$$L_0 = D - A, \tag{2}$$

where D is the diagonal matrix having the degrees of the nodes on the diagonal and A is the adjacency matrix of the network. This expression can be generalized in order to define higher-order Laplacians L_k (see Fig. 5) that describe diffusion from an k-simplex to another k-simplex [21,26]. The kth higher-order or combinatorial Laplacian L_k (also called the Hodge Laplacian) can be defined for each dimension k via two matrices that encode respectively the roles of upper and lower adjacencies in dimension k:

$$L_k = L_k^{up} + L_k^{low}, \tag{3}$$

where L_k^{up} and L_k^{low} are called the upper and lower adjacency Laplacians. The *upper Laplacian* $L_k^{up} = B_{k+1}B_{k+1}^T$ (B is the incidence matrix of simplicial complex) captures interactions between k-simplices through their cofaces (i.e., $(k+1)$-dimensional simplices that contain them as faces). This component governs diffusion-like processes that move "upward" through the simplicial hierarchy. The *lower Laplacian* $L_k^{low} = B_k^T B_k$ encodes interactions between k-simplices through their shared faces (i.e., $(k-1)$-dimensional simplices). This term governs processes that move "downward" through the complex. The higher-order combinatorial Laplacian L_k becomes then:

$$L_k = B_{k+1}B_{k+1}^T + B_k^T B_k. \tag{4}$$

A profound result from Hodge theory connects the spectral properties of L_k to the topology of the underlying simplicial complex [51]:

$$\dim(\ker(L_k)) = \beta_k, \tag{5}$$

where β_k is the kth Betti number. Thus, the number of (homological) k-holes is the same as the dimension of the kernel of L_k. The eigenvectors associated with zero eigenvalues (harmonic forms) localize around topological cavities in dimension k, providing geometric insight into the complex's void structure. For $k = 0$, this reduces to the classical result that the multiplicity of the zero eigenvalue in the graph Laplacian equals the number of connected components (β_0).
The spectrum of L_k contains rich information about the higher-order organization of the network:

  - The *spectral gap* (smallest non-zero eigenvalue) governs diffusion timescales on k-simplices.
  - The *spectral dimension* (asymptotic scaling of eigenvalue density) reveals fractal-like properties.
  - Non-harmonic eigenvectors identify clusters or other mesoscale structures in the k-skeleton.

The Laplacian operator has also been generalized to k-uniform hypergraphs [52–54].
The theoretical foundation linking these operators to the continuous Laplacian allows researchers to probe the diffusion properties of higher-order systems through spectral analysis. Reflecting this, a key research thrust has been the formulation of specialized Laplacian operators for hypergraphs to model distinct types of diffusion dynamics [55,56]. These operators have also been successfully applied to study higher-order diffusion in fMRI data, where the temporal evolution of activity patterns can be modeled using the heat kernel, $\exp(-tL_k)$. The resulting dynamics reveals how information propagates through multi-region interactions that cannot be captured by standard graph-based approaches. The study by Abdelnour et al. [57] and subsequent related works [58,59] have demonstrated the success of using heat diffusion kernels on brain networks to predict functional connectivity and understand information flow. Research exploring the Hodge Laplacian of brain networks (e.g., the work of Chung et al. [60]) aims to model cycles and higher-order signal transmission paths, indicating a move beyond standard graph-based approaches.
- *Q-analysis.* Introduced by Atkin in the 1970s [61,62], Q-analysis provides a systematic framework for examining the multilevel structure of simplicial complexes and quantifying their higher-order connectivity patterns [63]. It addresses the limitations of pairwise analysis by focusing on the connectivity between simplices through shared faces. Two simplices are considered *q-near* if they share a common face of dimension at least q, and they are *q-connected* if there exists a chain of simplices between them where each consecutive pair is q-near. This allows the grouping of simplices into *q-connected components*, revealing the structure of the complex at different dimensional levels. The core of Q-analysis lies in the calculation of the *structure vectors*. The *First Structure Vector (FSV)* $\mathbf{Q}$ captures the number of q-connected components for each dimensional level q, providing a means to visualize the graded substructures of the simplicial complex. The *Second Structure Vector (SSV)* $\mathbf{n}$ counts the number of simplices at each dimensional level, while the *Third Structure Vector (TSV)* $\bar{\mathbf{Q}}$ quantifies the degree of connectedness at each level, normalized by the number of simplices. Additional metrics include *topological entropy*, which measures the diversity of vertex participation in simplices of dimension q, and *topological dimensionality*, which extends the concept of vertex degree to account for participation in multi-node interactions across all dimensions. Q-analysis has been

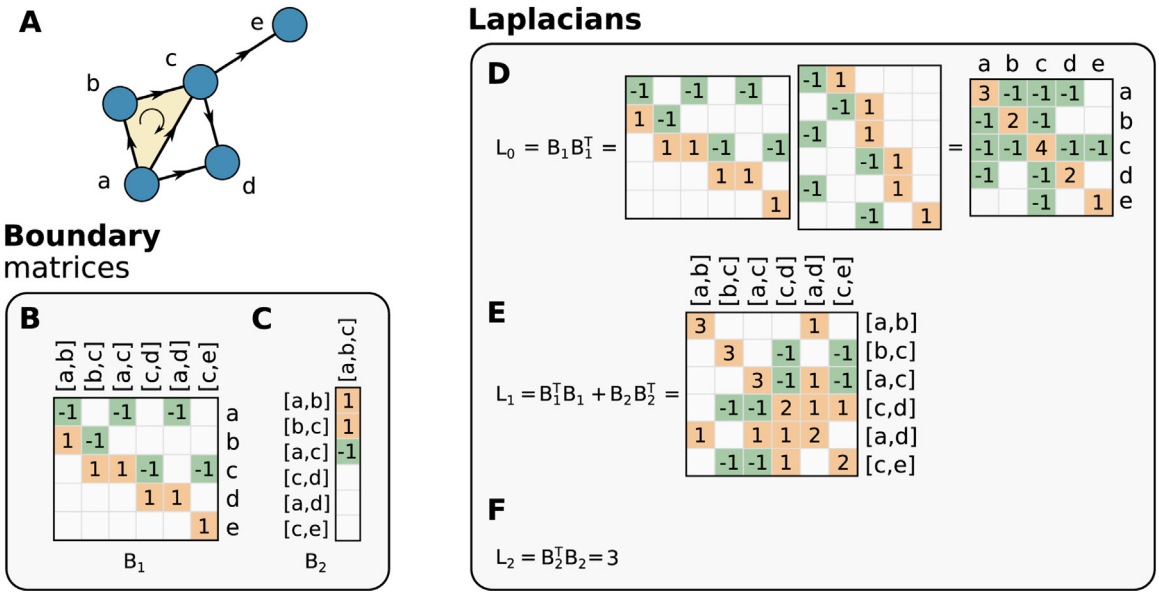

Fig. 5. Constructing the combinatorial Laplacian for a toy simplicial complex. (**A**) The complex is endowed with a lexicographic orientation, a prerequisite for defining boundary operators. The corresponding non-trivial boundary matrices, $\mathbf{B}_1$ and $\mathbf{B}_2$, are shown in (**B**) and (**C**), respectively. The combinatorial Laplacians, $\mathbf{L}_k$, are then built for each dimension k: (**D**) $\mathbf{L}_0$ (acting on nodes), which is identical to the standard graph Laplacian; (**E**) $\mathbf{L}_1$ (acting on edges); and (**F**) $\mathbf{L}_2$, which is a scalar in this case due to the presence of only one 2-simplex.
Source: Adapted from [21]; licensed under a Creative Commons Attribution 4.0 International license.

applied to study social networks, scientific collaboration, and, more recently, brain networks (connectomes) [64]. In neuroscience, it has revealed disruptions in higher-order functional assemblies in conditions such as Major Depressive Disorder, where patients show reduced connectivity at high q-levels compared to healthy controls [65]. This demonstrates the utility of Q-analysis in characterizing the integrity of multi-region functional coordination beyond pairwise interactions. More details on Q-analysis and the special Q-analysis package for Python can be found in Ref. [66] and on GitHub at https://github.com/pakrentos/q-analysis.

Thus, the application of TDA, particularly persistent homology, offers a principled way to address the common problem of thresholding in fMRI functional connectivity analysis while considering HOIs. Generally, an fMRI correlation matrix represents a weighted, fully connected graph [30]. By constructing a filtration of simplicial complexes (typically clique complexes) by systematically varying the correlation threshold, persistent homology tracks topological features across all possible thresholds. Features that persist over a wide range of thresholds are considered robust, while short-lived features are more likely to be noise. This multi-scale perspective is crucial for identifying significant HOIs that are stable across a range of connectivity strengths, rather than being artifacts of an arbitrarily chosen single threshold. This robustness is essential for discovering reliable biomarkers from fMRI data.

2.2.3. Dynamic and multilayer higher-order brain networks

Brain function is inherently dynamic, and its organization can be viewed through multiple lenses (e.g., different frequency bands or cognitive states). Static HOI models, while informative, average out these crucial temporal and contextual variations [67].

Dynamic HOIs. The motivation for studying dynamic HOIs is that brain activity patterns and interactions are not fixed but evolve over time, reflecting ongoing cognitive processes and state changes [68–70]. There are following basic methods for capturing dynamic HOIs:

- *Sliding Window Approach.* This common technique involves constructing HOI representations (simplicial complexes or hypergraphs from fMRI data) within successive, often overlapping, time windows [15,69,70]. The temporal evolution of HOI features (e.g., Betti numbers, simplex counts) is then analyzed across the sequence of these window-specific HOI structures.
- *Temporal Hypergraphs/Evolving Simplicial Complexes.* These are formalisms where hyperedges or simplices can be added or removed over time, directly modeling the dynamic formation and dissolution of multi-region co-activation patterns [39,71]. An example is the simplicial activity-driven model, where active brain regions (nodes) can dynamically form transient simplices.

- *Phase Space Reconstruction for HOIs.* While primarily developed for univariate time series, adapting such methods to multivariate fMRI data to reconstruct a joint phase space whose topology (analyzed via persistent homology) might reveal dynamic HOIs is an active area of research.
- *Persistent Homology for Dynamic Data.* Filtration can be constructed based on time itself (simplices appear as they become active and persist) or by analyzing evolving connectivity strengths within sliding windows using persistent homology to identify robust dynamic topological features.

However, analyzing dynamic HOIs presents several challenges, including the high dimensionality of the data, significant computational costs, the difficulty of distinguishing true dynamic changes from noise or sampling variability, and the necessity of developing appropriate null models for statistical inference of dynamic HOIs [70].

Multilayer HOIs. Brain networks can be conceptualized as multilayer systems, where layers might represent different frequency bands of neuroimaging signals (e.g., EEG or MEG) [72], distinct cognitive tasks, different subject groups, or the integration of fMRI (functional connectivity) with other neuroimaging modalities, such as diffusion tensor imaging (structural connectivity) [73,74]. Each layer in a multilayer network can itself be an HOI network (a hypergraph or simplicial complex). Inter-layer connections can also be higher-order, linking simplices or hyperedges across different layers. For instance, a hyperedge in a multiplex hypergraph could connect a group of nodes within one layer and their corresponding nodes in another layer.

The typical example is analyzing EEG or MEG data filtered into different frequency bands (e.g., delta, theta, alpha, beta, gamma). Each band can be represented as a layer of simplicial complexes. Investigating HOIs within each band and how these HOIs interact or couple across bands could reveal frequency-specific group processing and mechanisms of cross-frequency coupling at a higher-order level.

Single-layer HOI metrics (e.g., Betti numbers, Laplacian spectra) can be extended to the multilayer context to characterize, for instance, multilayer Betti numbers or joint topological features that span across layers.

The development of dynamic and multilayer frameworks for HOI is crucial for an ecologically valid model of brain function. Such models are necessary to describe how the brain dynamically assembles and disassembles higher-order functional units to flexibly orchestrate complex behaviors in response to changing internal states and external demands [68,69]. Static HOI models, by averaging over time and context, miss these crucial dynamics. Dynamic HOI models, such as evolving simplicial complexes derived from fMRI time windows, can capture these transient functional assemblies. Similarly, the nature and structure of HOIs might vary across different cognitive tasks or be expressed differently across various frequency bands. Multilayer HOI models can represent these distinct states or information channels as separate layers, facilitating the study of both within-layer HOI organization and inter-layer HOI dependencies [74]. For instance, a specific HOI pattern might be prominent during a working memory task (represented in one layer) but absent or altered during a motor task (another layer), or its topological characteristics might differ significantly across fast and slow frequency bands. This advanced modeling provides a powerful framework for investigating disorders characterized by abnormal brain dynamics or impaired context processing, yielding a more nuanced representation of brain complexity.

2.3. Role of HOIs in cognitive functions and neurological disorders

Exploring HOIs in fMRI-based brain networks is not just a methodological advancement; it is also driven by the hypothesis that these complex interactions are fundamental to brain function and change in dysfunction. Specifically, HOIs are increasingly considered to be the basis of sophisticated cognitive abilities that depend on the integration of information across widespread brain regions [33,75].

Information integration and processing. Simplicial complexes and their topological features, such as Betti numbers and persistent cycles derived from fMRI data, offer quantitative measures of the information integration. For instance, β_1 can quantify irreducible cyclic pathways of functional connectivity, while higher-dimensional Betti numbers (β_k, $k \geq 2$) might reflect the brain's capacity for more complex forms of information integration or the presence of multi-regional functional "voids" or "cavities" that shape information flow [76,77].

Learning and plasticity. The brain's ability to learn and adapt is a hallmark of its function. Dynamic HOI analysis, or the application of TDA to fMRI data acquired across different learning stages or conditions, can reveal changes in HOI patterns that may reflect underlying neural plasticity and the formation or dissolution of functional assemblies critical for new skills or knowledge [69].

Task performance and cognitive states. Specific HOI features derived from fMRI are being investigated for their correlation with performance on various cognitive tasks and their ability to characterize different cognitive states [33]. For example, the robustness (persistence) of certain topological cycles or the spectral properties of higher-order Laplacians computed from task-based fMRI data might predict cognitive efficiency. A notable example is the study by Petri et al. (2014) [77], which found that psilocybin-induced altered states of consciousness were associated with distinct "homological scaffolds" (topological backbones of functional networks), indicating profound changes in large-scale information integration patterns compared to placebo.

Pathophysiological mechanisms and clinical translation. The framework of HOIs provides a new lens for understanding brain disorders, suggesting that their pathophysiology may manifest primarily as a disruption in the brain's capacity to form integrated, multi-region functional ensembles. These impairments in synergistic integration are often invisible to standard pairwise connectivity analyses, positioning HOI analysis as a tool to uncover fundamental, system-level breakdowns.

This theoretical promise is driving a research program focused on identifying novel clinical biomarkers. The central hypothesis is that HOI metrics are sensitive to the subtle disintegration of functional ensembles before widespread pairwise connections are lost. Consequently, HOI analyses, including hypergraph models, simplicial topology, and multivariate cumulants, are being applied to differentiate clinical groups from healthy controls. For instance, in neurodegeneration, these methods are used to distinguish mild cognitive impairment and Alzheimer's disease from healthy aging [78,79].

The validity of this approach is demonstrated by its success in linking HOI dynamics directly to clinical outcomes. A key example comes from multiple sclerosis, where multivariate cumulants, which quantify genuine HOIs from time series, have not only classified patient groups but also explained their behavioral variability [78]. Similarly, in neurodevelopmental disorders, TDA has revealed altered functional brain topology in autism spectrum disorder (ASD) [28], and hypergraph-based methods are increasingly deployed to capture its atypical HOIs [39]. Together, these studies underscore the potential of HOIs to provide biomarkers for diagnosis, prognosis, and treatment monitoring across a spectrum of neurological and psychiatric conditions.

Thus, the investigation of HOIs provides a more sensitive and mechanistically informative lens for understanding brain disorders. Many conditions are conceptually framed as "disconnection syndromes", yet analyses based solely on pairwise connectivity often yield inconsistent results. HOI measures address this limitation by capturing a more fundamental pathology: the impaired capacity for synergistic, multi-region integration. A disorder might leave many pairwise connections intact while critically degrading the brain's ability to form coherent functional ensembles.

This principle manifests in distinct ways across different pathologies. In schizophrenia, the core deficit may be a breakdown in the global integration of information, which could be revealed topologically as a reduction in high-dimensional persistent cycles or altered spectra of higher-order Laplacians. Conversely, in the early stages of Alzheimer's disease, the initial pathology may subtly disrupt the organization of HOIs long before widespread pairwise disconnections become apparent [78]. Consequently, HOI-based biomarkers offer a pathway to increased diagnostic sensitivity and specificity, shifting the focus from which pairs of regions are disconnected to how the brain's capacity for integrated computation is compromised.

In summary, the transition from pairwise to HOI models represents a necessary evolution in the analysis of functional brain networks. By leveraging the mathematical frameworks discussed herein, researchers can now interrogate the complex, multi-region dynamics that underlie both healthy cognition and its dissolution in disease. While challenges in the robust inference of dynamic HOIs remain, this paradigm is essential for understanding the brain as a genuine complex system.

Section 5 delves into the specific prospective applications of this HOI framework, reviewing its most promising translational pathways.

3. Biophysical basics of fMRI and BOLD signals

Functional magnetic resonance imaging (fMRI) has revolutionized cognitive and clinical neuroscience by providing a noninvasive window into the functioning human brain. The predominant contrast mechanism underpinning this technology is the *Blood Oxygenation Level Dependent* (BOLD) signal, a complex physiological phenomenon that serves as an indirect proxy for neural activity. First introduced by Ogawa and colleagues (1990) [80], BOLD contrast exploits the magnetic susceptibility differences between oxygenated and deoxygenated hemoglobin to infer regional changes in brain metabolism and hemodynamics. The emergence of fMRI as a tool for studying brain activity was made possible by the work of Ogawa [81] and Kwong [82], who independently showed that the MR signal is sensitive to natural changes in blood oxygenation caused by neuronal activity.

Fig. 6 depicts the hemodynamic response function (HRF) within the human motor cortex, as measured by magnetic resonance (MR) techniques sensitive to cerebral blood flow and oxygenation during a 2-second finger-tapping task. Even transient stimuli evoke substantial perfusion changes, which are subsequently detected as subtle BOLD signal alterations. A principal advantage of this fMRI methodology over techniques such as X-ray or nuclear medicine is its noninvasive nature, eliminating the need for exogenous contrast agents or radioactive tracers. This capacity to assess neural function in vivo is founded on the physical principles of nuclear magnetic resonance (NMR) and the paramagnetic properties of deoxyhemoglobin, which intrinsically modulates the MR signal.

Indeed, the BOLD effect, which serves as the primary contrast mechanism for fMRI, is a hemodynamic correlate of neural activity originating from two interrelated yet distinct biophysical mechanisms. The first is a biophysical property of deoxyhemoglobin. The dissociation of oxygen from hemoglobin induces a transition in its magnetic properties, rendering deoxyhemoglobin paramagnetic. This paramagnetism increases the magnetic susceptibility of blood, creating a susceptibility gradient between vasculature and the surrounding parenchyma [84]. These gradients generate localized magnetic field inhomogeneities that accelerate the decay of the transverse magnetization ($T2^*$), thereby attenuating the net MR signal. Under baseline conditions, with a typical oxygen extraction fraction (OEF) of approximately 40%, the presence of deoxyhemoglobin in the cerebral microvasculature at a field strength of 3 T can reduce the MR signal by roughly 10% compared to a fully oxygenated state [85].

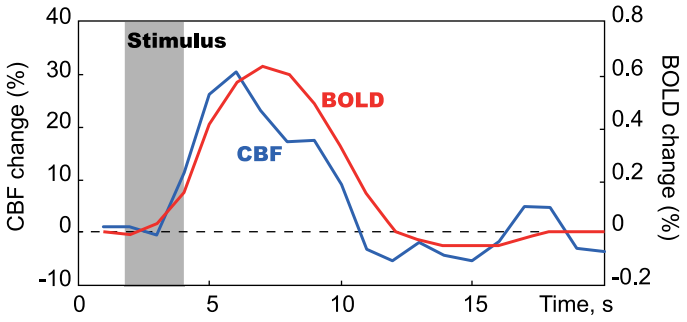

Fig. 6. Contrasting cerebral blood flow (CBF) and hemodynamic response function (HRF) as BOLD signal to a 2-second motor stimulus (gray box). A brief finger-tapping task elicits a strong, direct CBF response measured by arterial spin labeling—a non-invasive MRI technique used to quantify CBF (blue curve), which in turn drives an increase in venous blood oxygenation, giving rise to the weaker BOLD response measured with fMRI (red curve).
Source: Adapted from [83]; licensed under a Creative Commons Attribution International license.

Consequently, the MR signal exhibits an intrinsic sensitivity to the OEF. While this biophysical principle is noteworthy, it alone is insufficient for functional neuroimaging, as a constant OEF would yield no dynamic signal change. For instance, a matched, proportional increase in cerebral blood flow (CBF) and the cerebral metabolic rate of oxygen ($CMRO_2$) would preserve the OEF, leaving the MR signal unaltered. The utility of this mechanism for functional imaging emerges from a second, neurovascular physiological response: during neural activation, the increase in CBF is substantially greater than the concomitant rise in $CMRO_2$ [86]. This hemodynamic uncoupling precipitates a decrease in the OEF. This represents a seemingly paradoxical state wherein venous blood becomes more oxygenated despite an elevated metabolic demand, solely because the delivery of oxygenated hemoglobin via augmented perfusion outstrips its rate of consumption.

The confluence of these two phenomena – the magnetic susceptibility of deoxyhemoglobin and the neurovascular uncoupling of flow and metabolism – generates the BOLD effect. This is observed as a focal increase in the MR signal resulting from a task-induced reduction in deoxyhemoglobin concentration. Although the detection of this BOLD signal has established fMRI as a preeminent tool for non-invasive human brain mapping, a precise quantitative physiological interpretation of the BOLD response remains challenging. This complexity arises because the signal is an aggregate measure reflecting the dynamic interplay of multiple physiological variables, including CBF, $CMRO_2$, and cerebral blood volume (CBV), as will be discussed subsequently. We will start the discussion with basic questions of biophysical mechanisms of neurovascular coupling (see Section 3.1), then we will focus on the basics of fMRI and talk about the properties of BOLD signals (see Section 3.2), in particular about the possibilities of spatial and temporal resolution of brain activity using this technology. Finally, we will talk a little about the technical aspects of fMRI data preparation and quality assessment (see Section 3.3)

3.1. Neurovascular coupling

Despite its relatively small weight (about 2% of body weight), the human brain consumes around 20% of the oxygen and glucose supplied to the body at rest, and almost all of the adenosine triphosphate (ATP) produced in the brain is generated through the oxidative metabolism of glucose [87,88]. This high metabolic demand is combined with the extremely limited ability of neurons and glial cells to store energy, which necessitates the precise and dynamically regulated delivery of substrates to active regions of the brain. Therefore, one of the most important factors ensuring adequate blood supply is neurovascular coupling (NVC), i.e., the close temporal and regional relationship between neuron activation and cerebral blood flow regulation [89].

NVC is a fundamental physiological mechanism that precisely regulates CBF in response to neuronal activity, thereby sustaining optimal brain function. Maintaining this coupling has become possible thanks to the extremely high degree of vascularization of the brain and the presence of complex, excessively organized mechanisms of blood flow regulation, ranging from large vessels (internal carotid and vertebral arteries) to the microcirculatory bed, permeated by a network of capillaries surrounded by glial (mainly astrocytic) endings [90]. The anatomical substrate of NVC originates at the circle of Willis, which distributes blood via cerebral arteries coursing along the pial surface. These arteries give rise to meningeal branches and subsequently penetrate the brain parenchyma as deep penetrating arterioles. At this initial point of cortical penetration, perivascular spaces are established between the vessel wall and the pia mater. As these arterioles descend further, their walls fuse with the pial layer, the perivascular spaces are obliterated, and the vessels arborize into extensive capillary networks. This intricate architecture ensures the proximity of all neurons to a vascular supply, facilitating efficient nutrient delivery and waste clearance, which are critical for cerebral homeostasis [91,92]. An important feature of human cerebral hemodynamics is that large extracranial and superficial vessels are richly innervated by sympathetic and parasympathetic nerves, while parenchymal arterioles are largely controlled by local (intrinsic) mechanisms directly related to metabolic and functional activity (see Fig. 7).

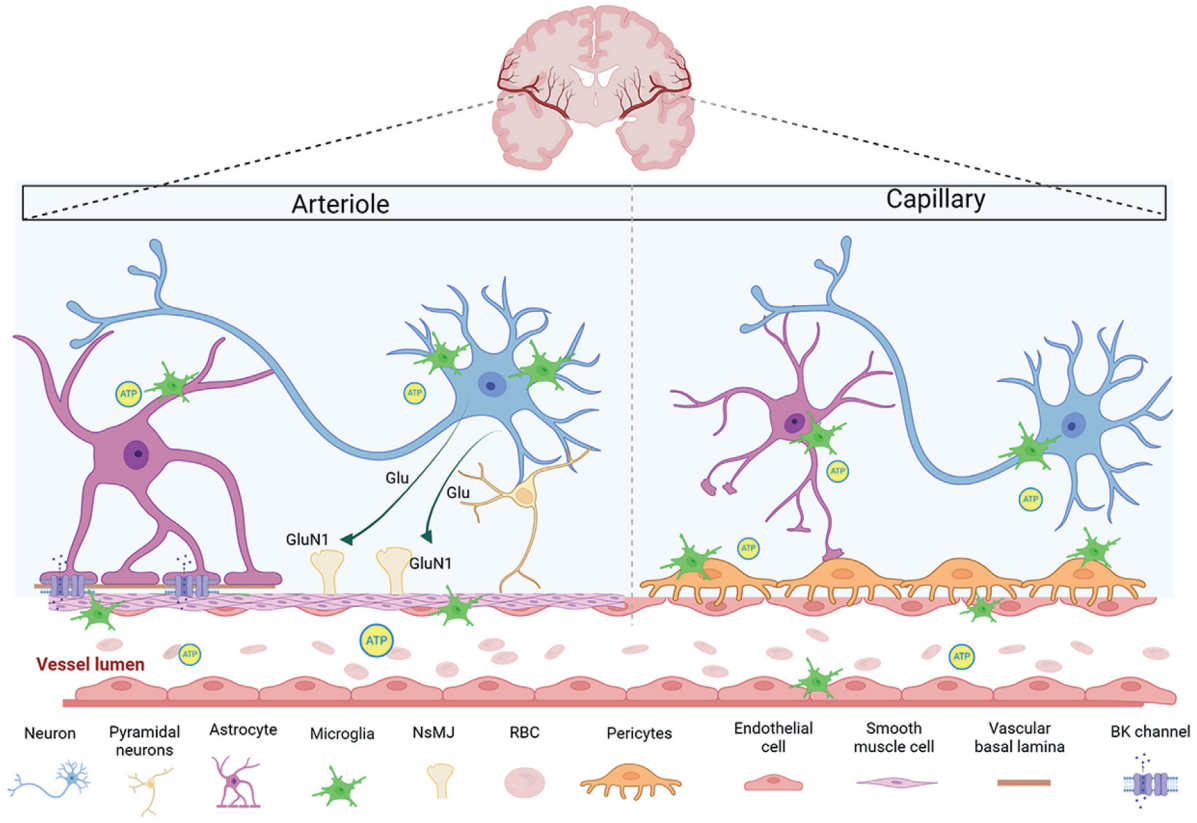

Fig. 7. Neurovascular coupling (NVC) is a complex process involving multiple cell types, including neurons, astrocytes, microglia, endothelial cells (ECs), smooth muscle cells (SMCs), and pericytes. Astrocytes extend perivascular endfeet that ensheath capillaries, facilitating intercellular communication and helping to maintain the blood–brain barrier (BBB) phenotype of ECs; this communication is partly mediated by BK channels within these endfoot processes. Microglia are recruited via ATP/ADP chemotaxis and engage in dynamic interactions with neurons, astrocytes, and the vasculature. At the level of precapillary arterioles, SMCs mediate vasodilation by responding to neuronal glutamate through surface GluN1 receptors. Finally, pericytes, which are embedded within the capillary basement membrane and form discontinuous coverage along microvessels, are critical for maintaining BBB integrity.
Source: Reproduced from [93]; licensed under a Creative Commons Attribution 4.0 International license.

At the functional level, the neurovascular unit (NVU) serves as the principal effector of NVC. The NVU is an multicellular ensemble – comprising neurons, astrocytes, vascular smooth muscle cells (VSMCs), and pericytes – that orchestrates the dynamic control of CBF (see Fig. 10). In response to heightened neural activity, neurons signal directly or via astrocytic intermediaries to induce vasodilation in adjacent VSMCs and pericytes. This localized hemodynamic adjustment augments perfusion to meet the elevated metabolic requirements of active neural tissue [94]. These vascular responses are both rapid, occurring within seconds of neuronal activation, and spatially precise, with observed changes in CBF extending several millimeters from the originating site of neural activity [91,95].

NVC refers to the integrated cellular processes that translate local neuronal activity into precise adjustments in CBF. This mechanism ensures the timely delivery of energy substrates and the clearance of metabolic waste products that are essential for normal brain function. The classical model posited that these vascular responses were driven primarily by local metabolic demand as shown in Fig. 8. However, contemporary research, as detailed by Hillman et al. [90], has elucidated a more complex framework involving a network of cellular and molecular mediators.

Regulation of CBF is achieved through complementary *feedback* and *feedforward* mechanisms. The feedback mechanism is initiated by metabolic activity, leading to the release of vasoactive metabolites such as lactate and nitric oxide (NO), which subsequently induce vasodilation and an increase in CBF. In contrast, feedforward mechanisms are primarily glutamate-mediated. In this pathway, neuronal synaptic activity triggers the release of vasoactive substances, including prostanoids and ions such as potassium (K^+). A key distinction is that the feedforward mechanism is directly driven by synaptic activity itself, rather than being a secondary consequence of the tissue metabolic state [96].

Concurrently, the hemodynamic shear stress mechanism provides a critical safeguard against vascular injury during CBF increases. Elevated flow enhances the frictional force exerted on the vascular endothelium, stimulating the release of vasoactive mediators that promote further vasodilation. Furthermore, autonomic mechanisms contribute to NVC regulation by modulating sympathetic and parasympathetic tone to influence vascular smooth muscle contraction, with

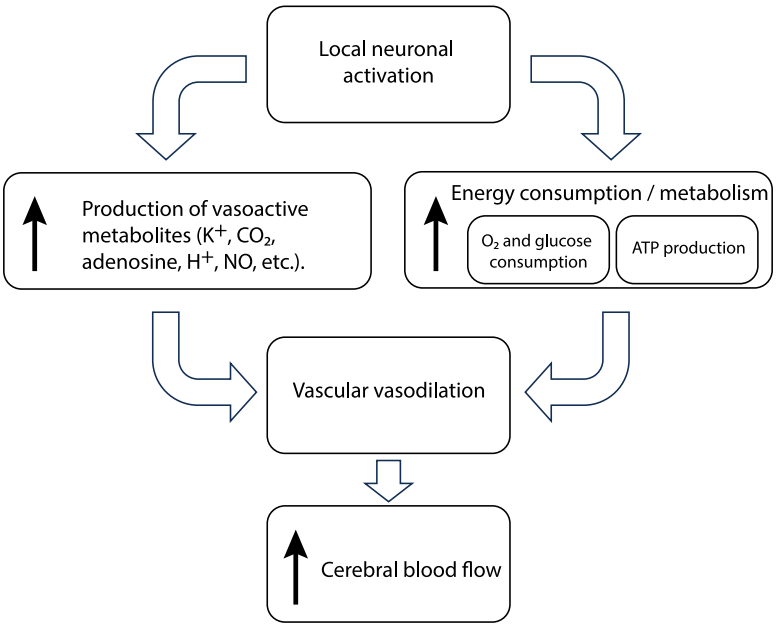

Fig. 8. The classical metabolic model of neurovascular coupling (NVC). This framework posits that cerebrovascular responses are governed by the local metabolic demands of neural tissue. The cascade begins when local neuronal activation increases energy consumption, driven by processes such as ionic gradient restoration and neurotransmitter cycling, requiring rapid ATP generation. This ATP is supplied primarily through oxidative glucose metabolism, which consumes both glucose and oxygen (notably, approximately 90% of cerebral glucose is metabolized aerobically). To sustain this elevated metabolic rate, cerebral blood flow (CBF) is tightly coupled to regional neural activity. The diagram illustrates the temporal sequence: a rise in neuronal firing leads to increased glucose and oxygen consumption, which is rapidly followed by a pronounced increase in CBF. A critical feature of this hemodynamic response is its stoichiometry: while glucose utilization and CBF increase in near parallel, the rise in cerebral metabolic rate of oxygen ($CMRO_2$) is significantly smaller. This mismatch results in a net increase in tissue oxygenation within the activated region. The precise interplay between neuronal metabolism and localized blood flow underpins the phenomenon of functional hyperemia, which is fundamental to healthy brain function.

parasympathetic activation notably inducing cerebral vasodilation [89]. Let us consider these principal mechanisms, in a little more detail.

Functionally, the neurovascular unit (NVU) operates as the core component of NVC. Comprising neurons, astrocytes, VSMCs, and pericytes, the NVU orchestrates the regulation of CBF (Fig. 1). Neurons, either directly or through astrocytes, signal VSMCs and pericytes to dilate nearby blood vessels. This response increases blood flow precisely where it is most needed to support the metabolic demands of active brain regions [4]. Such rapid and precise vascular responses to neural activity have been documented to occur within seconds and can affect areas several millimeters from the site of neuronal activation [2,9].

3.1.1. Astrocytes

Astrocytes are central regulators at the neurovascular interface, where their end-feet ensheath cerebral arterioles, capillaries, and venules. Synaptic glutamate release during neuronal activity activates metabotropic glutamate receptors (mGluRs) on astrocytes, triggering a rise in intracellular calcium. This calcium signal stimulates the production of arachidonic acid (AA) via phospholipase A2 (PLA2). AA is subsequently metabolized into vasoactive derivatives: by cyclooxygenases (COX1/3) into prostaglandins (PGs) and by cytochrome P450 epoxygenase into epoxyeicosatrienoic acids (EETs). These metabolites act as potent vasodilators, relaxing vascular smooth muscle cells (SMCs) by elevating cyclic AMP (cAMP), thereby increasing local blood flow.

3.1.2. Endothelial cells

Endothelial cells lining cerebral vessels constitute a potent signaling platform. These cells can be activated directly by neurotransmitters such as acetylcholine (ACh), bradykinin (BK), adenosine, ATP, adenosine diphosphate (ADP), and uridine triphosphate (UTP), triggering phospholipase C (PLC) and the release of calcium from intracellular stores. Elevated endothelial calcium activates endothelial nitric oxide synthase (eNOS), producing NO, which diffuses to SMCs and stimulates the conversion of GTP to cyclic GMP (cGMP), causing relaxation. Additionally, the opening of calcium-dependent potassium channels in endothelial cells induces cell hyperpolarization. This hyperpolarization, facilitated by gap junctions, can be rapidly propagated to neighboring endothelial cells, allowing efficient conduction of vasodilation over significant vascular distances.

Endothelial cells can also produce other vasodilators such as prostacyclin (PGI2), working in tandem with NO to modulate vascular tone through distinct second messenger pathways (cAMP, cGMP). This dual mechanism ensures both rapid-onset and sustained blood flow adaptations to neuronal activity. The concept of endothelium-derived hyperpolarizing factor (EDHF) captures various molecular entities, including K^+ efflux via SKCa and IKCa channels, that transmit hyperpolarization to SMCs and drive vasodilation.

3.1.3. Pericytes

Pericytes are contractile cells surrounding capillaries and small vessels. They respond to an array of vasoactive signals, including NO, PGI2, vasoactive intestinal peptide (VIP), and low pH, by modulating capillary diameter. Pericytes' contractile properties enable both dilation and constriction in response to neural and endothelial signals, facilitating precise microvascular control and fine-tuning nutrient delivery at the capillary level. Although their involvement in stimulus-evoked hyperemia is still under investigation, pericytes constitute a vital link between neural signals and capillary regulation.

3.1.4. Neuronal networks and interneurons

Neurons, particularly GABAergic interneurons, actively regulate local blood flow. Certain interneurons can release vasodilators such as NO and VIP or vasoconstrictors like neuropeptide Y (NPY) and somatostatin (SOM), refining hemodynamic responses. Cholinergic afferents, especially those arising from the basal forebrain, modulate regional perfusion via ACh-dependent pathways, interconnecting neural circuits with vascular responses. Subcortical networks (e.g., locus coeruleus) may exert global constraints on hyperemia via noradrenergic signaling.

3.1.5. Propagation and integration of vasodilation

A major recent advancement is the recognition of propagated vasodilation—the process by which signals initiated at capillaries are transmitted along the vascular tree to remote pial arteries, ensuring a coordinated blood flow response over spatially distributed cortical domains.

- *Fast endothelium-derived hyperpolarizing factor-mediated propagation:* A pronounced endothelial calcium increase ($>$ 340 nM based on the studies in isolated rat middle cerebral arteries [97]) triggers endothelial hyperpolarization and rapid, long-distance vasodilation via gap junctions. This mechanism allows electrical signals to travel retrograde from microvascular segments to distant arteries with minimal attenuation, enabling near-instantaneous adjustment of vascular conductance and supporting rapid BOLD-fMRI responses to short neuronal bursts [98].
- *Slow NO/prostanoid-dependent propagation:* A more modest elevation in endothelial calcium ($\geq$ 220 nM based on the studies in isolated rat middle cerebral arteries [97]) prompts a slower propagating wave of NO and prostanoid release, supporting sustained parenchymal hyperemia and meeting ongoing metabolic needs [99]. The synergy of these fast and slow pathways shapes the spatiotemporal profile of the hemodynamic response, underlying the nonlinearities observed in the BOLD signal during long or repetitive stimuli [90].

The vasculature itself thus emerges not merely as a passive responder but as an active integrator and conduit of neurovascular signals, with endothelial cells serving as key conductors of both rapid and sustained blood flow changes.

3.1.6. Integration and redundancy

Importantly, no single NVC pathway operates in isolation; instead, the neurovascular unit leverages multiple overlapping mechanisms, conferring redundancy and resilience to the regulation of CBF. Pharmacological blockade studies have revealed the persistence of functional hyperemia even with inhibition of key pathways, underlining the importance of integrated action among astrocytes, pericytes, neurons, interneurons, and vascular endothelium [100].

3.2. Fundamentals of fMRI: BOLD signal and temporal resolution

3.2.1. Neuroimaging techniques for NVC visualization

The study of NVC in humans presents inherent methodological challenges compared to animal and in vitro models. These limitations primarily stem from the necessity for non-invasive access and the potential confounding effects of anesthesia or underlying pathology. Consequently, a range of neuroimaging techniques has been developed to indirectly assess NVC, each with distinct advantages and limitations concerning spatial and temporal resolution, invasiveness, and practicality.

The primary modalities for assessing NVC include Transcranial Doppler ultrasonography (TCD), fNIRS, and fMRI (see Table 2).

- **TCD** is a portable, non-invasive technique that uses ultrasound to measure cerebral blood flow velocity (CBFv) in large cerebral arteries, most commonly the middle cerebral artery (MCA) [100]. CBFv acts as a proxy for CBF, assuming vessel diameter, blood pressure, and arterial CO_2 partial pressure remain constant during the measurement [101]. TCD offers excellent temporal resolution, detecting robust, region-specific hyperemic responses (increases in flow velocity) during well-defined stimulation paradigms (e.g., visual, motor, or cognitive tasks). A primary limitation is that approximately 10%–15% of individuals lack adequate acoustic bone windows for insonation, though this prevalence varies across populations.

Table 2
Comparison of primary neuroimaging modalities for assessing NVC in humans.

Method	Measured parameter	Temporal resolution	Spatial resolution	Key advantages	Key limitations
TCD	Blood flow velocity in large arteries	High (ms)	Low (vessel-specific)	Portable, excellent temporal resolution, well-tolerated	Limited to large vessels; $\sim 10 \div 15\%$ lack acoustic window; assumes constant vessel diameter
fNIRS	[O_2Hb], [HHb] in microvasculature	Low (s)	Low (superficial cortex)	Portable, measures oxygenation, well-tolerated	Superficial penetration only; limited spatial resolution
BOLD-fMRI	Magnetic susceptibility from dHb	Low (s)	High (mm)	Excellent spatial resolution; whole-brain coverage	Indirect measure; poor temporal resolution; expensive; not well-tolerated by all
PET/SPECT	Radioligand uptake (flow/metabolism)	Very low (min)	Moderate-High	Quantifies metabolism and absolute CBF	Ionizing radiation; very expensive; poor temporal resolution; limited availability

The notations are introduced here [O_2Hb] is the oxyhaemoglobin concentration; [HHb] is the deoxyhaemoglobin concentration; dHb is the deoxyhaemoglobin.

- **fNIRS** quantifies changes in oxygenated and deoxygenated hemoglobin concentrations in the cortical microvasculature based on optical absorption of infrared light (780–2500 nm). Like TCD, it is portable, non-invasive, but it provides low temporal resolution. Its key advantage is the direct measurement of hemodynamic changes related to blood oxygenation, offering additional insight into metabolic aspects of NVC. However, its utility is restricted to measuring superficial cortical regions and it possesses limited spatial resolution [102].
- **BOLD-fMRI Imaging** provides spatial maps of neural activation based on magnetic susceptibility changes from deoxyhemoglobin, providing superior spatial resolution compared to TCD and fNIRS [103,104]. It has become the primary method in both cognitive neuroscience research and clinical practice due to its ability to visualize deep brain structures noninvasively and with millimeter-level precision. This enables detailed studies of sensory processing, motor control, emotional regulation, memory, attention, decision-making, and network connectivity across the whole brain, including cortical and subcortical regions such as the hippocampus and amygdala.
  Despite these advantages, BOLD-fMRI has relatively poorer temporal resolution than some other methods because it measures hemodynamic changes that lag behind neural activity by several seconds. The BOLD signal is also an indirect and complex hemodynamic measure, rather than a direct measure of neuronal activity or absolute CBF. Moreover, fMRI requires expensive, immobile equipment, and the constrained scanning environment can be uncomfortable or unsuitable for certain populations like those with claustrophobia or movement disorders [105]. Nonetheless, due to ongoing technological improvements, including enhanced spatial sensitivity and integration with machine learning [106], BOLD-fMRI remains the gold standard for noninvasive imaging of brain function in both cognitive and clinical neuroscience settings. Consequently, the following discussion in this Review will be focused exclusively on the BOLD-fMRI technique.

Other time-dependent neuroimaging techniques, such as positron emission tomography (PET) and single-photon emission computed tomography (SPECT), use radiolabelled tracers to measure regional metabolic activity and blood flow. While valuable, these methods are associated with risks of false positives/negatives, high cost, technical complexity, and exposure to ionizing radiation, limiting their routine use for NVC assessment.

3.2.2. The MRI scanner

A modern MRI scanners consist primarily of a superconducting electromagnet generating a powerful static magnetic field, typically ranging from 1.5 to 7.0 T for human brain research, orders of magnitude greater than the Earth's magnetic field. Let us recall that the Earth's magnetic field is only 50 μT. This strong static field B_0, which is always active, necessitates strict safety precautions to prevent ferromagnetic objects from becoming hazardous projectiles. Importantly, no long-term biological effects have been associated with MRI exposure, supporting its wide use for human studies.

Additional key hardware includes radio frequency (RF) coils, positioned close to the target (e.g., the head), which transmit RF signal with B_i amplitude and receive energy at the resonance frequency of the imaged tissue, and gradient coils, which introduce controlled spatial variations G_x, G_y and G_z in the magnetic field essential for spatial encoding. These components collectively enable the acquisition of various image types tailored to anatomical structure, tissue contrast, or physiological properties such as water diffusion (diffusion-weighted imaging (DWI) used to measure white-matter tracts) or flow of cerebrospinal fluid. The corresponding schematic diagram illustrating a typical MRI scanner is shown in Fig. 9(a). A more detailed description of the physical principles and technical details can be found in [107].

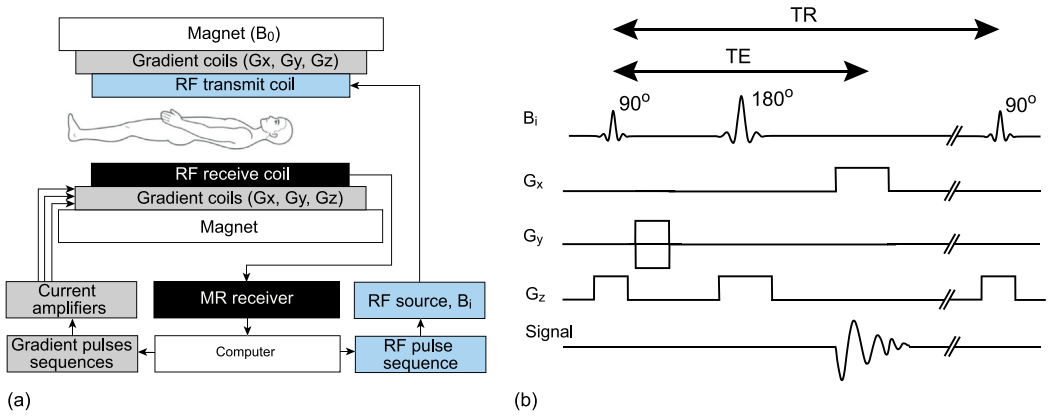

Fig. 9. Principles of magnetic resonance imaging (MRI). (a) Block diagram of a clinical MRI system, showing the core components: the main magnet generating the static field ($\mathbf{B}_0$), gradient coils (G_x, G_y, G_z) for spatial encoding, and radiofrequency (RF) coils for transmission (B_1) and signal reception. (b) Schematic of a generic MRI pulse sequence, illustrating the synchronized application of an RF excitation pulse, slice-selection, phase-encoding, and frequency-encoding gradients, followed by the received signal (echo). The imaging process begins by placing a subject within the $\mathbf{B}_0$ field, establishing a net tissue magnetization. A resonant RF pulse, emitted by the transmit coil, rotates this magnetization. The resulting precessing magnetization, detected by the receive coil as it returns to equilibrium, constitutes the MR signal. Spatial localization is achieved by superimposing magnetic field gradients (G_x, G_y, G_z) to encode position into the signal's frequency and phase. Crucially, image contrast is not inherent but is *generated* by the pulse sequence timing, primarily through the repetition time (TR) and echo time (TE). By varying TR and TE, images can be weighted to reflect different tissue properties: proton density, T_1, T_2, T_2^*, or diffusion. The acquired signal is complex; its magnitude provides anatomical structure and enables quantitative parameter mapping (e.g., relaxation times, diffusion coefficients), while its phase encodes information on physiological processes such as blood flow, temperature, and tissue stiffness.

Particularly significant is fMRI, which exploits rapid imaging sequences to capture dynamic changes associated with neuronal activity. Structural scans are always included with fMRI protocols, as precise anatomical localization is critical for interpreting functional data. Overall, a single MRI scanner supports a spectrum of modalities – structural, functional (fMRI), and connectivity (DWI) imaging – within the same session, making it an indispensable instrument for noninvasive human brain research.

3.2.3. Physical basis of the MRI

MRI fundamentally relies on the magnetic properties of atomic nuclei, with hydrogen nuclei (^{1}H protons) being the primary target due to their abundance and strong magnetic moment. Each proton behaves like a tiny spinning charged sphere, generating a magnetic moment. Although individual proton magnetization cannot be detected, MRI measures the net magnetization **M** of a large ensemble of nuclei within a volume. This magnetization vector has two components: the longitudinal component M_z aligned with the external magnetic field $\mathbf{B_0}$, and the transverse component M_{xy} perpendicular to it.

In the absence of $\mathbf{B_0}$, protons are randomly oriented with no net magnetization. Exposure to a strong magnetic field aligns them, producing a net longitudinal magnetization. Protons precess about the field at the Larmor frequency: $\omega_0 = \gamma B_0$, where γ is the gyromagnetic ratio.

When an RF pulse at the resonance frequency is applied, protons absorb energy, tipping the net magnetization vector into the transverse plane and creating measurable transverse magnetization. After the pulse, the system relaxes back to equilibrium via two key processes: longitudinal (T_1) relaxation and transverse (T_2) relaxation. These are described by exponential functions:

- Longitudinal relaxation (recovery of M_z):

$$M_z(t) = M_0\left(1 - e^{-t/T_1}\right). \tag{6}$$

- Transverse relaxation (decay of M_{xy}):

$$M_{xy}(t) = M_0 e^{-t/T_2}. \tag{7}$$

Here, M_0 is the equilibrium magnetization, T_1 is the longitudinal relaxation time, and T_2 is the transverse relaxation time. One more parameter, T_2^*, reflects transverse relaxation influenced by magnetic field inhomogeneities and underlies fMRI contrast:

$$\frac{1}{T_2^*} = \frac{1}{T_2} + \frac{1}{T_2'}, \tag{8}$$

where T_2' captures inhomogeneity effects.

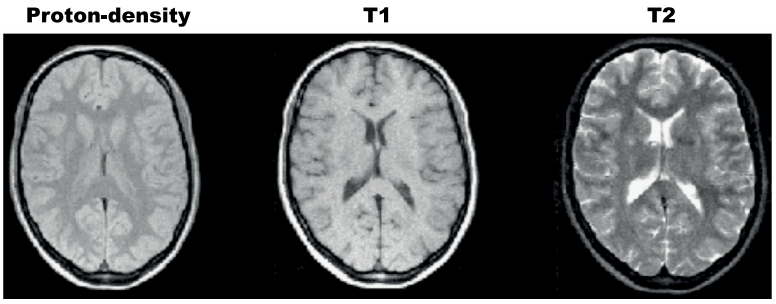

Fig. 10. Examples of proton density, T_1-weighted, and T_2-weighted 2D images. Based on data from [108].

The versatility of MRI stems from controlling repetition time (TR, time between excitations) and echo time (TE, time after excitation to data acquisition), which together govern image contrast as shown in Fig. 9(b). Taking into account Eqs. (6) and (7), the MRI signal intensity S can be approximated as:

$$S \propto M_0 \left(1 - e^{-TR/T_1}\right) e^{-TE/T_2}. \tag{9}$$

The contrast in MRI is governed by the strategic selection of TR and TE parameters. To generate a *proton-density weighted image*, where signal intensity is approximately proportional to the native spin density (M_0) of the tissue, a long TR and a short TE are employed. This minimizes weighting from both T_1 and T_2 relaxation processes according Eq. (9).

Conversely, T_1-*weighted images*, which are essential for delineating anatomical structures, are obtained by employing a short TE together with an intermediate TR. This combination increases the contrast that arises from differences in the longitudinal relaxation times (T_1) across tissues.

For T_2-*weighted imaging*, a long TR and an intermediate TE are selected to maximize contrast based on transverse relaxation time T_2 variations. As both T_1 and T_2 are intrinsic properties that differ across tissue types, T_1- and T_2-weighted images provide high-resolution visualization of anatomical boundaries, such as those between gray matter, white matter, and CSF.

fMRI relies on T_2^*-*weighted imaging*, which is sensitive to magnetic field inhomogeneities induced by changes in blood flow and oxygenation. These images are acquired with parameters analogous to T_2-weighting; the critical distinction lies in the specific design of the pulse sequence and its manipulation of magnetic gradients—a technical detail beyond the scope of this discussion. Consequently, each weighting scheme (proton-density, T_1, T_2, T_2^*) highlights distinct tissue properties, as shown in Fig. 10 and their application is determined by the specific objectives of the study.

Magnetic resonance images are represented as a three-dimensional (3D) matrix of numbers corresponding to spatial locations within the brain or other imaged tissue. This 3D representation is typically constructed from a series of two-dimensional (2D) slices acquired sequentially or in an interleaved manner. Each slice corresponds to a thin section of the brain, and together these slices span the entire volume of interest.

The process of forming such a 3D image involves exciting nuclei within each slice and measuring their signal contributions. However, the signal measured directly corresponds only to the net magnetization within that slice and does not inherently contain spatial localization information within the slice. To resolve spatial details across the plane of each slice and in the direction perpendicular to it, MRI employs gradient coils with the spatially varying magnetic field gradients G_x, G_y and G_z as shown in Fig. 9(b) that manipulate the magnetic field to encode spatial information.

This spatial encoding enables each MRI signal measurement to be represented as a sample in the frequency domain, known as k-space. k-space data are acquired at discrete spatial frequency coordinates, $(k_x(t_j), k_y(t_j))$, at time points $t_j = j\Delta t$, where Δt is determined by the sampling bandwidth of the MRI scanner. Mathematically, the measured complex-valued signal at each time point can be described by the fast Fourier transform (FFT) of the spin density $M(x, y)$ modulated by a phase factor dependent on k-space coordinates:

$$S(t_j) \approx \iint M(x, y) e^{-2\pi\sqrt{-1}(k_x(t_j)x + k_y(t_j)y)}\, dx\, dy. \tag{10}$$

This is the quantity we aim to measure in each voxel of the brain image.

To fully reconstruct a 3D MR image at a desired resolution, a large number of samples must be collected from k-space, each at unique spatial frequency coordinates. The density and coverage of k-space sampling determine the final spatial resolution and quality of the reconstructed image. For example, to fully reconstruct a 64×64 image, a total of 4096 separate measurements are required. FFT methods are commonly employed to convert the sampled k-space data back into image space, yielding the spatial distribution of MR signal intensities that form the image slices.

To obtain a spatial image, it is necessary to perform the inverse Fourier transform (IFT) on the entire k-space data set:

$$M(x, y) = \iint S(k_x, k_y) e^{2\pi\sqrt{-1}(k_x x + k_y y)}\, dk_x\, dk_y. \tag{11}$$

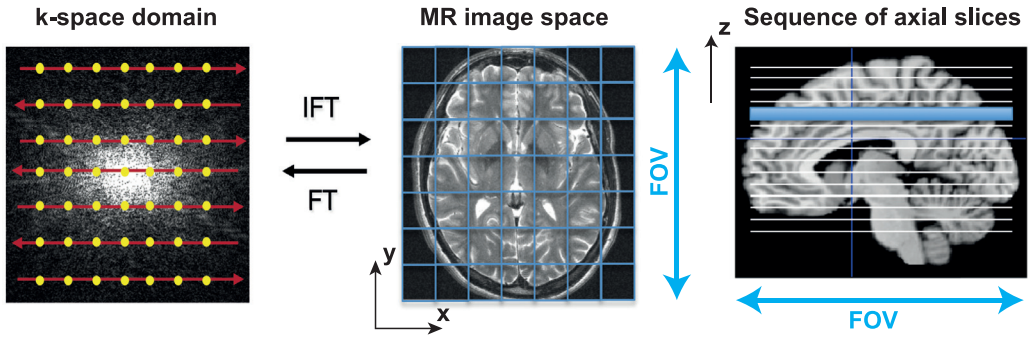

Fig. 11. Original *k*-space data, typically acquired on a uniform Cartesian grid, is reconstructed into the image domain via an inverse Fourier transform (IFT). This transformation is a prerequisite for subsequent quantitative analysis and interpretation. A brain volume is acquired as a set of axial z slices spanning a specific area referred to as field-of-view (FOV). The spatial resolution is governed by the matrix size, which is the number of voxels within the imaging xy-plane. The final voxel volume is determined by the matrix size, the FOV, and the slice thickness.

Finally, stacking these slices reconstructs the full 3D volume of the brain. This approach enables the flexible acquisition of images of the brain's structure and function with controlled resolution and contrast.

Common *k*-space sampling trajectories include uniform Cartesian grids, which facilitate rapid and easy reconstruction using FFT, as shown in Fig. 11, as well as other non-Cartesian trajectories like Archimedean spirals.

Standard acquisition of 3D neuroimaging volumes entails obtaining sequential axial slices (over the xy-plane with a fixed z value). Each slice, characterized by a defined thickness, is sampled across a specific spatial region known as the field-of-view (FOV). The in-plane spatial resolution is governed by the matrix size, which specifies the number of voxels along the x and y dimensions; a larger matrix yields superior resolution. The voxel dimensions are consequently determined by the interplay of the FOV, slice thickness, and matrix size (see Fig. 11). For instance, an illustrative protocol employing thirty 5 mm-slices with a 192 mm FOV and a 64 × 64 matrix (common for full brain coverage) results in individual voxel dimensions of 3 × 3 × 5 mm.

The Kotel'nikov–Nyquist–Shannon theorem dictates that the sampling interval must be less than twice the reciprocal of the signal's maximum frequency (the Nyquist criterion). This constraint establishes the following fundamental relationships between MR imaging parameters and resolution for rectilinear sampling in a spin echo pulse sequence:

$$\Delta x = \frac{\mathrm{FOV}x}{N_x} = \frac{2\pi}{N_x \gamma G_x T_W}, \quad \Delta y = \frac{\mathrm{FOV}y}{N_y} = \frac{2\pi}{N_y \gamma G_y T_\varphi}, \tag{12}$$

where N_x and N_y are the number of partitions (typically, 128 or 256), G_x and G_y are the magnitude of the x (read) and y (phase) encoding gradients (typically, 1–200 G/cm), and T_W and T_φ are the duration of the acquisition window (typically, 1–10 ms) and the phase encoding gradient (typically, $\leq$ 5 ms), respectively.

The position z and thickness of a slice are determined by the modulation of the transmitted RF pulses (B_1 in Fig. 9). For standard sinc modulation, the slice thickness can be described by the following expression:

$$\Delta z = \frac{4\pi}{\gamma G_z \tau}, \tag{13}$$

where τ is the duration of the 90° B_1 pulse (typically, 5 ms).

3.2.4. From MRI to BOLD-fMRI

The data acquisition and reconstruction methodologies outlined previously facilitate the generation of static 3D neuroanatomical images. Importantly, neuronal activity induces localized changes in cerebral hemodynamics, which in turn modulate the intensity of the MR signal as discussed above. Consequently, a temporally resolved sequence of appropriately acquired T_2^*-weighted images enables the investigation of dynamic neural processes. This fMRI approach is operationalized through the rapid sequential acquisition of T_2^*-weighted volumetric scans, typically at intervals of several seconds. The temporal interval between successive 3D volume acquisitions is designated as the repetition time (TR). While the TR in most fMRI paradigms is approximately 2 s, this parameter can be adjusted, ranging from 0.1 to 6 s, to address specific experimental requirements and hypotheses. Fig. 12 shows an illustrative example of BOLD signal formation based on a series of 3D T_2^*-weighted functional images (volumes). Each volume consists of a multidimensional matrix of voxels (volume pixels). The temporal evolution of intensity values for each voxel constitutes the BOLD signals of an individual voxel, and the entire set of voxels forms a set of signals from all areas of the brain. Often, signals from individual voxels are summed or averaged over certain anatomical areas of the brain, characterizing the integral dynamics.

During the scanning session, participants may be instructed to engage in a prescribed task, be exposed to an induced psychological or behavioral manipulation, or maintain a state of rest. In recent years, resting-state fMRI (rs-fMRI) protocols,

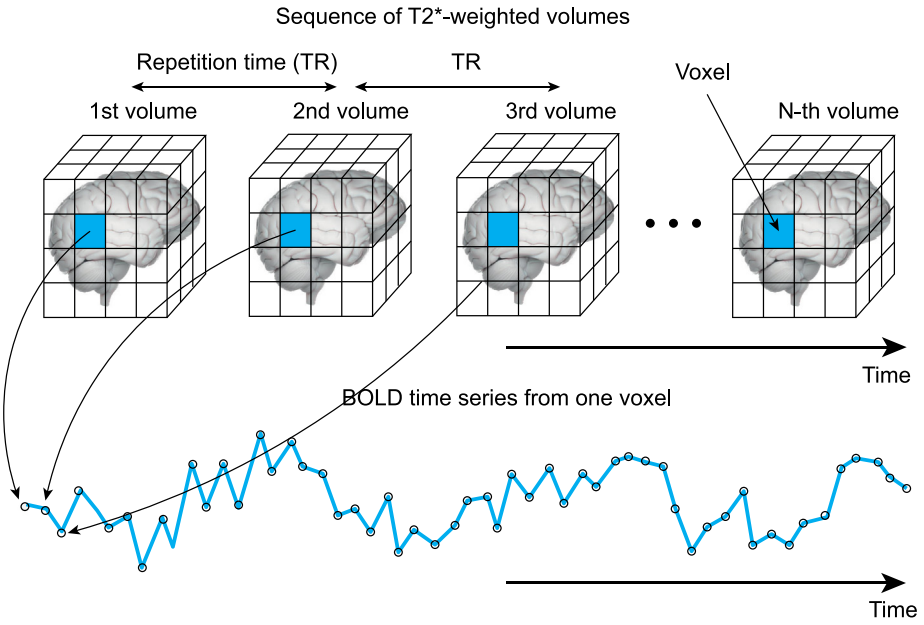

Fig. 12. fMRI data comprises a time series of volumetric 3D T_2^*-weighted images (volumes) of the living human brain. Each volume is composed of a high-dimensional matrix of voxels (volumetric pixels), typically numbering in the hundreds of thousands. The temporal evolution of intensity values for a single voxel constitutes the BOLD signal, which serves as a proxy for neural activity.

wherein participants remain awake but do not perform an explicit task, have become increasingly prevalent. These studies are designed to analyze spontaneous, low-frequency fluctuations in the BOLD signal. The temporal coherence of these fluctuations across spatially discrete brain regions is interpreted as evidence of intrinsic functional connectivity within brain large-scale neural networks. The implications and findings of resting-state research will be discussed in more detail later in this review.

The predominant methodological approach in fMRI utilizes the BOLD contrast mechanism. This technique derives its signal from a time series of T_2^*-weighted images (see Fig. 12), capitalizing on the paramagnetic properties of deoxygenated hemoglobin which shorten the T_2^* relaxation time. Although alternative techniques exist, such as various arterial spin labeling methods sensitive to cerebral blood flow or volume (see Fig. 6), BOLD fMRI remains the most extensively adopted paradigm. Its ascendancy followed the pivotal discovery that oxygenated hemoglobin exhibits a longer T_2^* relaxation rate than its deoxygenated counterpart, superseding earlier methods that relied on exogenous paramagnetic contrast agents. Given its current ubiquity, the present review will focus exclusively on the analysis of the BOLD signal.

As previously noted, BOLD-fMRI permits the investigation of hemodynamic responses subsequent to neural firing. Elevated neuronal activity induces an increase in metabolic demand, triggering a neurovascular coupling (NVC) process that culminates in an augmented inflow of oxygenated blood to active cerebral regions. This process can be formalized as follows:

$$\text{Neural Activity} \xrightarrow{\text{signaling}} \text{Vasodilation} \xrightarrow{\text{increased CBF}} \uparrow [O_2\text{Hb}], \downarrow [\text{HHb}] \xrightarrow{\text{MR physics}} \uparrow \text{BOLD signal},$$

where $[O_2\text{Hb}]$ and [HHb] are the oxyhaemoglobin and deoxyhaemoglobin concentrations, respectively.

The transient change in the MR signal consequent to a neural event is termed the hemodynamic response function (HRF); a canonical example is illustrated in Fig. 6. Crucially, the oversupply of oxygenated blood results in a net decrease in local deoxyhemoglobin concentration, thereby producing a positive BOLD signal. This signal rise initiates approximately 1–2 s post-stimulus, peaks 5–8 s after peak neural activity, and is typically followed by a post-stimulus undershoot—a sustained signal dip below baseline lasting roughly 10 s. This undershoot is attributed to a slower recovery of cerebral blood volume relative to cerebral blood flow, temporarily increasing the concentration of deoxyhemoglobin.

It is imperative to recognize that the BOLD signal constitutes an indirect proxy for the underlying neural activation of primary interest. Consequently, a critical question pertains to the fidelity with which the BOLD signal reflects genuine increases in neuronal spiking. This relationship is complex and has been a subject of extensive research [109]. Empirical evidence indicates that the BOLD signal correlates strongly with the local field potential (LFP), which is thought to predominantly reflect integrated post-synaptic activity [110]. However, neurovascular decoupling can occur under certain conditions, meaning the BOLD signal may capture only a subset of the neural activity alterations induced by a task or state, potentially overlooking changes that do not significantly alter net metabolic demand. Early models of the BOLD

signal assumed linearity, where the HRF could be convolved with neural activity to predict responses [109,111]. However, numerous studies have shown that this assumption does not always hold. Nonlinearities emerge in both amplitude and temporal characteristics of the response, particularly when stimuli differ in duration, frequency, or intensity [112–114]. For example, very brief and relatively long visual stimuli can evoke almost identical BOLD responses, contrary to linear predictions of proportional scaling [115].

These deviations suggest that vascular dynamics impose nonlinear constraints, including plateauing responses for longer stimulus durations and saturation effects [116]. Simultaneous recordings of neural activity and BOLD signals further indicate that the correspondence depends on the neural measure used: BOLD changes correlate more strongly with local field potentials than with spiking activity [110,117].

The *temporal resolution* of an fMRI study is principally governed by the repetition time (TR), which commonly ranges from 0.5 to 4 s. This sampling rate presents a fundamental disparity with the millisecond-scale temporal dynamics of neuronal firing. Nonetheless, the statistical analysis of fMRI data is predicated on modeling the slow hemodynamic response rather than the neural activity itself. Therefore, the critical limiting factor for temporal resolution is generally not the data acquisition speed but the kinetics of the evoked hemodynamic response. As inference is based on oxygenation changes that evolve over several seconds (peaking at 5–8 s), a TR on the order of 2 s is conventionally deemed sufficient.

fMRI offers comparatively high *spatial resolution* relative to other functional imaging modalities such as PET, MEG, and EEG. While sub-millimeter resolution is achievable in high-field animal studies, typical human studies operate at a voxel size of approximately 27–36 mm^3. Consequently, small-scale features, such as cortical columns and sub-nuclei, remain difficult to resolve. The effective spatial resolution of fMRI is constrained by both biophysical and methodological factors. The BOLD signal exhibits a point-spread function, as oxygen-rich blood drains into venous structures beyond active neuronal sites, thereby blurring neural specificity. This effect is partially mitigated at higher magnetic field strengths but is exacerbated by head motion and physiological noise. Analytical procedures further limit resolution. Preprocessing steps, such as spatial smoothing (see Section 3.3), reduce effective precision, while inter-subject comparisons require image registration across variable brain anatomies, introducing additional blurring and noise.

The principal challenge in interpreting BOLD-fMRI data stems from the complex, nonlinear nature of neurovascular coupling, which cannot be adequately captured by simplified models. The limited spatial resolution (typically, $> 1\,mm^3$), which averages signals across heterogeneous neural ensembles and vascular compartments, combined with a inherently slow temporal resolution (governed by a TR $\in$ $[0.5, 4]$ s and an underlying hemodynamic delay of several seconds), fundamentally decouples the measured signal from the millisecond-scale neural dynamics that underlie it. Consequently, accurate interpretation necessitates accounting for a multitude of factors, ranging from local vascular properties and vasomotor reactivity to stimulus-dependent nonlinearities in metabolic demand and blood flow, thereby challenging the feasibility of making simple and direct quantitative inferences about underlying neural activity.

3.3. Preprocessing of BOLD-fMRI data: Methods and quality assessment

BOLD-fMRI data requires rigorous preprocessing before any reliable analysis can be performed. This preprocessing ensures the removal of artifacts and standardizes data across subjects, enabling meaningful group-level statistical inferences. Let us briefly touch on these points, which are not central to the topic of the review, but are important for understanding the kind of data the researcher has to deal with.

3.3.1. Overview of preprocessing steps

The principal steps in fMRI preprocessing typically include:

- *Motion correction*: Head motion during scanning introduces significant artifacts that confound the BOLD signal. Motion correction algorithms realign the sequential fMRI volumes to a common reference frame, typically the first or middle volume, to reduce these artifacts. Techniques often rely on rigid-body transformations with six degrees of freedom (three translations and three rotations). Popular algorithms estimate and correct motion parameters to minimize intensity differences as presented in Refs. [118,119]. Thresholds for excessive motion are often set around 2 mm of translation or 2 degrees of rotation [120].
- *Nuisance Signal Regression*: This is arguably one of the most critical steps for connectivity analysis [121]. The BOLD signal is contaminated by various non-neural physiological fluctuations (e.g., from cardiac and respiratory cycles) and residual motion artifacts. These are statistically removed through linear regression. Common nuisance regressors include the six motion parameters derived from realignment (and their derivatives, and squares), as well as average signals extracted from white matter and cerebrospinal fluid masks [122]. Mathematically, this process can be framed as a projection. If we let $\mathbf{y}$ be the n-dimensional time series vector for a given voxel (where n is the number of time points) and $\mathbf{X}$ be the $n \times p$ design matrix containing the p nuisance regressors, the goal is to remove the component of $\mathbf{y}$ that lies in the space spanned by the columns of $\mathbf{X}$. The cleaned signal, $\mathbf{e}$, is the residual from the linear model $\mathbf{y} = \mathbf{X}\beta + \mathbf{e}$, and is given by:

$$\mathbf{e} = (\mathbf{I} - \mathbf{H})\mathbf{y}. \tag{14}$$

  Here, $H = \mathbf{X}(\mathbf{X}^T\mathbf{X})^{-1}\mathbf{X}^T$ is a projection matrix that projects $\mathbf{y}$ onto the nuisance subspace. The resulting signal $\mathbf{e}$ resides in a subspace that is orthogonal to the nuisance regressors, ensuring they are uncorrelated [122].

- *Normalization (spatial registration)*: To enable statistical group analyses and comparisons across subjects, individual fMRI data are geometrically warped into a standard anatomical space, such as the Montreal Neurological Institute (MNI)-labeled space using a full-brain template [123] or Talairach space [124,125]. This step involves estimating nonlinear deformations and applying these transformations to all volumes. Spatial normalization could be performed using nonlinear registration algorithms, such as DARTEL in SPM or FNIRT in FSL, with warp resolution of approximately 1–2 mm [126].
- *Spatial smoothing*: Smoothing the normalized images with a Gaussian kernel (typically 4–8 mm full width at half maximum (FWHM), kernel width selection balances between noise reduction and spatial specificity) increases the signal-to-noise ratio by averaging signals over neighboring voxels and accounts for anatomical variability. This is also important for satisfying the assumptions of Gaussian random field theory in statistical inference [127].
- *Temporal filtering (optional)*: High-pass filtering (cutoff about 0.008–0.01 Hz) removes slow drifts. Band-pass filters or empirical mode decomposition may be used in resting-state fMRI [128,129].

These main steps can be realized within software statistical processing packages [130] such as `SPM` [131], `FSL` [132], and `AFNI` [133], which provide standardized, automated preprocessing pipelines. Recently, frameworks such as `fmriprep` [121] and `CONN Toolbox` [134] have emerged, integrating best practices and multiple tools to produce reproducible preprocessing with detailed reports.

Importantly, the sequential application of modular steps, such as motion regression, temporal filtering, and nuisance regression, can lead to the reintroduction of artifacts that were previously removed [122]. This occurs because linear projection operations used in these steps are not commutative; later steps may project the data back into subspaces associated with earlier nuisance regressors, reintroducing artifacts and nuisance variables. For instance, performing high-pass filtering after motion regression can reintroduce motion-related variance, while the reverse order may reintroduce low-frequency drift. This geometric insight underscores the importance of either combining preprocessing steps into a single joint model or carefully orthogonalizing sequential operations to avoid such artifacts and ensure valid inference in fMRI studies [122].

3.3.2. Assessing quality of preprocessing

Assessing the quality of preprocessing is an essential step in BOLD-fMRI neuroimaging data analysis to guarantee the validity and reliability of subsequent results [135]. One fundamental aspect of this evaluation involves examining motion parameters and calculating framewise displacement (FD). By plotting estimated motion parameters over time, researchers can identify sudden spikes or gradual trends in head movement. FD serves as a quantitative measure of instantaneous head displacement between successive volumes and is commonly used to detect problematic motion. Thresholds around 0.5 mm are widely accepted to identify volumes that may need to be censored to mitigate motion-related artifacts.

The accuracy of spatial normalization is also scrutinized during preprocessing quality assessment. This typically involves visual inspection of the alignment between individual normalized anatomical images and a standard brain template to ensure proper registration. In addition to subjective visual checks, automated metrics such as mutual information or correlation coefficients between the normalized anatomy and the template can provide objective measures to assist in evaluating the success of normalization procedures [136].

Smoothness estimation constitutes another aspect of quality control, where the spatial smoothness achieved after applying smoothing algorithms is verified. This step ensures that the applied smoothing kernel matches the intended size and characteristics, which is important to maintain consistency across datasets and to optimize the sensitivity of statistical analyses [127].

Outlier detection and volume censoring are important for identifying volumes contaminated by excessive motion or other artifacts. The proportion of flagged volumes is quantified, and a high percentage of affected volumes may indicate the need for data re-acquisition or exclusion from further analysis to preserve the integrity of the study. Overall, thorough quality assessment at the preprocessing stage is paramount to ensure the robustness and interpretability of neuroimaging findings [137].

Another critical indicator of preprocessing quality is based on signal quality assessment, which can be based on several metrics, among which temporal signal-to-noise ratio (tSNR) and contrast-to-noise ratio (CNR) play an important role [138,139]. tSNR is defined as the ratio of the average signal to its standard deviation in the time series for each voxel. This metric reflects the quality of temporal data, providing an indication of signal stability over time. A high tSNR indicates a low level of noise relative to the signal, which is important for reliable detection of changes in brain activation. CNR is the ratio of the contrast value (the difference in average signal values between activated and non-activated states) to the noise level. Unlike tSNR, CNR directly indicates the ability to distinguish functional activation or differences between states. In fMRI, CNR reflects the quality of experiment detection, showing how pronounced the signal change is during stimulation relative to noise. Formally, one of the CNR definitions can be expressed as [139]:

$$\mathrm{CNR} = \frac{S_{activate} - S_{base}}{\sigma^{noise}}, \tag{15}$$

where $S_{activate}$ and S_{base} are the average signal values in activated and baseline areas, σ^{noise} is the standard deviation of background noise.

Table 3
Summary of methodologies for HOI assessment.

Methodology	Core principle	Example methods	Primary output
Multivariate Statistical Models	Model systems of multiple interacting time series to disentangle direct vs. indirect interaction	Edge Functional Connectivity, Partial Correlation, SEM, MVAR, Granger Causality (Conditional, Spectral), Multivariate Cumulants	Directed/undirected graphs of unconfounded connections; maps of "genuine" HOIs
Information-Theoretic Measures	Quantify the flow, distribution, and nature (synergistic/redundant) of information in multivariate systems	Transfer Entropy, O-information, Partial Information/Entropy Decomposition (PID/PED)	Directed information flow networks; maps of synergistic and redundant systems
Machine Learning & AI	Discover complex, nonlinear HOIs by framing the problem as one of feature selection or end-to-end representation learning	LASSO (Group, Structurally-Weighted), Graph Neural Networks (GNNs), Transformers	Sparse hypergraphs representing predictive relationships; predictive models with implicitly learned HOIs

Thus, in fMRI tasks, it is not so much the absolute signal quality (tSNR) that is important, but rather the ability to detect experimental changes, which is more fully reflected by CNR. Some studies show that CNR correlates better with activation detection power than tSNR. It should be noted that imaging parameters and hardware settings affect tSNR and, indirectly, CNR. For example, increasing the magnetic field significantly improves both tSNR and CNR of fMRI data. However, CNR depends on the magnitude of activation and its contrast, while tSNR depends on the stability of the temporal signal and the noise level in the data. As a result, tSNR assesses the quality of the time series signal, while CNR assesses how well functional changes can be detected. In fMRI studies, it is advisable to use CNR to assess the ability to detect activations, although tSNR is widely used for the initial assessment of fMRI data quality.

Robust preprocessing of fMRI data including motion correction, spatial normalization, and smoothing is essential for valid interpretation of the BOLD signal. Utilizing established tools such as `SPM`, `FSL`, `AFNI`, and `fmriprep` facilitates reproducible workflows. Systematic quality assessment using motion-related metrics, tSNR and CNR, and normalization accuracy helps ensure the efficiency of preprocessing and the reliability of the fMRI data, which is then used to analyze more sophisticated entities such as fMRI-based functional brain networks.

4. Evolution of methodologies for assessing higher-order interactions

The shift from a pairwise to a higher-order perspective represents a critical evolution in the field of modern neuroscience, promising to unlock a deeper understanding of the brain's integrative mechanisms. This section provides a comprehensive review of the methodologies for assessing HOIs that enable this shift. We will systematically survey three major classes of these advanced methodologies: (1) statistical models that account for multivariate influences to disentangle complex dependencies (see Section 4.3); (2) information-theoretic frameworks that provide a model-free quantification of how information is shared, transferred, and synergistically integrated within groups of brain regions (see Section 4.4); and (3) machine learning (ML) and artificial intelligence (AI) techniques that leverage powerful algorithms to discover complex, nonlinear dependencies directly from high-dimensional neuroimaging data (see Section 4.5).

Before delving into the specific methodologies, Table 3 provides a high-level roadmap, categorizing the diverse approaches into three coherent families based on their core scientific principles. This framework will help organize the detailed information that follows and highlight the conceptual relationships between different classes of methods.

4.1. The foundation: Pairwise functional connectivity

To appreciate the necessity and novelty of higher-order methods, it is essential to first understand the foundational paradigm they seek to extend: the construction and analysis of brain networks using pairwise measures of functional connectivity (FC). This section briefly details the standard pairwise connectivity measures that result in static network graphs and critically examines the assumptions and limitations of this classical approach.

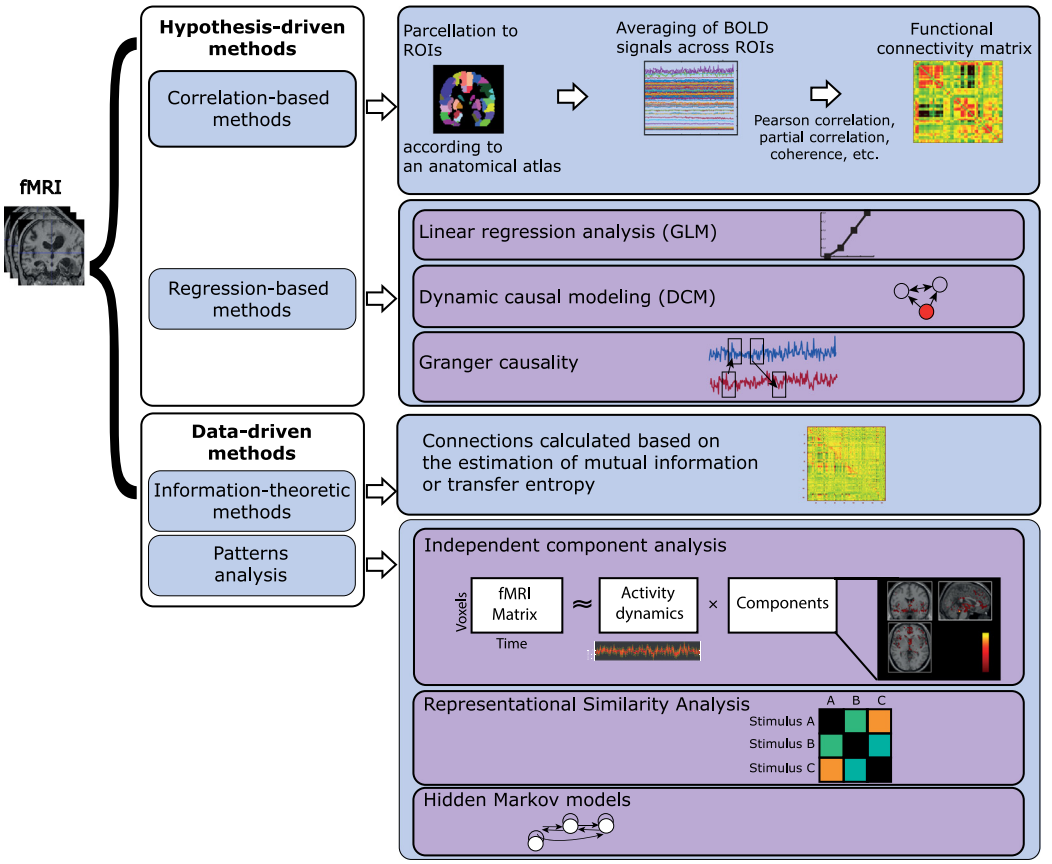

Fig. 13. Basic methods for extracting a static functional connectivity (FC) using fMRI data. There are two main types of methods: hypothesis-driven and data-driven.

4.1.1. Defining network nodes: ROI time series extraction

After preprocessing (see Section 3.3.1), the continuous voxel-wise data must be parcellated into a discrete set of nodes to form a network [37]. These nodes are termed Regions of Interest (ROIs) [134]. The representative activity of each ROI is typically calculated by averaging the BOLD time series of all voxels contained within its boundaries. This crucial step is most commonly accomplished using a predefined brain atlas that partitions the brain into anatomically or functionally distinct parcels.

A wide variety of atlases are available, such as the Automated Anatomical Labeling (AAL) atlas [30,140], the Harvard-Oxford atlas [141], and functionally derived parcellations like the Craddock atlases [142]. Software packages like `FSL`, `AFNI`, `CONN`, and `C-PAC`, as well as programming libraries such as `nilearn` in `Python`, provide extensive toolsets for applying these atlases and extracting the corresponding ROI time series. The procedure yields N time series (one per ROI in the chosen atlas). These form the basic data structure on which all subsequent connectivity analyses – pairwise and higher-order – are based.

4.1.2. Pairwise connectivity: Basic measures

Once a set of N ROI time series is available, the next step is to quantify the relationships between them. In the pairwise framework, a static functional network is constructed by computing a chosen connectivity measure for each pair of ROIs. The results are assembled into an $N \times N$ adjacency matrix, A, where the entry A_{ij} represents the weight of the functional edge connecting node i and node j. There are numerous measures, both directed and undirected.

Fig. 13 schematically illustrates the basic types of the measures. There are two main types of methods: hypothesis-driven and data-driven [15]. These classes include correlation-based methods in time and frequency domains, regression-based methods, information-theoretic methods, pattern-based methods, matrix decomposition-based methods, clustering-based methods, and deep learning methods. However, the field has historically relied on a few foundational metrics.

Pearson correlation. The Pearson correlation coefficient [143] is, by a significant margin, the most widely used measure of functional connectivity in fMRI research [30,144]. It provides a simple, intuitive, and computationally efficient way to

quantify the degree of linear temporal association between the BOLD time series of two regions, X and Y, each of length T. The formula is given by the covariance of the two series divided by the product of their standard deviations:

$$r_{XY} = \frac{\sum_{t=1}^{T}(X_t - \bar{X})(Y_t - \bar{Y})}{\sqrt{\sum_{t=1}^{T}(X_t - \bar{X})^2}\sqrt{\sum_{t=1}^{T}(Y_t - \bar{Y})^2}}. \tag{16}$$

The resulting value, r_{XY}, ranges from -1 (perfect anti-correlation) to $+1$ (perfect positive correlation), with 0 indicating no linear relationship. It is a symmetric ($r_{XY} = r_{YX}$), zero-lag, time-domain measure that implicitly assumes the relationship between the signals is linear and that their joint distribution is approximately bivariate Gaussian [145]. For the purpose of statistical hypothesis testing, the correlation coefficients are often converted to z-scores using the Fisher transformation, which stabilizes the variance and makes the sampling distribution approximately normal.

Coherence. Recognizing that brain activity is fundamentally oscillatory, coherence was introduced as a frequency-domain alternative to correlation [144]. Coherence, or more specifically magnitude-squared coherence, quantifies the consistency of the phase relationship between two signals as a function of frequency, f. It is particularly useful because it is insensitive to constant time lags between signals, which could otherwise attenuate a time-domain correlation value [146]. The magnitude-squared coherence, $C_{XY}(f)$, is defined as the squared magnitude of the cross-spectral density, $G_{XY}(f)$, normalized by the auto-spectral densities of the individual signals, $G_{XX}(f)$ and $G_{YY}(f)$:

$$C_{XY}(f) = \frac{|G_{XY}(f)|^2}{G_{XX}(f)G_{YY}(f)}. \tag{17}$$

The value of $C_{XY}(f)$ ranges from 0 to 1 for each frequency bin, where 1 indicates a perfect linear relationship (i.e., a consistent phase lag) at that specific frequency. This allows for a more nuanced analysis of connectivity, revealing, for example, whether two regions are coupled primarily through slow fluctuations or faster oscillations.

Mutual information. Both correlation and coherence are limited to assessing linear relationships. To capture more complex, nonlinear dependencies, information-theoretic measures can be employed. The most fundamental of these is mutual information (MI) [144,147]. MI quantifies the statistical dependence between two variables by measuring the reduction in uncertainty about one variable given knowledge of the other. For two fMRI time series, represented as vectors $\mathbf{X}$ and $\mathbf{Y}$, the MI is defined by the integral over their joint and marginal probability distributions, $P_{(X,Y)}$, P_X, and P_Y:

$$I(\mathbf{X};\mathbf{Y}) = \int_{\mathcal{Y}}\int_{\mathcal{X}} P_{(X,Y)}(x,y)\log\left(\frac{P_{(X,Y)}(x,y)}{P_X(x)P_Y(y)}\right)dxdy. \tag{18}$$

MI is a powerful and general measure, but its application to fMRI data is challenging. Estimating the underlying probability distributions from finite, noisy, and temporally correlated data is non-trivial and prone to significant bias, making the results highly dependent on the choice of estimator (e.g., k-nearest neighbor or kernel-based methods).

Numerous comprehensive reviews provide more detailed considerations of various measures of pairwise functional connectivity (see, e.g., [14,15,148] and references therein).

4.2. Limitations of pairwise measures in capturing complex brain interactions

While the pairwise framework has been immensely productive, its inherent simplifications impose fundamental constraints on our ability to model the brain's true operational complexity [149]. The limitations are not merely statistical artifacts but conceptual shortcomings that prevent the observation of crucial network phenomena. The very progression of methods from Pearson correlation to coherence and then to mutual information illustrates a drive to relax statistical assumptions – from linear time-domain, to linear frequency-domain, to nonlinear – but this evolution does not address the core conceptual flaw of the pairwise view. All these measures are fundamentally blind to the distributed and synergistic nature of brain function [31,32].

4.2.1. The confound of direct vs. Indirect effects

A primary and critical limitation of any bivariate measure is its inability to distinguish between a direct functional link between two regions ($A \leftrightarrow B$) and an indirect connection that is mediated by a third region or a common input ($A \leftrightarrow C \leftrightarrow B$). A strong correlation observed between regions A and B might be entirely spurious, arising simply because both are driven by a third, unobserved region C. This ambiguity severely limits the interpretability of standard FC networks, as the presence of an edge does not guarantee a direct interaction. Methods like partial correlation were developed to address this by statistically removing the linear influence of other regions, but this only partially solves the problem and relies on strong linear assumptions.

4.2.2. Blindness to emergent group dynamics: Synergy and redundancy

Perhaps the most profound limitation of the pairwise approach is its definitional inability to detect emergent phenomena that arise from the collective, simultaneous interaction of multiple brain regions. Information theory provides a powerful language to describe these phenomena, decomposing multivariate interactions into two key components: synergy and redundancy [150].

Synergy refers to information that is newly created by the interaction of a group of elements. It is information that is available only when considering the regions jointly and cannot be obtained from any individual region or smaller subgroup within the set. This corresponds to the brain's capacity for information integration.

Redundancy refers to information that is duplicated or shared across multiple regions. It is information that could be obtained from any one of several sources, providing the system with robustness against noise or damage [151]. Traditional FC, which measures the similarity of temporal fluctuations, is conceptually much closer to redundancy. Two regions that receive the same inputs will exhibit correlated time series, reflecting a redundant relationship. By contrast, FC is largely blind to synergy. It cannot answer questions such as: how does the joint state of regions A and B provide novel information about region C that neither A nor B carries alone? Answering such questions is crucial for understanding cognitive processes that rely on the integration of information, and this is precisely the regime in which pairwise methods are fundamentally inadequate [31,32].

4.2.3. Statistical and biophysical complications

The interpretation of pairwise FC is further complicated by the statistical properties of fMRI data and its indirect relationship to neural activity. The following main problems are recognized:

- *High Dimensionality and Spurious Findings.* In whole-brain analyses with hundreds of ROIs, the number of possible pairwise connections is enormous ($N(N-1)/2$), which greatly increases the probability of observing strong correlations purely by chance. This necessitates stringent correction for multiple comparisons, which can in turn reduce statistical power [149,152].
- *Sampling Variability and Noise.* The BOLD signal is slow, with most neurally-driven power concentrated below 0.2 Hz, and has a relatively low signal-to-noise ratio (SNR). FC measures like correlation are second-order statistics (as they involve the product of two signals), and measures of FC variability are fourth-order statistics. Higher-order statistics are inherently more susceptible to sampling error. This means that with the limited number of independent samples available in a typical fMRI scan, estimates of FC can be highly variable and noisy, making robust inference challenging [70].
- *Agnosticism to Mechanism.* Finally, all pairwise FC measures are descriptive, not mechanistic. They quantify statistical co-fluctuation but are agnostic to the direction of influence or the underlying causal mechanisms that give rise to the observed patterns. A strong correlation does not imply causation, a limitation that has spurred the development of methods for "effective connectivity" [153], many of which are inherently multivariate and form the basis of the next section.

In summary, the classical pairwise framework, while foundational, constructs a simplified model of the brain that ignores mediated effects, is blind to emergent synergistic interactions, and is susceptible to statistical confounds. This conceptual wall, more than any specific limitation of Pearson correlation or its alternatives, necessitates a move toward methodologies capable of assessing higher-order interactions.

4.3. Statistical approaches: from foundational models for pairwise analysis to techniques for assessing HOIs

To overcome the fundamental limitations of the pairwise framework, a suite of more sophisticated statistical methods has been developed. These approaches explicitly model the brain as a multivariate system, allowing for the statistical disentanglement of direct from indirect influences and, in some cases, the direct quantification of interactions among three or more regions. This section reviews these methods, starting with foundational multivariate models and progressing to techniques specifically designed to isolate "genuine" higher-order dependencies.

4.3.1. Edge functional connectivity

One of the most commonly used measure for higher-order connectivity is the *edge functional connectivity* (eFC) [154]. Unlike node-centric FC, which measures temporal correlations between regional time series, eFC quantifies the similarity between the time-varying co-fluctuations of pairs of edges. Specifically, for each pair of brain regions i and j, an edge time series c_{ij} is constructed as the element-wise product of their z-scored BOLD signals, capturing moment-to-moment co-fluctuation magnitudes (see Fig. 14 for details). The eFC between two edges (i, j) and (u, v) is given by the correlation between their edge time series:

$$\mathrm{eFC}_{ijuv} = \frac{\sum_t c_{ij}(t) \cdot c_{uv}(t)}{\sqrt{\sum_t c_{ij}(t)^2} \cdot \sqrt{\sum_t c_{uv}(t)^2}}. \tag{19}$$

The correlation between the edge time series across all possible pairs of edges yields the eFC matrix, which encodes how the strength of functional connections covaries over time [154].

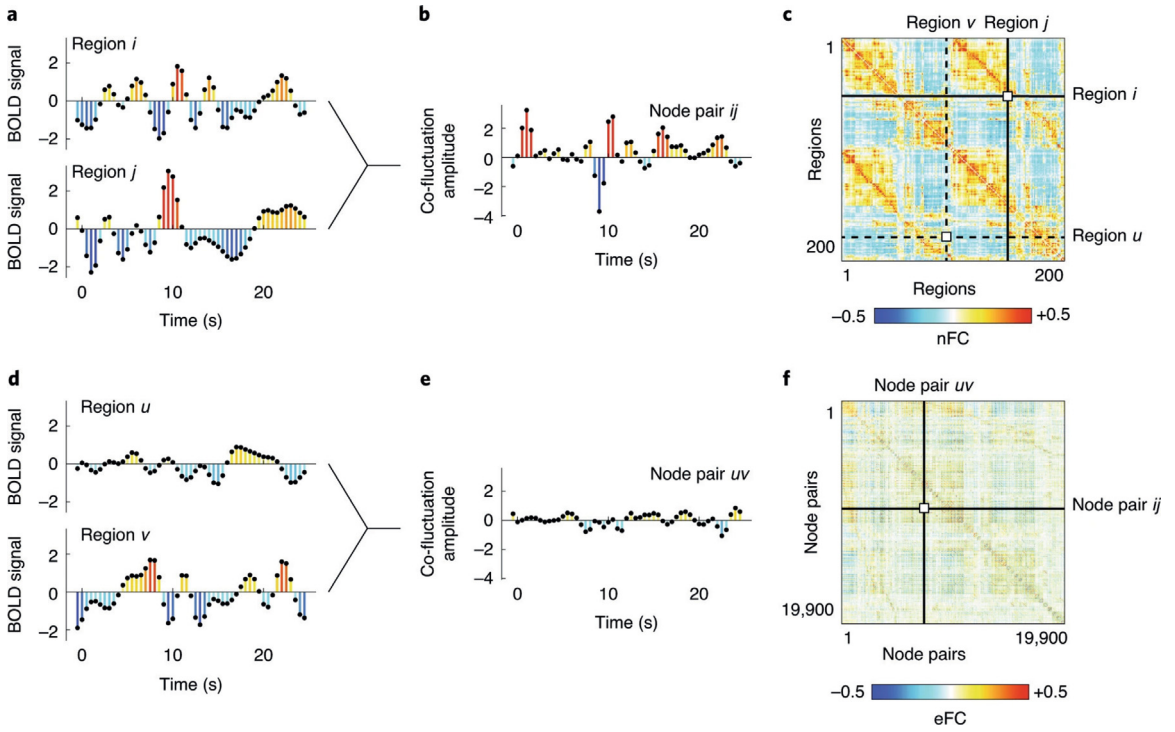

Fig. 14. Edge functional connectivity (eFC) construction from fMRI time series. Each element of the eFC matrix is computed from the fMRI BOLD time series of four nodes (brain regions). Panels (a) and (d) show representative time series from regions i, j, u, and v. (c) Pairwise FC is typically obtained by z-scoring each time series, taking the element-wise product (dots) of region pairs, and averaging the resulting product time series. In contrast, eFC retains the full product time series for every pair of regions. Panels (b) and (e) show product time series for the pairs $\{i, j\}$ and $\{u, v\}$. The elements of these product time series represent the instantaneous co-fluctuation magnitude of each pair (i.e., edge) across time. The eFC between two edges is then obtained by element-wise multiplication of their product time series and normalizing the sum by the product of their standard deviations, which constrains the result to $[-1, 1]$. (f) The resulting value is stored in the corresponding entry of the eFC matrix.
Source: Reproduced from [154].

This edge-centric framework provides a natural foundation for capturing more complex, higher-order interactions. For instance, the co-fluctuation of two edges may indicate coordinated engagement of three or more regions, suggesting the presence of group-level dynamics that cannot likely be reduced to pairwise correlations. A potential drawback of this method is that it does not definitively determine whether the observed higher-order connectivity can be reduced to the pairwise connectivity of the participating brain regions [78]. Nevertheless, the study [154] demonstrated empirically that eFC is not well approximated using only linear combinations of the pairwise elements of the initial FC matrix. However, the inclusion of nonlinear transformations and interaction terms allows the pairwise FC matrix to approximate eFC. This suggests that the eFC measure encompasses both pairwise interactions and more intricate nonlinear HOIs.

EFC has been shown to be highly reproducible within individuals, stable across sessions, and modulated by cognitive tasks, indicating its sensitivity to brain state changes [33,154,155]. Moreover, clustering eFC matrices reveals overlapping community structures at the edge level, which, when projected back to nodes, show that brain regions, particularly in sensorimotor and attentional systems, participate in multiple functional communities simultaneously [154]. This overlap suggests a more nuanced and multifunctional organization of the brain than what is captured by traditional non-overlapping modular partitions.

To support the inference of HOIs, Santoro et al. [155] introduced a related but more general measure. This measure quantifies the strength of the connectivity between k brain regions (i.e., kth order connectivity) for $k > 2$. Specifically, the generic element of the z-scored k-order co-fluctuations between $(k + 1)$ time series at time t is calculated as follows:

$$\xi_{0\ldots k}(t) = \frac{\prod_{p=0}^{k} z_p(t) - \mu\left[\prod_{p=0}^{k} \mathbf{z}_p\right]}{\sigma\left[\prod_{p=0}^{k} \mathbf{z}_p\right]}, \tag{20}$$

where $\mu[\bullet]$ and $\sigma[\bullet]$ are the time-averaged mean and standard deviation functions. A sign remapping is applied to emphasize perfectly coherent contributions: concordant signs in a k-order product are always positively mapped, while discordant signs are negatively mapped. In this way, all the perfectly coherent contributions (namely, either all positive or all negative) will be mapped as positive.

Later, the same group used a topological approach to construct instantaneous weighted simplicial complexes from edge time series and their higher-order generalizations (e.g., products of three or more z-scored time series) [33]. This method allows for the identification of "violating triangles" – triplets of regions whose joint co-fluctuation exceeds what would be expected from their pairwise connections – and the extraction of homological scaffolds, which highlight edges critical to maintaining cyclic topological structures in the functional network.

However, eFC – and especially its higher-order extensions – comes with substantial computational challenges. The eFC matrix scales quadratically with the number of edges, and incorporating higher-order interactions (e.g., triplets, tetrahedra) further increases the combinatorial burden. To manage this complexity and to extract stable functional modules, subsequent work has introduced dimensionality-reduction and clustering approaches.

A key evolutionary step involves grouping edge-time series based on their similarity before calculating the high-order correlations. As demonstrated in the work by Pan et al. [156], instead of correlating every pair of edges, the edge-time series from all subjects are first clustered into a manageable number of representative functional modules using an algorithm like Ward's method [157]. The high-order functional connectivity network is then constructed by computing the correlations between the averaged edge-time series of these clusters. This "clustering-before-correlation" approach significantly reduces the computational burden and mitigates the risk of overfitting by creating a more compact and interpretable representation of the higher-order network topology. It effectively shifts the analysis from individual edges to coherent groups of edges that exhibit similar temporal dynamics, highlighting large-scale coordination between functional systems. This methodological refinement underscores a broader trend in the field towards leveraging data-driven clustering and dimensionality reduction to make the analysis of higher-order interactions both tractable and biologically meaningful.

In summary, edge functional connectivity provides a powerful bridge between classical pairwise connectivity and higher-order interactions. By capturing the temporal dynamics of edge co-fluctuations, it enables the detection of complex, multi-node functional patterns that are otherwise obscured in traditional analyses, offering a more comprehensive view of brain network organization.

4.3.2. Multivariate statistical models

The first step beyond pairwise analysis is to consider all regions of interest simultaneously within a single statistical model. Two major classes of models have emerged for fMRI data: Structural Equation Modeling (SEM) and Multivariate Autoregressive (MVAR) Models.

Structural Equation Modeling (SEM). SEM is a powerful, hypothesis-driven statistical technique used to test pre-specified models of effective (i.e., causal) connectivity [158,159]. Unlike exploratory methods, SEM requires the researcher to posit a specific anatomical model based on prior neurobiological knowledge. This model defines a set of ROIs and the directed (causal) pathways assumed to exist between them [159].

The core of SEM is a system of simultaneous linear equations that describes the relationships among the variables. For a set of brain regions with activity vector $\mathbf{x}$, the model can be expressed as:

$$\mathbf{x} = \mathbf{A}\mathbf{x} + \omega, \tag{21}$$

where $\mathbf{A}$ is the matrix of path coefficients representing the connection strengths between regions, and ω is a vector of Gaussian noise or unexplained variance [158,159]. The SEM algorithm then estimates the values of the coefficients in $\mathbf{A}$ that best reproduce the observed covariance matrix of the fMRI time series data, typically using maximum likelihood estimation. The significance of these path coefficients can then be tested, and different models can be compared.

The primary strength of SEM is its ability to test specific, directional hypotheses about brain circuitry. However, its major drawback is this very reliance on an a priori model. If the specified model is incorrect or incomplete (e.g., omits a critical mediating region), the results can be misleading. Furthermore, the classical formulation of SEM for fMRI is based on the covariance matrix, meaning it does not explicitly model the temporal, time-series nature of the data [160].

Multivariate autoregressive (MVAR) models. Unlike the hypothesis-driven approach of SEM, MVAR models provide a data-driven framework for analyzing network dynamics [161]. They characterize each region's activity as a linear combination of its own past and the past of all other regions in the network. For a K-dimensional multivariate time series $\mathbf{x}(t)$ (representing the activity of K ROIs at time t), an MVAR model of order p (the number of time lags considered) is defined as:

$$\mathbf{x}(t) = \sum_{k=1}^{p} \mathbf{A}(k)\mathbf{x}(t-k) + \mathbf{E}(t), \tag{22}$$

where $\mathbf{A}(k)$ is the $K \times K$ matrix of model coefficients for lag k, and $\mathbf{E}(t)$ is a vector of white noise residuals, or prediction errors [162].

The MVAR framework is inherently multivariate and serves as the mathematical foundation for several important directed connectivity measures, most notably Granger Causality. By modeling all ROIs simultaneously, it implicitly accounts for their mutual influences when estimating the model coefficients [161,163]. However, MVAR models are not without limitations. The number of parameters to be estimated, $p \times K^2$, grows quadratically with the number of ROIs, K.

This "curse of dimensionality" makes the model intractable for large-scale brain networks (e.g., hundreds of ROIs) unless the number of time points is very large or advanced regularization techniques are employed to enforce sparsity [160]. Additionally, the standard MVAR model assumes linearity and stationarity (i.e., that the statistical properties of the signals and their relationships do not change over time), which may not hold true for fMRI data, especially during task-based experiments.

The tension between the hypothesis-driven SEM and the data-driven MVAR frameworks highlights a central challenge in connectivity analysis: balancing inferential power with exploratory flexibility. SEM provides strong causal inference but is constrained by what is already known, while MVAR is more exploratory but can be difficult to interpret in complex systems and is sensitive to confounds. This has led to the development of hybrid approaches that seek to bridge this gap, using data-driven methods that are guided or constrained by anatomical priors, a theme that reappears in the ML section.

4.3.3. Partial correlation and extensions of granger causality

Building upon the multivariate framework, several specific measures have been developed to more precisely probe higher-order dependencies by disentangling direct from indirect effects.

Partial correlation. Partial correlation is a direct extension of the Pearson correlation that addresses one of the primary weaknesses of bivariate measures [164]. It quantifies the linear relationship between two variables, X and Y, after statistically controlling for the linear influence of a third variable or a set of variables, Z [153]. For the simple case of controlling for a single variable Z, the partial correlation $r_{XY \cdot Z}$ is computed from the pairwise correlations:

$$r_{XY \cdot Z} = \frac{r_{XY} - r_{XZ} r_{YZ}}{\sqrt{(1 - r_{XZ}^2)(1 - r_{YZ}^2)}} \tag{23}$$

In the general multivariate case, the partial correlation between any two variables, controlling for all other variables in the set, can be efficiently calculated from the inverse of the full covariance matrix [153]. By "partialling out" the influence of other regions, this method aims to produce a sparser, more interpretable connectome that reflects direct connections more accurately than a standard correlation matrix.

Granger causality and its multivariate extensions. Granger Causality (GC) is a statistical concept of causality based on temporal precedence and predictability [165]. In simple terms, a time series Y is said to "Granger-cause" a time series X if the past values of Y contain information that helps to predict the future values of X better than using the past values of X alone.

In its original formulation, GC is a bivariate measure applied to a pair of time series. However, this is susceptible to the same confounds as Pearson correlation, where a third variable Z driving both X and Y can create a spurious causal link. The crucial extension for HOI analysis is Conditional GC, which is assessed within a full MVAR model. The causal influence from Y to X is tested conditional on all other time series Z included in the model [161]. This move from a bivariate to a multivariate context is a fundamental step toward modeling higher-order dependencies, as it attempts to isolate the direct influence of Y on X from the influences mediated through other nodes in the network.

Since neural communication often occurs within specific frequency bands, it is useful to resolve directed connectivity in the frequency domain. Spectral extensions of multivariate GC have been developed for this purpose, most notably Partial Directed Coherence (PDC) [166,167] and the Directed Transfer Function (DTF) [168,169]. PDC is a frequency-domain measure of direct causal influence from region j to region i, normalized by the total inflow of information to region i [170]. Its key strength is its design to separate direct causal links from indirect, polysynaptic pathways. DTF, in contrast, quantifies the total causal influence from region j to region i, including both direct connections and indirect effects that are cascaded through other nodes in the network [163]. By comparing the PDC and DTF between two regions, one can potentially infer the nature of the connection: a strong PDC suggests a direct link, whereas a strong DTF in the absence of a strong PDC suggests an indirect, mediated pathway.

A related technique, also based on vector autoregressive processes, known as directed partial correlation (dPC), has been proposed to estimate the likelihood of a directed direct interaction between variables, allowing for statistical assessment of connections at specific time lags [171].

4.3.4. Other statistical approaches: Isolating genuine HOIs with multivariate cumulants

While methods like conditional GC and partial correlation represent a significant advance by attempting to isolate direct pairwise links within a multivariate context, they do not directly quantify interactions that are intrinsically of a higher order (e.g., a three-way or four-way dependency). A major conceptual and statistical challenge in this endeavor is the problem of redundancy: an apparent higher-order statistical dependency might be nothing more than a complex reflection of the underlying pairwise correlation structure, especially if the data generating the signals is Gaussian [78,172]. For instance, the popular HOI measure "edge connectivity" – the correlation between the time series of two different edges – can be shown to be a simple function of the six pairwise correlations among the four participating nodes if the signals are Gaussian [154,172]. This raises a critical question: are we discovering any genuinely new information beyond what is already contained in the pairwise connectome? [78].

A rigorous answer to this question comes from the statistical theory of multivariate cumulants. Cumulants are statistical quantities that are mathematically constructed to be "blind" to lower-order correlations. By their very definition, they

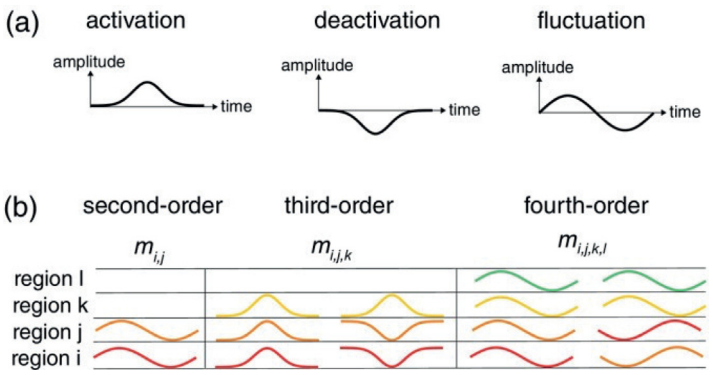

Fig. 15. Functional interpretation of multivariate moments. (a) Left: A positive deflection of the fMRI signal relative to baseline (activation). Middle: A negative deflection of the fMRI signal relative to baseline (deactivation). Right: The concatenation of an activation and a deactivation (i.e., a fluctuation). (b) Schematic illustration of the functional interpretation of higher-order moments. A positive second-order moment $m_{i,j}$ between fMRI signals from regions i and j reflects coherent fluctuations (i.e., both activations and deactivations) in regions i and j. A positive third-order moment $m_{i,j,k}$ between fMRI signals in regions i, j, k can reflect coherent activations in all three regions i, j, k or coherent deactivations in two of the regions (regions i and j) and simultaneous activation of the third region (region k). A positive fourth-order moment $m_{i,j,k,l}$ between fMRI signals in regions i, j, k, l can reflect coherent fluctuations (i.e., both activations and deactivations) in all four regions or coherent fluctuations in two pairs of regions (pairs (i, j) and (k, l)) that are anti-correlated.
Source: Reproduced from [78]; licensed under a Creative Commons Attribution 4.0 International license

quantify the part of a higher-order moment that is "non-redundant"—that is, the part that cannot be explained by any combination of lower-order moments [78]. This makes them ideal tools for identifying genuine HOIs.

Let $x = (x_1, \ldots, x_n)$ be the fMRI activity of n brain regions at a given time-point. We treat x as a realization of a random vector $X = (X_1, \ldots, X_n)$. Different realizations of X correspond to different time-points. Without loss of generality, we assume that the expectation $E[X_i] = 0$ for all brain regions i. This assumption reflects the fact that the information in fMRI signals is contained in their fluctuations, and not in their off-sets. Then,

- The second-order cumulant of two zero-mean random variables is identical to their second-order moment or covariance (Fig. 15):

$$c_{i,j} = E[X_i X_j]. \tag{24}$$

  Its normalized version, the non-redundant second-order correlation, $r^c_{i,j} = c_{i,j}/\sigma_i\sigma_j$, is the Pearson correlation coefficient. It quantifies the extent to which the fluctuations in regions i and j are coherent, that is, co-fluctuate.
- The third-order cumulant of three zero-mean random variables is identical to their third-order moment:

$$c_{i,j,k} = E[X_i X_j X_k]. \tag{25}$$

  Its normalized version, the non-redundant third-order correlation or coskewness, $r^c_{i,j,k} = c_{i,j,k}/\sigma_i\sigma_j\sigma_k$, quantifies the degree of asymmetric co-fluctuation among three regions. A significant non-zero value indicates a genuine three-way interaction that is not simply an artifact of the pairwise correlations among regions i, j, and k [78].
- The fourth-order cumulant is where the power of this approach becomes most apparent. It is defined based on the fourth-order moment by subtracting the contributions from all possible combinations of second-order moments:

$$c_{i,j,k,l} = m_{i,j,k,l} - m_{i,j}m_{k,l} - m_{i,k}m_{j,l} - m_{i,l}m_{j,k}, \tag{26}$$

  where $m_{i,j,k,l}$ is the fourth-order moment and $m_{*,*}$ are the corresponding second-order moments. The normalized version, the non-redundant fourth-order correlation or cokurtosis, $r^c_{i,j,k,l} = c_{i,j,k,l}/\sigma_i\sigma_j\sigma_k\sigma_l$, vanishes for any multivariate Gaussian distribution. Therefore, a significant non-zero cokurtosis provides unambiguous evidence for a genuine four-way interaction – a hyperedge – that is irreducible to pairwise effects [78].
- The same applies to higher orders.

The introduction of multivariate cumulants marks a pivotal moment in the statistical analysis of HOIs. It directly confronts the potent critique of reducibility. By providing a mathematically sound method for defining and measuring "genuine" HOIs, this framework elevates the field from exploratory observation to quantifiable science. When a study reports a significant cokurtosis between four brain regions, it can make a robust claim of having detected a true higher-order interaction. Empirical applications have already demonstrated the value of this approach, revealing that higher-order networks defined by cumulants are topologically distinct from conventional pairwise networks and can possess unique clinical relevance, such as explaining variance in cognitive impairment in multiple sclerosis patients beyond what can be captured by pairwise connectivity alone [78].

4.4. Evolution of information-theoretical measures for assessing HOIs

Information theory offers a powerful, model-free alternative to the statistical methods described above. Rather than assuming a specific underlying model (e.g., linear regression), information-theoretic approaches quantify the statistical dependencies between variables in terms of uncertainty and information. This framework is particularly well-suited for capturing nonlinear relationships and for dissecting multivariate interactions into conceptually distinct components like synergy and redundancy. We begin this section with a brief description of foundational pairwise approaches, followed by advanced techniques for HOI quantification.

4.4.1. Transfer entropy, multi-information, and interaction information

Transfer entropy. Transfer Entropy (TE) is a non-parametric, information-theoretic measure of directed information flow between two time series [173,174]. It is often described as the nonlinear generalization of Granger causality, as it makes no assumptions about the linearity of the interactions. TE from a source process Y to a target process X quantifies the reduction in uncertainty about the future state of X that is gained from knowing the past states of Y, over and above the uncertainty reduction gained from knowing the past of X alone. Mathematically, it is expressed as a conditional mutual information:

$$T_{Y\to X} = I(X_{t+1}; Y_t^{(l)} | X_t^{(k)}) = H(X_{t+1}|X_t^{(k)}) - H(X_{t+1}|X_t^{(k)}, Y_t^{(l)}), \tag{27}$$

where $X_t^{(k)}$ and $Y_t^{(l)}$ represent the past histories (of length k and l, respectively) of the processes, and $H(\bullet|\bullet)$ is the conditional entropy.

The main advantage of TE is its model-free nature, allowing it to detect nonlinear directed coupling. However, it is computationally very demanding, requiring the estimation of high-dimensional probability distributions [175]. Furthermore, in its standard bivariate form, it is susceptible to the same confounds from common drivers as bivariate Granger causality. To mitigate the detection of spurious connections in complex networks, multivariate extensions of TE that condition on the activity of other relevant processes are required.

Multi-information (total correlation). Multi-information, also known as total correlation, is a direct multivariate generalization of mutual information. It quantifies the total amount of statistical dependency present in a set of variables $\mathbf{X} = X_1, \ldots, X_N$ [31,176]. It measures the gap between the information contained in the whole system and the sum of the information contained in its individual parts. It is equivalent to the Kullback–Leibler divergence between the true joint probability distribution $p(\mathbf{X})$ and the factorized distribution of independent marginals $\prod p(X_i)$:

$$T(\mathbf{X}) = D_{KL}(p(\mathbf{X}) \parallel \prod_{i=1}^{N} p(X_i)) = \sum_{i=1}^{N} H(X_i) - H(\mathbf{X}), \tag{28}$$

where $H(X_i)$ is the entropy of a single variable and $H(\mathbf{X})$ is the joint entropy of the entire set. While multi-information provides a single, scalar value representing the overall "connectedness" or complexity of a system, its primary limitation is that it does not decompose this total dependency into its constituent parts. It does not distinguish, for example, between a system with many strong pairwise links and a system with weak pairwise links but strong, emergent three-way interactions.

Interaction information. Interaction information was one of the earliest attempts to extend mutual information to quantify interactions among more than two variables. For a triplet of variables X_1, X_2, X_3, it is defined as the difference between the mutual information of two variables with and without knowledge of the third:

$$I(X_1; X_2; X_3) = I(X_1; X_2|X_3) - I(X_1; X_2). \tag{29}$$

For $n > 3$ variables, interaction information is defined recursively as follows:

$$I(X_1; X_2; \ldots; X_n) = I(X_1; X_2; \ldots; X_{n-1} \mid X_n) - I(X_1; X_2; \ldots; X_{n-1}). \tag{30}$$

It was initially proposed that a positive value indicated synergy (e.g., the context of X_3 enhances the relationship between X_1 and X_2) while a negative value indicated redundancy. However, this interpretation has been shown to be ambiguous and problematic, and the measure does not generalize gracefully to systems with more than three variables, limiting its utility for modern HOI analysis [150].

4.4.2. Synergy and redundancy decomposition methods

The conceptual ambiguity of interaction information highlighted the need for a more principled way to dissect multivariate information. This led to the development of frameworks that decompose the information that a set of source variables provides about a target into distinct, non-overlapping components ("atoms"): unique, redundant, and synergistic information [32,177].

- **Redundant information** is information about a target that is common to multiple sources. For a system with two sources X_1, X_2 and a target Y, it is the information that can be obtained from observing source X_1 or source X_2. This duplication of information provides robustness to the system.

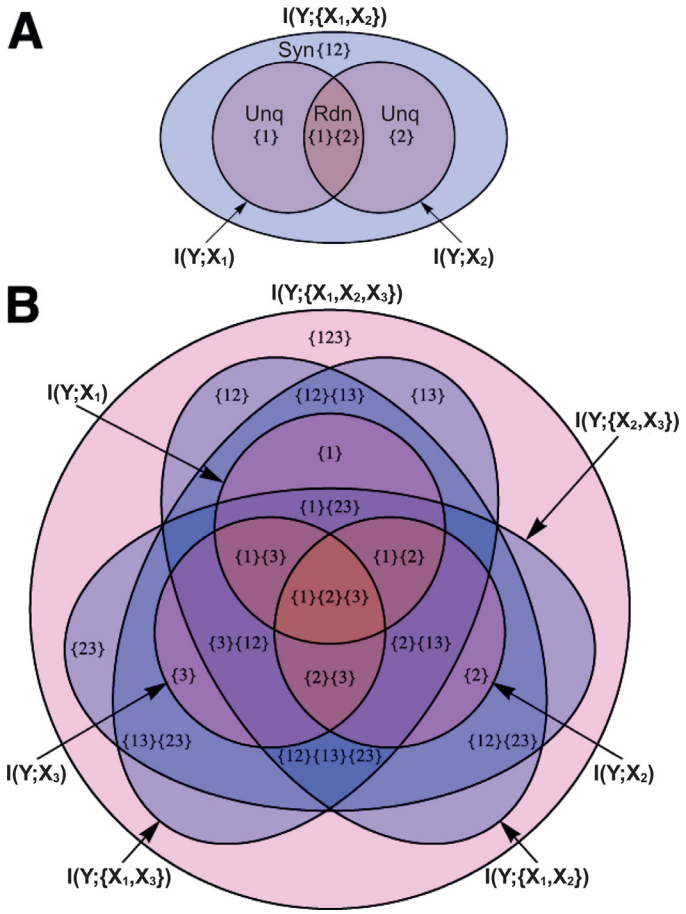

Fig. 16. Partial information diagrams for (A) 3 and (B) 4 variables. Labeled regions correspond to unique information (Unq), redundancy (Rdn), and synergy (Syn).
Source: Adapted from [150]; licensed under a Creative Commons Attribution 4.0 International license

- **Unique information** is information that is available from one source and one source only. For example, information about the target that can be obtained from X_1 but *not* from X_2.
- **Synergistic information** is the most direct information-theoretic signature of an HOI. It is emergent information that is only available when considering the sources jointly. It cannot be obtained from any individual source or any smaller subgroup of sources [32,178]. It represents the creation of novel information through the integration of parts.

Partial information decomposition. Partial Information Decomposition (PID), introduced by Williams and Beer in 2010 [150], is a formal mathematical framework designed to perform this decomposition [177,179]. PID breaks down the total multivariate mutual information between a target variable (e.g., a brain region's activity) and multiple source variables (e.g., other interacting regions) into a number of "atoms" representing the unique, redundant, and synergistic information between all subsets of source variables [180]. For a system with two sources X_1, X_2 and a target Y, PID decomposes the total mutual information $I(Y; X_1, X_2)$ into four non-negative, non-overlapping "atoms" (see Fig. 16A):

$$I(Y; X_1, X_2) = I_\delta(Y; \{X_1\}\{X_2\}) + I_\delta(Y; \{X_1\}) + I_\delta(Y; \{X_2\}) + I_\delta(Y; \{X_1, X_2\}), \tag{31}$$

where I_δ is the partial information function (see [150,180] for details), which measures the unique information contributed by only that node (redundant, synergistic or unique information within or between subsets of variables). Thus, the bivariate mutual information is split into four terms representing a contribution shared between both variables, unique to each variable and synergistic between them.

Fig. 16B illustrates a more complex case of the PID involving four variables, providing an exhaustive account of all higher-order dependencies. This lattice-based structure generalizes to any number of variables [150]. Unlike interaction information, the atoms of the PID are never negative and always support a clear interpretation as informational quantities.

PID offers a powerful framework for uncovering the intricate topology of brain networks by quantifying how information is jointly processed across multiple neural regions. Central to this approach is its ability to identify synergistic

networks, configurations in which neural computations arise not from individual regions in isolation, but from the collective, interdependent activity of multiple areas. This synergy, a hallmark of HOIs, is particularly evident in cognitive control networks, where distributed brain regions must integrate information dynamically to support complex functions.

A pivotal demonstration of PID's utility comes from Sherrill et al. [181], who applied PID to cortical cultures to quantify synergistic integration. Their findings reveal that recurrent information flow within neural motifs significantly amplifies HOIs, thereby enhancing the network's computational capacity. Crucially, this work establishes a direct link between synergistic information, as formally measured by PID, and the emergent computational properties of neural circuits.

Building on this foundation, Wibral et al. [177] argue that PID provides a principled framework for dissecting information processing beyond pairwise dependencies. By decomposing the contributions of multiple sources into unique, redundant, and synergistic components, PID enables researchers to pinpoint how groups of brain regions jointly encode and transform information. In cognitive systems, such synergy is not merely a byproduct but a signature of emergent computation, where the whole system achieves more than the sum of its parts. Together, these studies underscore PID's unique capacity to illuminate the organizational principles underlying complex brain dynamics.

The process of estimating a synergistic network begins with defining the relevant neural variables, where source regions $(X_1, X_2, \ldots, X_n)$ represent interacting brain areas and the target (Y) corresponds to either a downstream neural region or behavioral output influenced by these sources. The core analytical step involves computing information components that decompose the joint activity into unique contributions from individual regions, redundant overlapping signals, and most importantly, the synergistic information that emerges specifically from the combined interaction of multiple regions.

This calculation uncovers information that emerges only when considering the collective activity of the regions, information that cannot be inferred from their individual contributions alone. To ensure the robustness of these findings, rigorous statistical validation is essential. This typically entails comparing the observed synergy values against null distributions generated via surrogate data methods, such as phase randomization or time-series shuffling, followed by network-level thresholding procedures to control for multiple comparisons.

The mapping of synergistic networks can be approached through both region-pair analysis and graph-theoretical methods. The former identifies specific connections (hyperedges) demonstrating significant synergy, while the latter models the broader network architecture of these higher-order interactions. These approaches have proven particularly valuable in task-based experimental designs, where researchers can examine how synergy strength correlates with cognitive performance metrics, as well as in clinical investigations comparing integration patterns in neurological or psychiatric disorders.

Additionally, PID plays a crucial role in quantifying redundancy by highlighting overlapping information across neural pathways, which may reflect functional robustness in brain systems. Another important application is dynamic connectivity analysis, where extending PID to time-resolved fMRI data allows researchers to track how HOIs evolve over time during both task performance and resting states.

Several practical challenges must be addressed in this analytical pipeline. Data quality concerns, particularly the potential for noise to produce spurious synergy signals, may be mitigated through denoising techniques and longer acquisition times. The framework itself does not uniquely specify how to calculate the atoms. It requires an additional definition of the redundancy function. Several competing definitions have been proposed (e.g., Imin, BROJA PID, MMI-PID) [182–184], which may yield different results, necessitating careful methodological validation. PID requires estimating high-dimensional probability distributions, which is challenging given fMRI's limited temporal resolution and noise. Furthermore, computational demands can be substantial, potentially requiring optimized PID estimators or hardware acceleration for large-scale analyses. Analytical solutions have only recently been derived for the special case of multivariate Gaussian variables [185].

Partial entropy decomposition. While PID decomposes the information a set of sources provides about a target, a complementary framework is needed to understand the intrinsic statistical structure of a multivariate system itself. Partial Entropy Decomposition (PED), introduced by Ince in 2017 [180], addresses this by deconstructing the joint entropy of a set of brain regions into non-negative "atoms" that quantify all possible redundant, unique, and synergistic interactions within the system. This provides a complete picture of the system's informational architecture, revealing higher-order structures that are invisible to standard functional connectivity. In general, PED is very similar to PID, but the main difference is that the PED uses entropy to calculate information "atoms". For a two-region system, the PED takes the following form:

$$H(X_1, X_2) = H_\delta(\{X_1\}\{X_2\}) + H_\delta(\{X_1\}) + H_\delta(\{X_2\}) + H_\delta(\{X_1, X_2\}), \tag{32}$$

where H_δ is partial entropy function, which measures the unique entropy contributed by only that node (redundant, synergistic or unique entropy within or between subsets of variables) [180]. The first term in Eq. (32) is the redundant component, the second and third are the unique components, and the fourth is the synergistic one.

PED offers a powerful analytical lens to critique standard bivariate functional connectivity (FC). First, the latter lacks specificity: a high pairwise correlation (or mutual information) between regions X_1 and X_2 does not reflect a unique dyadic interaction. PED reveals that $I(X_1; X_2)$ conflates true pairwise redundancy with non-local, higher-order redundancies shared with other regions (e.g., $H_\delta(\{X_1\}, \{X_2\}, \{X_3\})$ [180]. This means a single redundant piece of information copied across many regions inflates all pairwise connections between them, violating the common assumption that FC edges are independent.

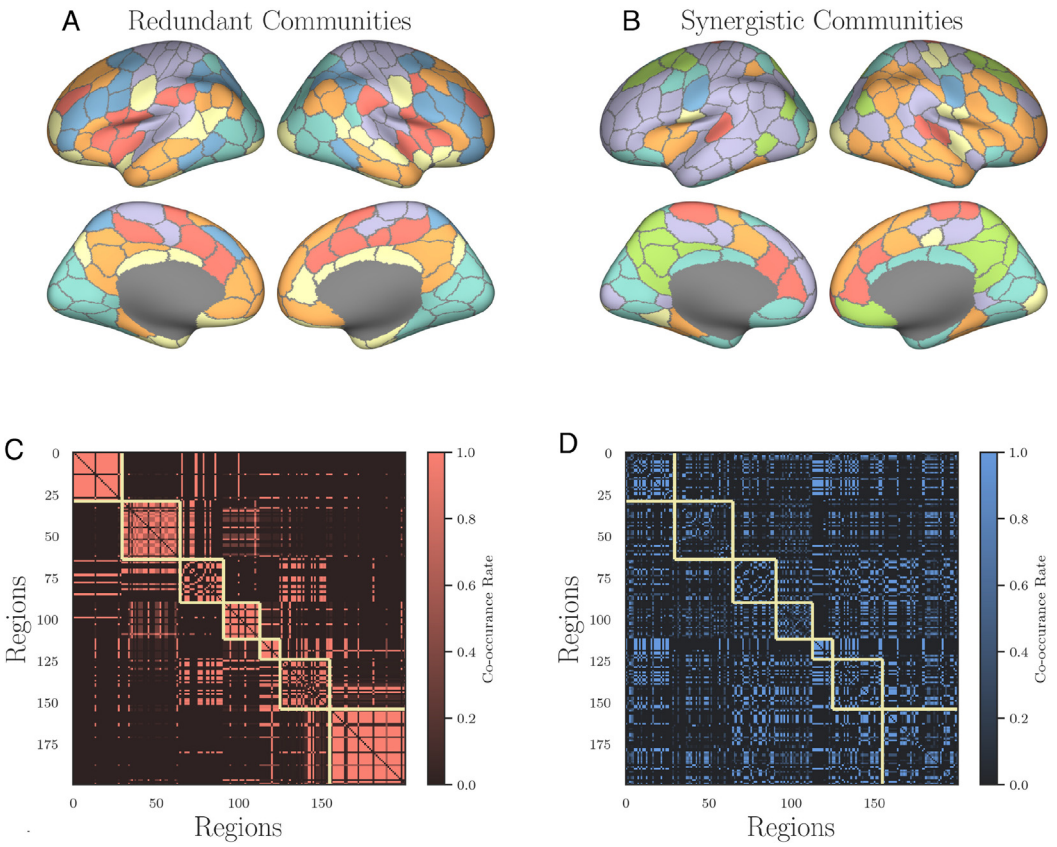

Fig. 17. Redundant and synergistic hypergraph community structure. (A,B) Surface renderings of the two dominant hypercommunity configurations identified via higher-order information decomposition. (A) Redundant structure: regions share information redundantly across triplets. (B) Synergistic structure: information arises only through the joint interaction of three regions. Both patterns exhibit approximate bilateral symmetry, though the synergistic structure features two prominent, lateralized communities. (C, D) Coclassification matrices showing the frequency with which pairs of brain regions are assigned to the same hypercommunity by hypergraph modularity maximization [186]. Higher values (darker hues) indicate more consistent coassignment. Yellow outlines delineate the seven canonical Yeo functional networks [187]. The redundant hypercommunity structure aligns closely with these established bivariate networks, even though it reflects triadic redundancy, whereas the synergistic structure shows little correspondence with the canonical organization.
Source: Reproduced from [31]; licensed under a Creative Commons Attribution-NonCommercial-NoDerivatives 4.0 International license

The second problem with standard bivariate FC is its lack of completeness; it is largely ignores synergy. PED shows that synergistic information $H_\delta\{X_1, X_2\}$ is actually subtracted from the pairwise mutual information calculation. Furthermore, conditional mutual information and partial correlation, often used to "control" for confounders, also fail to achieve specificity and actively penalize higher-order synergies, making them incomplete measures of the system's true structure [180].

When applied to resting-state fMRI data, PED uncovers a rich landscape of higher-order interactions [31]:

- Redundancy mirrors canonical networks (Fig. 17A). The spatial pattern of high redundant entropy strongly reflects well-established functional large-scale networks like the Default Mode, Visual, and Somato-motor networks [187]. This confirms that the architecture captured by traditional FC is predominantly redundant in nature.
- Synergy reveals a novel architecture (Fig. 17B). In contrast, the synergistic structure forms a qualitatively different, robust organization. It is more lateralized and does not align with canonical large-scale networks. This represents a vast "shadow structure" of brain organization that has been missed by decades of pairwise analysis.
- There is a redundancy-synergy gradient in the brain. Consistent with other methods [32], a clear gradient emerges: primary sensory and motor regions are dominated by redundancy, supporting robust, segregated processing. Conversely, transmodal association areas (e.g., prefrontal and parietal cortex) are dominated by synergy, supporting flexible, integrative computations.
- Dynamic temporal properties. Because PED can be computed in a time-resolved manner, it reveals that the balance of redundancy and synergy is highly dynamic. Whole-brain synergy and redundancy fluctuate anti-correlated over time, and the redundancy-synergy dominance of individual regions can transiently shift. These dynamics are structured, forming distinct brain states that transition in a non-random sequence. Notably, periods of high global

functional connectivity (high-amplitude co-fluctuations) are associated with high redundancy and low synergy, further emphasizing that standard FC primarily captures redundant dynamics.

O-information. Given the computational difficulties of full PID/PED, the O-information was developed as a scalable and practical heuristic to assess the overall balance between synergy and redundancy in a multivariate system of three or more variables. It does not provide the full decomposition into unique, redundant, and synergistic atoms, but instead yields a single value indicating which mode of interaction dominates.

The O-information ($\Omega(\mathbf{X})$), introduced by Rosas et al. in 2019 [188], is defined as the difference between two well-known multivariate information measures—total correlation $T(\mathbf{X})$ (see Eq. (28)) and dual total correlation $D(\mathbf{X})$ [189]:

$$\Omega(\mathbf{X}) = T(\mathbf{X}) - D(\mathbf{X}), \tag{33}$$

where

$$D(\mathbf{X}) = H(\mathbf{X}) - \sum_{i=1}^{N} H(X_i|\mathbf{X}_{-i}). \tag{34}$$

Here, $\mathbf{X}_{-i}$ means all variables in $\mathbf{X}$ except X_i. Total correlation measures the total amount of dependency among the variables. It is high when the variables are highly correlated. Meanwhile, dual total correlation captures the information shared across all the variables. It is high when information is widely shared.

Consequently, the O-information of the system can be written as:

$$\Omega(\mathbf{X}) = (N-2)H(\mathbf{X}) + \sum_{i=1}^{N} [H(X_i) - H(\mathbf{X}_{-i})]\,. \tag{35}$$

The power of the O-information lies in its interpretable sign. If $\Omega > 0$, the system is redundancy-dominated. The information shared by the variables is largely overlapping and can be accessed by observing individual elements. Conversely, when $\Omega < 0$, the system is synergy-dominated. Finally, when $\Omega \approx 0$, the system has a balance between redundant and synergistic interactions. Clearly, the main drawback of O-information is that it does not highlight multiplets of balanced variables [190]. In contrast, approaches like PID evaluate both quantities and can, in principle, handle these cases.

Additionally, the O-information is connected to the Synergy-Redundancy Index (SRI), which was developed in [178, 191]. Although the SRI does not provide separate quantifications of synergy and redundancy as PID/PED does, it considers the respective contributions of signal and noise correlations to synergy and redundancy [192,193]. Therefore, the SRI should be regarded as complementary to the PID/O-information approaches.

Recently, Varley et al. [31] used PED to provide a nuanced view of what the O-information actually captures. Their decomposition reveals that:

- It is a heuristic, not a pure measure. O-information is not simply the sum of all redundancies minus the sum of all synergies. Its algebraic structure, as shown through PED, is complex. For example, in a 3-variable system, it counts the highest-order synergy atom ($H_\delta(\{X_1, X_2, X_3\})$ positively, which is counterintuitive for a measure intended to decrease with synergy.
- There is a potential for misinterpretation. Due to its structure, it is possible for a system with no true redundancy to still have a positive O-information if it contains a very strong highest-order synergy. The authors found that, in brain data, a significant portion of triads that were classified as synergy-dominated by a more precise, PED-based measure were incorrectly classified as redundancy-dominated by the O-information.
- Despite not being pure, the O-information is still a highly useful tool. Varley et al. empirically found [31] that was strongly positively correlated with their measure of redundant structure and strongly negatively correlated with their measure of synergistic structure in fMRI data, confirming its overall validity for assessing the redundancy-synergy balance at a population level.

The scalability of O-information has made the large-scale analysis of HOIs in the brain feasible for the first time. Applications to neuroimaging data have revealed that synergistic interactions are crucial for complex cognition and that the brain's dynamics involve transient fluctuations between states of high synergy and high redundancy [194].

The framework for computing O-information has recently undergone expansion, with the introduction of gradients of this metric. These gradients measure the irreducible contribution of a variable (or a group of variables) to the higher-order informational circuits of a system [190].

Partial information rate decomposition. A critical theoretical issue with applying measures like PID and O-information to fMRI data is that these measures were defined for sets of random variables, implicitly assuming the data points are independent and identically distributed (i.i.d.) [179]. However, fMRI time series are anything but i.i.d.; they possess a rich temporal correlation structure due to the slow hemodynamic response and underlying neural dynamics. Applying i.i.d.-based measures to time-correlated data is theoretically incorrect and can lead to a mischaracterization of the system's interactions.

To address this fundamental gap, the framework of Partial Information Rate Decomposition (PIRD) has recently been introduced [179]. PIRD extends the principles of PID to random processes with temporal structure. Instead of decomposing the mutual information between variables, PIRD decomposes the mutual information rate, a quantity from information theory that correctly accounts for the memory and temporal dynamics of the processes. This is a crucial theoretical development that paves the way for a more rigorous and accurate application of information decomposition techniques to fMRI and other neurophysiological time series.

4.4.3. Statistical validation of HOI measures

Given the high dimensionality, low SNR, and complex correlation structure of fMRI data, any claim of detecting HOIs must be supported by robust statistical validation to rule out spurious findings. Two primary methods are used for this purpose: surrogate data testing and bootstrap analysis [149].

Surrogate data testing is a non-parametric approach used to assess the statistical significance of an observed quantity against a well-defined null hypothesis [195]. In the context of HOI analysis, a commonly adopted null hypothesis posits that the observed HOIs arise purely as a byproduct of pairwise correlations, with no genuine higher-order structure present in the data. To evaluate this hypothesis, one constructs an ensemble of surrogate datasets that preserve key statistical properties of the original time series, such as their power spectra and amplitude distributions, while deliberately destroying the specific dependencies hypothesized to generate HOIs (e.g., higher-order phase coupling). A widely used method for generating such surrogates is the iterative amplitude-adjusted Fourier transform (iAAFT) algorithm [196]. The HOI measure is computed both for the empirical data and for each surrogate realization. The observed value is considered statistically significant if it lies in the extreme tail of the surrogate distribution, for instance, exceeding the 95th percentile (corresponding to a significance level of $p < 0.05$).

Bootstrap analysis is a methodological framework employed to estimate the uncertainty of a measure and to construct confidence intervals [197]. This is of particular importance when comparing HOIs between different conditions or groups, or for assessing significance at the single-subject level. For time series data, the block bootstrap procedure is most appropriate [78,198,199]. This method involves resampling the original time series not by individual points, but by randomly sampling and concatenating contiguous blocks of data. This procedure partially preserves the autocorrelation structure of the original signals. By re-computing the HOI measure on hundreds or thousands of these bootstrapped datasets, one can construct a sampling distribution of the measure and thereby derive confidence intervals or perform statistical tests between conditions.

4.5. Machine learning techniques for assessing HOIs

The most advanced approaches to quantifying HOIs leverage the power of AI, specifically, modern ML methods. Unlike traditional statistical or information-theoretic methods, which rely on explicit, pre-defined mathematical formulations to measure interactions, ML-based techniques aim to uncover complex, nonlinear dependencies directly from data. This is typically achieved by casting the problem in terms of prediction or representation learning: HOIs emerge as the latent structures or patterns that a model learns in order to successfully perform a given task, such as forecasting, classification, or generative modeling. By doing so, these methods offer a data-driven, flexible framework for detecting and characterizing higher-order dependencies that may elude conventional analytical approaches.

4.5.1. Feature selection and dimensionality reduction for HOIs

One powerful and intuitive way to conceptualize HOIs is through the lens of regression. The functional interaction underlying a hyperedge can be thought of as the collective influence of a set of source regions, $\{x_1, \ldots, x_p\}$, on a target region, y. The goal, then, is to identify the specific subset of source regions that best predicts the activity of the target. Given the high number of potential source regions in the brain, this becomes a problem of high-dimensional feature selection [200,201].

Sparse representation based methods and least absolute shrinkage and selection operator (LASSO). A prominent application of sparse regression in the context of HOIs is the *Sparse Representation (SR)*, which directly constructs functional connectivity hyper-networks from fMRI time series [202]. In this framework, the time series of a target brain region is expressed as a sparse linear combination of the time series of all other regions by solving a LASSO-type optimization problem. LASSO is a penalized regression method that is exceptionally well-suited for the "small n, large p" problem (few time points, many potential predictors) characteristic of fMRI data [200,203,204]. It modifies the standard least-squares regression by adding a penalty term proportional to the sum of the absolute values of the regression coefficients (the L^1-norm). The optimization problem is:

$$\hat{\beta} = \arg\min_{\beta} \left\{ \frac{1}{2n} \|\mathbf{y} - \mathbf{X}\beta\|_2^2 + \lambda \|\beta\|_1 \right\}, \tag{36}$$

where $\hat{\beta}$ is the vector of coefficients we are solving for and λ is the regularization parameter ($\lambda \geq 0$). The key property of the L^1-penalty is that it forces the coefficients of many irrelevant or redundant features to become exactly zero. This performs automatic feature selection, yielding a sparse model. In the context of HOIs, one can regress the time series of

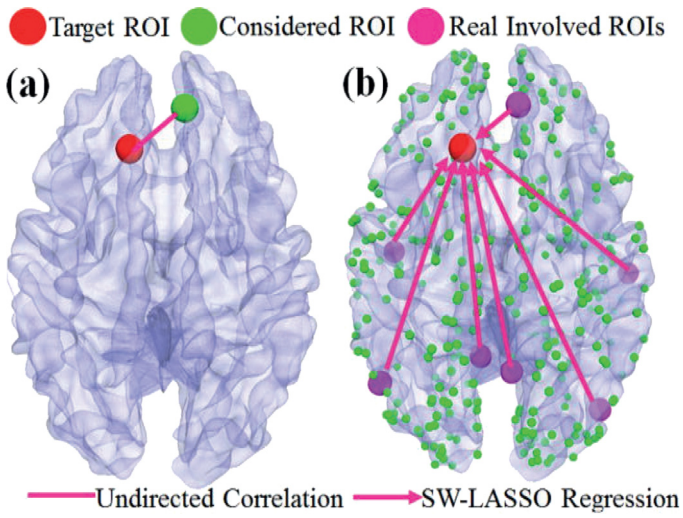

Fig. 18. (a) Pairwise functional connectivity and (b) higher-order interactions (HOIs) identified via the sliding-window LASSO (SW-LASSO) approach. Green dots denote all candidate regions of interest (ROIs) considered in the analysis; pink dots highlight the subset of ROIs that were actively selected by the SW-LASSO regression at a given time window. In (a), undirected lines represent conventional pairwise correlations. In (b), directed arrows indicate the influence of predictor ROIs on the target ROI within the SW-LASSO regression framework, reflecting the directionality inherent in the predictive modeling of HOIs.
Source: Adapted from [200].

each ROI against the time series of all other ROIs. The non-zero coefficients in the resulting model identify the sparse set of regions that collectively predict the target's activity, thereby defining a directed hyperedge.

This SR-based hyper-network model offers several advantages. It automatically filters out spurious or weak connections, leading to a more interpretable and robust network topology. Moreover, by varying the sparsity parameter λ, multiple hyper-edges can be generated for each region, reflecting different levels of interaction granularity. This multi-level representation enriches the feature set extracted from the hyper-network, such as clustering coefficients, which can then be used for downstream tasks like disease classification [202].

However, standard LASSO has a notable limitation in the context of brain networks: when faced with a group of highly correlated predictors (as is common for regions within a single functional network), it tends to arbitrarily select just one predictor from the group and discard the others [204].

Extensions of LASSO for structured brain data. To address the limitations of standard LASSO and better adapt it to the unique structure of brain data, several important extensions have been proposed:

- *Group LASSO.* This variant is designed specifically for situations where predictors have a known group structure [204, 205]. Instead of penalizing individual coefficients, it penalizes the L^2-norm of entire groups of coefficients. This encourages sparsity at the group level, meaning the model selects or discards entire groups of correlated variables together. For brain data, groups can be defined based on anatomical atlases or known functional networks.
- *Sparse Group LASSO (sgLasso).* This method provides a powerful compromise between standard and group LASSO. It incorporates both an L^1-penalty (promoting sparsity of individual features within groups) and a group-level penalty (promoting sparsity between groups). This bi-level selection allows the model to discard unimportant entire networks, while also refining the selection to only the most relevant regions within the important networks [204].
- *Structurally-Weighted LASSO (SW-LASSO).* This approach represents a sophisticated integration of multimodal data [200]. It uses prior information from structural connectivity, typically derived from Diffusion Tensor Imaging (DTI), to guide the functional interaction model. The LASSO penalty is adaptively weighted such that regression coefficients corresponding to pairs of regions with strong anatomical connections receive a smaller penalty, making them more likely to be included in the final model. This biases the search towards neurobiologically plausible interactions and provides a principled way to constrain the vast model space, improving both computational efficiency and interpretability. The example is shown in Fig. 18.

4.5.2. Deep learning approaches for capturing nonlinear HOIs

The most recent and rapidly advancing frontier in HOI assessment involves the application of DL. The fundamental paradigm shift offered by DL is its capacity for *end-to-end representation learning*. Instead of relying on the researcher to first engineer features from the data (e.g., by calculating a correlation matrix or defining a regression model), deep

neural networks can learn complex, hierarchical, and nonlinear feature representations directly from the raw or minimally processed fMRI time series [206]. By doing so, they can implicitly capture spatiotemporal dependencies of arbitrary complexity, including HOIs, that are optimized for a given predictive task.

Early approaches: CNNs and RNNs. Early applications of DL to fMRI often employed architectures that were successful in other domains. Convolutional Neural Networks (CNNs), renowned for their success in image analysis, were adapted to learn spatial patterns from fMRI volumes. Specifically, the study by Meszlényi et al. [207] developed a CNN architecture for functional connectome classification, called the connectome convolutional neural network (CCNN). This architecture has demonstrated high efficiency in distinguishing between subject groups.

Recurrent Neural Networks (RNNs) and their more advanced variants like Long Short-Term Memory (LSTM) networks, designed for sequential data, were used to model the temporal evolution of BOLD signals. Ensembles of RNNs, for example, have been used to predict general intelligence directly from fMRI regional time series, successfully bypassing the intermediate step of FC calculation [208]. Vieira et al. [206] adapted the Inception Time temporal CNN architecture, which jointly predicted human traits directly from regional time series through representation learning. While promising, these architectures have known limitations in capturing the complex, long-range spatiotemporal dependencies characteristic of whole-brain dynamics.

Graph neural networks. A particularly natural framework for network neuroscience is the Graph Neural Network (GNN)—a class of DL architectures explicitly designed to operate on graph-structured data [209]. In typical applications, the brain is first modeled as a graph in which ROIs serve as nodes, and edges are defined by an initial connectivity matrix, often derived from simple pairwise measures such as Pearson correlation. The GNN then learns node-level representations through a message-passing (or neighborhood aggregation) mechanism: at each layer, the representation of a node is updated by aggregating information from its immediate neighbors in the preceding layer [39,210].

The true strength of GNNs for detecting HOIs lies in their hierarchical receptive field expansion. After a single message-passing layer, a node's representation encodes information from its 1-hop neighborhood; after L layers, it integrates signals from nodes up to L hops away. Consequently, the deep, multi-layer architecture of a GNN enables it to construct increasingly global representations that implicitly capture complex, multi-node interaction patterns—effectively uncovering higher-order topological structures that are not present in the original pairwise connectivity matrix. This capacity to go beyond dyadic relationships makes GNNs especially powerful for modeling the brain's intricate functional architecture. Indeed, GNNs have shown remarkable success in neuroimaging applications, consistently outperforming conventional neural networks in tasks such as disease classification, cognitive state prediction, and individual subject identification [211].

Transformers. The current state-of-the-art in modeling complex sequential data comes from Transformer architectures, which have revolutionized natural language processing and are now being successfully applied to fMRI time series [212]. The core innovation of the Transformer is the *self-attention mechanism*. This mechanism allows the model, when processing a single element in a sequence (e.g., the brain state at one time point), to dynamically weigh the importance of all other elements in the sequence and construct a context-aware representation [213].

This is exceptionally powerful for fMRI data. A Transformer can simultaneously attend to both spatial context (which other regions are co-active?) and temporal context (what were the relevant preceding brain states?), enabling it to capture long-range spatiotemporal dependencies in a highly flexible, data-driven manner. Crucially, many Transformer-based models, such as the BolT architecture [212], operate directly on the multivariate time series from all ROIs without requiring a pre-specified graph structure. The self-attention mechanism effectively learns the relevant connectivity patterns, both pairwise and higher-order, that are most informative for the task at hand. These models have demonstrated superior performance against other state-of-the-art methods in a range of challenging neuroimaging prediction tasks [212,213].

The evolution within the machine learning domain – from LASSO, to GNNs, to Transformers – reflects a clear and accelerating trend away from explicit, human-driven feature engineering and towards automated, end-to-end representation learning. This progression represents a growing confidence in the ability of powerful, data-hungry models to discover functionally relevant HOIs implicitly, without the need for a researcher to define them with a precise statistical formula. However, this power comes at the cost of interpretability. While a significant cokurtosis value has a clear mathematical meaning, the "higher-order interaction" learned by a Transformer is embedded implicitly within millions of model weights and is notoriously difficult to extract and interpret. This creates a productive tension in the field: statistical and information-theoretic methods are superior for testing specific, interpretable scientific hypotheses, whereas deep learning models often provide superior predictive power for clinical or diagnostic applications. A key direction for future research lies in developing methods for "explainable AI" (XAI) that can bridge this gap, allowing us to peer inside the "black box" of these powerful models to extract the novel and interpretable principles of brain function they have learned.

5. HOIs in neuroscience and clinical applications

Traditional models of functional brain connectivity, which are based on pairwise correlation analysis, have laid the foundation for the study of brain function and computational diagnosis of neurological and psychiatric disorders. However, our growing understanding of the brain as a complex, hierarchical system whose functioning cannot be reduced to

Table 4
Summary on the most relevant studies on the application of the higher-order interactions (HOIs) concept to fMRI-derived functional networks (see Table A.1 in the Appendix for the detailed description.

Application \ Method	Information-Theoretic Approaches	Statistical Approaches	ML-based Approaches	Simplicial Complexes Identification
Normal Brain Function	[31,215]	[216–218] [33,78]	[219,220]	[221]
AD/MCI	[222]	[223–225] [228–230] [234,235]	[202,226,227] [231–233] [75]	–
PD	[236]	–	–	[221]
ASD	[237]	[238–240] [67]	[241–243] [232,233,244] [39]	–
ADHD	–	–	[39,202,243] [245]	–
MDD	–	[246]	[247–249] [245,250]	[65]
SCZ	[214]	[156]	–	–
AnD	–	–	[251]	–
Other: disorders of consciousness, multiple sclerosis, altered states of consciousness	[149]	[78]	–	[77]

binary connections has revealed the limitations of these approaches. Modeling HOIs, which account for the simultaneous influence of multiple neural populations, has emerged as a relevant research direction. This section reviews findings on neurological and psychiatric disorders, as well as normal brain function, obtained by investigating HOIs. Analysis of existing studies shows that considering the high-level organization of brain networks improves classification accuracy and precision in identifying biomarkers. Consequently, this opens new avenues for understanding normal brain function, its development, and the pathophysiological mechanisms underlying various disorders.

5.1. Landscape of current studies

First, we have compiled a summary of key studies that use HOI methods to analyze fMRI-derived functional networks in order to synthesize the rapidly growing body of literature on this topic (see Table 4 for a summary and Table A.5 in the Appendix for the detailed description). The table is organized by the primary methodological approach used to assess HOIs: Information-Theoretic, Statistical, ML-based, and Approaches Based on Simplicial Complexes. This section describes the scope of the table and discusses the observed methodological trends, evolution of application domains, and the emerging distinction between different conceptual uses of "higher-order" in the field.

The application of HOIs has evolved in both methodology and scope. Early pioneering studies, such as those by Plis et al. [214] and Petri et al. [77], demonstrated that HOIs could detect disease-related changes and altered states of consciousness missed by pairwise methods. These works primarily employed information-theoretic measures and topological data analysis, establishing the foundational premise that brain dynamics are fundamentally high-order.

Subsequently, the field saw a surge in statistical approaches, particularly methods based on "correlation's correlation" or edge-based functional connectivity (eFC). These methods, which construct hypergraphs where hyperedges represent correlated time series between pairs of connections, proved highly effective for improving classification accuracy in various disorders, including Autism Spectrum Disorder (ASD), Mild Cognitive Impairment (MCI), Alzheimer's Disease (AD), and Major Depressive Disorder (MDD). A consistent finding across these studies is that HOI features provide complementary information to low-order networks, and their fusion often yields superior discriminative power for ML classifiers.

More recently, ML-based approaches have become dominant, particularly with the rise of hypergraph neural networks (HGNNs). These methods leverage the flexible structure of hypergraphs not only to represent complex brain connectivity but also to build powerful predictive models. This shift has been accompanied by a growing emphasis on dynamic HOIs, multimodal data integration (e.g., combining fMRI with DTI or sMRI), and the development of more sophisticated, learnable hypergraph constructions.

While a significant driver of HOI research has been the search for clinical biomarkers, these methods are equally powerful for investigating fundamental neurobiology in healthy and developing populations. For instance, studies have leveraged HOIs to trace developmental changes in the youth brain, showing that the organization of hyperedges evolves with age, particularly within the brain's functional core [217,220]. Furthermore, the study of healthy aging across the lifespan has revealed a systematic shift in the brain's functional architecture [215]. HOIs have also been used to probe

normal brain function during tasks and individual differences, demonstrating their utility in mapping the full spectrum of human brain organization beyond pathology [33,218].

Alongside hypergraphs, another mathematical framework for capturing HOIs is gaining traction: simplicial complexes analyzed with Topological Data Analysis (TDA). While currently less prevalent than hypergraph-based methods, this approach offers a distinct and powerful perspective. Instead of modeling arbitrary groups of regions (hyperedges), simplicial complexes enforce a combinatorial structure where, for example, a connection between three regions (a 2-simplex) requires the existence of all three constituent pairwise connections (1-simplices). This provides a more constrained but topologically rich representation of brain connectivity.

TDA techniques, such as persistent homology, can then be used to identify and quantify the presence of higher-order topological features like cycles and cavities in the network's structure, which are thought to reflect robust communication pathways and computational capacity. Early applications have shown promise, for example, in revealing how psilocybin alters the stability of mesoscopic cycles in the brain [77], in identifying local HOI "homological scaffolds" that outperform pairwise methods in task decoding and brain fingerprinting [33], and in uncovering reduced topological complexity in MDD [65]. These approaches directly characterize the shape of the data, offering a multiscale, noise-robust view of network architecture. Although the computational interpretation of these topological features is an ongoing challenge, their ability to reveal global, invariant properties of the connectome suggests they have significant potential for uncovering fundamentally new principles of brain organization.

The choice of application domain in HOI research is often heavily influenced by the availability of large, well-characterized, publicly available datasets. The widespread use of datasets like the Autism Brain Imaging Data Exchange (ABIDE) for ASD, the Alzheimer's Disease Neuroimaging Initiative (ADNI) for AD/MCI, and others for ADHD and MDD, is evident in Appendix. This has enabled rapid benchmarking and comparison of new HOI methods against established baselines. While this has accelerated methodological development, it has also concentrated research efforts on these specific disorders, with other neurological conditions being less explored.

A notable trend, particularly within ML-based approaches, is the expansion of the term "higher-order interaction". In classical neuroscience usage, HOIs refer to the simultaneous, non-decomposable interactions between multiple brain regions within a single subject's brain—the genuine polyadic dependencies that this review has focused on thus far. However, in many modern ML and HGNN applications, the "higher-order" concept is repurposed. Here, a hypergraph is often constructed where hyperedges represent relationships between subjects (e.g., connecting subjects with similar functional connectivity profiles), or to integrate multi-view data (e.g., where each brain parcellation atlas is a view) or multi-task data for a single subject. In this context, the hypergraph is a tool for representing complex sample relationships or data structures for a downstream classification task, rather than directly modeling the higher-order dependencies between regions in an individual's functional network. This is a powerful and valid approach, but it is conceptually distinct from using HOIs to describe the intrinsic multi-region dynamics of the brain itself. This distinction is important for interpreting the findings of such studies, as the "HOI features" they identify may reflect group-level similarities or fused multimodal patterns, rather than the classical definition of within-brain polyadic neural interactions.

For example, a study by Zu et al. [252] used the "higher-order" concept to model the complex, multisubject relationships between individuals based on their brain network features (see Fig. 19). In this framework, a hypergraph is constructed where each vertex represents a subject. Hyperedges are then formed by grouping subjects that show similar functional connectivity patterns within a specific, pre-defined brain subnetwork (e.g., a triad of regions). This creates a higher-order structure where a single hyperedge can connect multiple subjects, capturing group-wise similarities that go beyond simple pairwise subject comparisons. The goal of the subsequent hypergraph learning is to identify which of these subnetworks give rise to hyperedges that best separate the clinical groups (e.g., patients vs. controls), thereby serving as diagnostic biomarkers.

5.2. Normal brain function in healthy people

5.2.1. Resting-state functional connectivity in healthy youth

The application of hypergraph theory to neuroscience represents a methodological advancement for characterizing higher-order interactions in brain networks. This approach was notably implemented in the study by Gu et al. [217], which investigated the functional brain organization of 780 youth from the Philadelphia Neurodevelopmental Cohort, aged 8–22 years. The cohort included 333 males and 447 females, all scanned using identical Siemens Tim Trio 3T MRI protocols with resting-state fMRI acquisition parameters of TR/TE = 3000/32 ms, providing 124 volumes per subject. This substantial developmental sample enabled the examination of how functional connectivity patterns co-vary across individuals and evolve during adolescence.

The methodological framework treated functional connections rather than brain regions as the fundamental unit of analysis as shown in Fig. 20(A). For each subject, functional connectivity matrices were constructed using wavelet coherence between 264 functionally defined regions from the Power atlas, operating within the frequency interval of 0.01–0.08 Hz. This approach generated 34 716 unique functional connections per subject. The critical innovation lay in constructing a hypergraph where edges became nodes: for each possible pair of functional connections (i, j) and (k, l), the Pearson correlation coefficient was computed between their weight vectors across all subjects, forming a massive edge-by-edge adjacency matrix $\mathbf{H}$ of dimensions $34\,716 \times 34\,716$. This approach is an evolution of edge functional connectivity

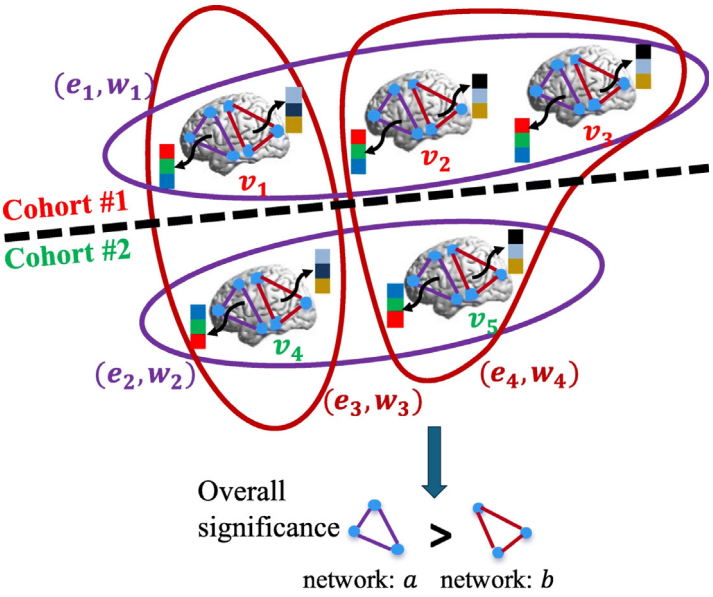

Fig. 19. Hypergraph construction for identifying disease-related subnetworks through higher-order subject relationships. Subjects from two cohorts (e.g., patients and controls) are represented as vertices (v_1 to v_5). For each candidate brain subnetwork (illustrated here by the purple and red triangular motifs), hyperedges (curved connectors) are formed by linking a subject – acting as a centroid – with its k-nearest neighbors, where neighborhood is defined by similarity in functional connectivity patterns within that specific subnetwork. This yields a hypergraph in which each hyperedge can simultaneously connect multiple subjects, thereby encoding complex, group-wise similarity structures that go beyond pairwise relationships and enable the detection of disease-associated network signatures.
Source: Adapted from [252].

(eFC). This hypergraph representation captured how groups of functional connections co-varied in strength across the population, with statistical thresholding applied to control false positives ($p < 0.05$).

Community detection applied to this hypergraph revealed 363 significant hyperedges – groups of co-varying functional connections – that segregated into three distinct topological classes with specific neurophysiological interpretations (see Fig. 20(B)). The most numerous were star hyperedges (326 instances), characterized by focal architectures where multiple connections converged onto a small set of hub regions (1–3 nodes). These stars demonstrated significantly higher edge-wise correlation than traditional node-based functional modules ($Q < 0.001$ for 11 of 13 major systems), suggesting they represent fundamental, highly cohesive functional units. Neuroanatomically, star hyperedges were widely distributed across the cortex, particularly in frontal-parietal regions, indicating their role as localized integration centers.

In contrast, cluster hyperedges (6 instances) formed densely interconnected systems that closely recapitulated known functional networks, including visual, somatomotor, default mode, and salience systems. These clusters occupied a central position in the hypergraph architecture, with two clusters, one in the visual system and another in the default mode network, showing significant strengthening with age (visual: $t = 3.25$, $p = 0.0012$; default mode: $t = 5.70$, $p = 1.69 \times 10^{-8}$). This developmental trajectory suggests cluster hyperedges represent the maturing functional core of the brain's functional network architecture.

Finally, bridge hyperedges (31 instances), exhibited bipartite topology, exclusively connecting two disjoint sets of brain regions without within-set connections. Fig. 20(C) illustrates how bridges connect stars to clusters. Statistical analysis revealed these bridges preferentially linked cluster hyperedges to star hyperedges ($p < 1 \times 10^{-20}$), forming integrative pathways between the densely connected core and the distributed periphery (see Fig. 20(D)). This connectivity pattern suggests a core–periphery organization where bridges facilitate information transfer between established functional systems and specialized processing centers.

The neurophysiological implications of this hypergraph decomposition are substantial. The tripartite architecture – stable core clusters, widely distributed stars, and integrative bridges – provides a novel perspective on functional brain organization that transcends traditional node-based modular descriptions. Developmentally, the concentration of age-related effects in cluster hyperedges suggests that adolescence is characterized primarily by the strengthening of within-system connectivity in major functional networks, while the architecture of local integrators (stars) and their long-range links (bridges) remains relatively stable. This pattern aligns with theories emphasizing network segregation during this developmental period.

Methodologically, this hypergraph approach demonstrates that treating edges as computational units reveals organizational principles invisible to conventional node-centric analyses. The findings establish that functional connections

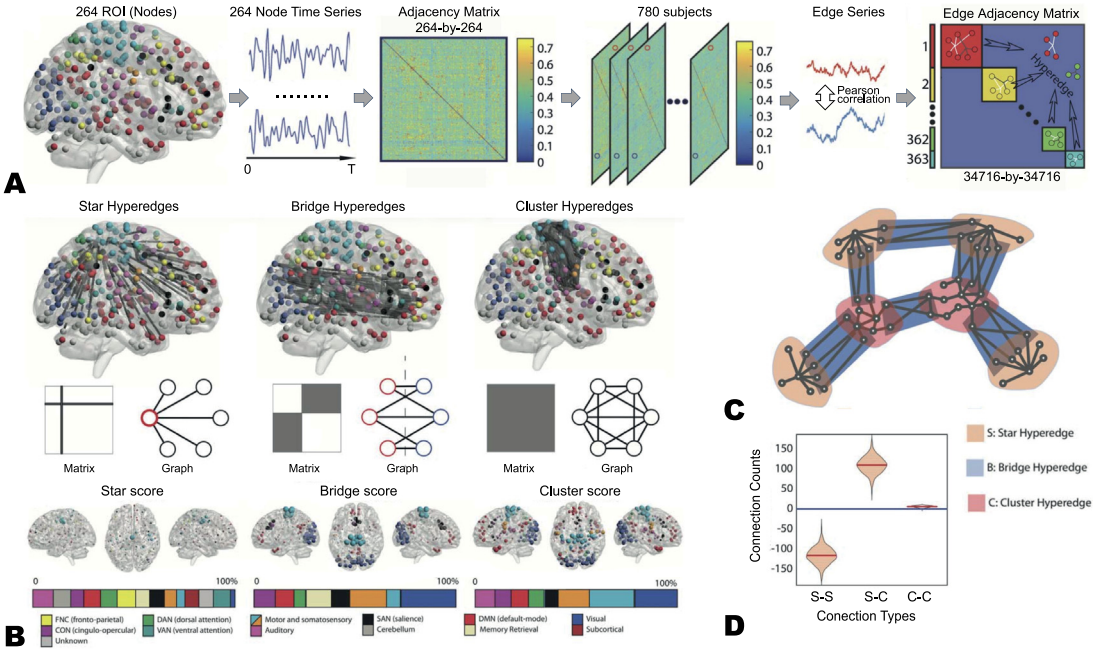

Fig. 20. Functional hypergraph to uncover covariant structures over neurodevelopment. (A) Schematic overview of hypergraph construction from resting-state functional MRI data. The process begins with the extraction of regional BOLD time series from 264 brain regions of interests (ROI) for each of the 780 subjects. For each subject, a functional connectivity matrix is computed using wavelet coherence between all pairs of regions. These subject-specific adjacency matrices are stacked to form a 3D data structure. The vector of connection strengths for each possible edge (regional pair) is then extracted across all subjects. Finally, a hypergraph is generated by computing the Pearson correlation between every pair of these edge-wise vectors, resulting in an edge-by-edge adjacency matrix. In this hypergraph, clusters of significantly co-varying edges, known as hyperedges, are identified using community detection techniques. (B) Hyperedge archetypes and their spatial distributions. The functional hypergraph revealed three distinct classes of co-varying connections: star, bridge, and cluster hyperedges. Regional participation was quantified through star, bridge, and cluster scores, showing differential involvement across brain systems. The star score of a node is defined as the number of times it serves as the core of a star hyperedge. The bridge score and cluster score are defined as the number of edges from bridge or cluster hyperedges, respectively, that are incident to the node. Bar plots show the distribution of these weighted scores across major functional systems, normalized by the number of ROIs. (C) Schematic illustration of the integrative role of bridge hyperedges (blue) connecting star (peach) and cluster (pink) structures demonstrating that bridge hyperedges preferentially link core clusters to peripheral stars. (D) Statistical comparison against a null model confirms that star-cluster connections are significantly enriched, while star-star connections are significantly suppressed.
Source: Adapted from [217]; licensed under a Creative Commons Attribution 4.0 International license.

organize into coherent higher-order structures with distinct topological roles and developmental trajectories. Future applications could extend this framework to longitudinal designs, clinical populations, and multimodal data integration, potentially revealing how alterations in hyperedge architecture relate to cognitive development and neuropsychiatric disorders.

5.2.2. Multi-hypergraph learning for cognitive prediction

The multi-hypergraph learning framework introduced by Xiao et al. [219] represents a substantial methodological leap beyond earlier hypergraph-based approaches in neuroscience. Whereas conventional methods typically assign uniform weights to all hyperedges and extract only basic topological descriptors, Xiao et al. propose a data-driven, adaptive weighting scheme that learns the functional relevance of each hyperedge through a principled optimization process. Specifically, hyperedge weights are tuned to best explain the observed dynamics of resting-state fMRI time series, under the biologically plausible assumption that the BOLD signal varies smoothly over the underlying higher-order functional architecture.

This is formalized as a regularized optimization problem that minimizes the trace of the product between the hypergraph Laplacian and the empirical covariance matrix of the fMRI data—effectively aligning the geometric structure of the hypergraph with the statistical dependencies in the neural signals. The regularization term ensures non-degenerate solutions and enhances generalizability. By endowing hyperedges with context-sensitive weights, the framework captures nuanced, behaviorally relevant patterns of multi-node interaction that uniform-weight models inevitably overlook.

A key limitation in neuroimaging research is the reliance on single experimental paradigms, which, despite engaging partially overlapping neural systems, fail to capture the full complexity of human cognition. To address this, multi-hypergraph learning extends the hypergraph framework by enabling the joint integration of data across multiple fMRI paradigms. In this approach, incidence matrices from each paradigm are concatenated to form a unified representation,

and hyperedge weights are optimized jointly across all tasks. This yields a single, integrated hypergraph similarity matrix that synthesizes complementary information from diverse cognitive contexts, thereby providing a more comprehensive characterization of an individual's functional brain architecture.

Empirical validation on the Philadelphia Neurodevelopmental Cohort (PNC) demonstrates the power of this approach: multi-hypergraph learning significantly outperformed conventional methods in predicting cognitive ability, as indexed by scores on the Wide Range Achievement Test (WRAT). This performance gain highlights the added value of modeling higher-order, multi-node interactions – beyond pairwise connectivity – in capturing behaviorally relevant neural signatures.

Analysis of the learned hypergraph similarity matrices revealed that the most discriminative connections for WRAT prediction were concentrated within a distributed network involving frontal, temporal, and posterior midline regions. Specifically, high- and low-performing individuals were most strongly differentiated by hyperedges linking: (i) the right superior frontal gyrus and the right angular gyrus, (ii) the right middle frontal gyrus and the right precuneus, and (iii) the left medial frontal gyrus and the bilateral middle temporal poles.

Moreover, a subset of regions consistently emerged as hubs within these discriminative hyperedges. Ranked by frequency of participation, the top discriminative ROIs were: the right precuneus, right superior frontal gyrus, left middle temporal gyrus, right posterior cingulate cortex, right insula, and left middle temporal pole—highlighting a core set of higher-order association areas that support learning and academic achievement.

These findings are neurophysiologically significant as they align with established knowledge about the brain's functional architecture for higher cognition. The identified network strongly implicates the frontoparietal control network (involving superior/middle frontal gyri and angular gyrus) and the default mode network (involving posterior cingulate, precuneus, and medial frontal regions). The hypergraph method specifically highlighted the interaction between these typically anti-correlated networks, suggesting that their coordinated higher-order interaction is a key neurophysiological feature underlying learning ability. The involvement of the temporal lobe regions further points to the integration of semantic and memory-related processes with executive control systems.

In essence, the novel contribution is not the discovery of these regions in isolation, but the revelation that their complex, high-order functional interplay – captured uniquely by the weighted hypergraph model – serves as a more sensitive and informative biomarker for individual cognitive differences than the pairwise connections identified by traditional graph-based methods.

5.2.3. Brain functional connectome analysis using dynamic weighted hypergraphs

Wang et al. [220] introduce a significant advance in functional connectome modeling through the development of the dynamic weighted hypergraph convolutional network (dwHGCN)—an end-to-end deep learning framework that unifies dynamic hypergraph learning with neural representation learning. In contrast to conventional hypergraph neural networks, which operate on static hypergraphs with fixed edge weights derived a priori, dwHGCN dynamically refines hyperedge weights during training (see Fig. 21), allowing the model to emphasize hyperedges that carry the greatest discriminative information for the task at hand.

This adaptive mechanism enables the network to capture time-varying, higher-order interactions among brain regions with greater fidelity. Moreover, by incorporating a manifold regularization term that enforces smoothness of the fMRI signal over the evolving hypergraph structure, dwHGCN ensures that the learned representations remain grounded in neurophysiological plausibility. The result is a model that not only achieves superior performance in downstream classification tasks but also enhances interpretability, explicitly identifying task-relevant brain regions and their multi-way functional interactions. Consequently, dwHGCN represents a marked improvement over both standard graph-based approaches and static hypergraph methods, offering a more expressive and biologically informed framework for probing the brain's functional architecture.

The core mathematical constructs center around a dynamically weighted hypergraph structure. A hypergraph is formally defined as $\mathcal{G} = (\mathcal{V}, \mathcal{E}, \mathbf{w})$, where $\mathcal{V}$ represents the set of vertices corresponding to brain ROIs, $\mathcal{E}$ denotes the set of hyperedges capturing higher-order interactions, $\mathbf{w}$ constitutes the vector of hyperedge weights, and $\mathbf{A} = diag(\mathbf{w}) \in \mathbf{R}^{M\times M}$ denotes the diagonal matrix of the hyperedge weights, where hyperedges with larger weights are considered more informative in representing the hyper network. The incidence relationships are encoded in the matrix $\mathbf{H} \in \mathbb{R}^{N\times M}$, with elements defined by $H_{ij} = 1$ if vertex v_i belongs to hyperedge e_j, and 0 otherwise.

A fundamental advancement over conventional approaches lies in the dynamic weighting mechanism, where hyperedge weights $\mathbf{w}$ are adaptively updated during model training according to

$$\mathbf{w}^{(t)} = \mathbf{w}^{(t-1)} - \eta \frac{\partial \mathcal{L}}{\partial \mathbf{w}^{(t-1)}}. \tag{37}$$

This dynamic adjustment enables the model to prioritize hyperedges with greater discriminative power. Furthermore, the framework incorporates manifold regularization to ensure topological consistency with the underlying neurobiological data. The regularization term

$$\mathcal{L}_m(\mathbf{w}) = \mathrm{tr}(\mathbf{F}^T \mathbf{L}_{(\mathbf{w})} \mathbf{F}) + \rho \|\mathbf{w}\|_2^2 \tag{38}$$

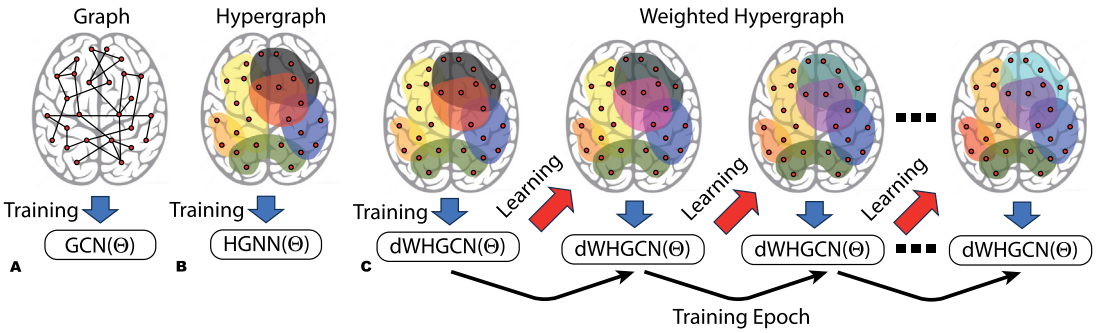

Fig. 21. Comparison of graph and hypergraph neural architectures for modeling brain connectivity. **(A)** The graph convolutional network (GCN) operates on pairwise functional connectivity graphs and has been widely used in neuropsychiatric classification tasks (e.g., autism spectrum disorder [253], Alzheimer's disease [253,254], major depressive disorder [255]). **(B)** The hypergraph neural network (HGNN) [256] extends graph-based learning to HOIs by representing the brain as a hypergraph. However, most existing HGNN implementations assume uniform hyperedge weights, thereby neglecting potentially informative variations in the strength or relevance of multi-region interactions [257]. **(C)** The dynamic weighted hypergraph convolutional network (dwHGCN) [220] overcomes this limitation by jointly optimizing both the neural network parameters Θ and the hyperedge weights w in an end-to-end fashion. At each training epoch, the hypergraph $\mathcal{G}(\mathbf{w})$ is updated to emphasize hyperedges with greater discriminative power, yielding a data-adaptive, weighted representation of functional brain connectivity that better captures behaviorally relevant higher-order organization. Based on data from [220].

imposes smoothness constraints on the fMRI signals $\mathbf{F}$ over the learned hypergraph structure, where ρ is a positive coefficient for the ℓ_2 penalty. A small value of ρ leads to a decrease in weights, while a large value of ρ—to the assignment of equal weights to all hyperedges. $\mathbf{L}$ represents the normalized hypergraph Laplacian operator

$$\mathbf{L} = \mathbf{I} - \mathbf{D}_v^{-1/2}\mathbf{H}\mathbf{A}\mathbf{D}_e^{-1}\mathbf{H}^\top\mathbf{D}_v^{-1/2}, \tag{39}$$

where $\mathbf{I}$ is an identity matrix, $\mathbf{D}_v$ and $\mathbf{D}_e$ are the diagonal matrices of vertex degrees and hyperedge degrees, respectively.

The empirical evaluation was conducted using the Philadelphia Neurodevelopmental Cohort (PNC), a comprehensive neuroimaging dataset. The cohort comprises over 1 400 typically developing adolescents and young adults aged 8 to 22 years. Multimodal functional MRI data were acquired, including resting-state fMRI, task-based fMRI during working memory performance (n-back paradigm), and task-based fMRI during emotion identification (emoid paradigm). Whole-brain parcellation was performed according to the functional template by Power et al. [258], resulting in 264 ROIs. The study addressed two primary classification tasks: age group discrimination (children under 12 years versus young adults over 18 years) and cognitive ability classification based on WRAT scores (high versus low performance groups).

The proposed dwHGCN substantially outperforms static hypergraph models, achieving a 4.9% absolute improvement in accuracy on age classification tasks. This performance enhancement stems from the model's capacity to dynamically adjust hyperedge weights during training, effectively prioritizing neurobiologically meaningful interactions. Beyond predictive accuracy, the framework offers significant advances in model interpretability. Through integration of Gradient-weighted Class Activation Mapping (Grad-CAM) and analysis of learned hyperedge weights, the model identifies and visualizes the most discriminative brain regions and their higher-order interactions. The incorporation of manifold regularization further ensures that the learned hypergraph structure maintains physiological plausibility by enforcing smoothness of fMRI signals across connected nodes, thereby enhancing the neurobiological validity of the extracted features.

From a neuroscientific perspective, the analysis reveals several key brain regions associated with neurodevelopment and cognitive function. In the context of brain maturation, the model identifies the cingulate gyrus as a crucial region regulating cognitive and emotional development during adolescence. The inferior temporal gyrus demonstrates a characteristic late maturation pattern extending into young adulthood, while the fusiform gyrus shows prolonged developmental trajectories consistent with established literature on gray matter volume changes.

For cognitive ability classification based on WRAT scores, the framework identifies networks predominantly located within parietal and frontal cortices. The inferior parietal lobule emerges as a key component of the cerebello-parietal network previously associated with general intelligence. The precuneus shows positive association with cognitive performance, while superior and middle frontal gyri contribute significantly to working memory capabilities. The anterior cingulate cortex, identified across analyses, appears to play a modulatory role in both developmental processes and cognitive control functions. These findings collectively demonstrate that hypergraph representations can capture complex, higher-order interactions between brain regions that transcend simple pairwise connectivity, providing a more comprehensive framework for understanding the neural substrates of cognitive development and function.

5.2.4. Multitask feature selection across cognitive domains

The application of hypergraph-based multitask learning to fMRI data represents a significant methodological advancement for identifying task-related brain regions across diverse cognitive domains. The fundamental mathematical framework, as exemplified by Qu et al. [259], formulates feature selection as a multitask learning problem where distinct

temporal segments of the fMRI time series are treated as separate but related tasks. The core objective function integrates several regularization terms to leverage the intrinsic structure of the neural data:

$$\min_{\mathbf{W}} \frac{1}{2} \sum_{i=1}^{m} \left\| \mathbf{Y}^i - \mathbf{X}^i \mathbf{w}^i \right\|_2^2 + \lambda_1 \|\mathbf{W}\|_{2,1} + \lambda_2 \sum_{i=2}^{m} \left\| \mathbf{w}^i - \mathbf{w}^{i-1} \right\|_2 + \lambda_3 \mathbf{R}, \tag{40}$$

where $\mathbf{W} = [\mathbf{w}^1, \mathbf{w}^2, \ldots, \mathbf{w}^m] \in \mathbb{R}^{d \times m}$ is the feature weight matrix across m tasks (time windows); $\mathbf{X}^i = (\mathbf{x}_1^i, \mathbf{x}_2^i, \ldots, \mathbf{x}_N^i)^\top \in \mathbb{R}^{d \times m}$ consists of training samples from N subjects for ith task, where $\mathbf{x}_j^i \mathbb{R}^d$ represents the signals from d brain regions for jth subject at time i; $\mathbf{Y}^i \in \mathbb{R}^N$ represents the class labels, which indicate whether subjects are in a resting state or engaged in specific task states. The term $\|\mathbf{W}\|_{2,1} = \sum_{i=1}^{d} \|\mathbf{w}_i\|_2$ defines $\ell_{2,1}$-norm of $\mathbf{W}$ with $\mathbf{w}_i$ denoting the ith row of $\mathbf{W}$ and promotes group sparsity, encouraging the model to select a common set of relevant brain regions across all temporal tasks. The temporal smoothness term $\sum_{i=2}^{m} \left\| \mathbf{w}^i - \mathbf{w}^{i-1} \right\|_2$ imposes a constraint on the temporal consistency of the feature weights, reflecting the premise that neural representations evolve smoothly over time. The hypergraph regularization term is crucial for preserving the high-order relationships among subjects and defined as $\mathbf{R} = \sum_{i=1}^{m} \mathbf{w}^{i\top} \mathbf{X}^{i\top} \mathbf{L} \mathbf{X}^i \mathbf{w}^i$ based on the normalized hypergraph Laplacian (39).

Thus, each hypergraph vertex represents a subject, not a brain region. A key step in constructing a hypergraph is assembling hyperedges based on the distance between vertices. The k-nearest neighbors (kNN) method can be used to select a fixed-size subset of adjacent vertices, namely k vertices, as hyperedges for each vertex. When constructing a hypergraph, each vertex is connected to a set of neighbors if their distance from the vertex is less than a given threshold. Therefore, given N vertices, the corresponding incidence matrix $\mathbf{H} \in \mathbb{R}^{N \times N}$ contains N hyperedges, each of which connects a subset of vertices of flexible size, unlike the kNN-based method with a fixed size of $(k+1)$ vertices.

The empirical validation of this framework on the large-scale Human Connectome Project dataset yielded compelling results. The model achieved a remarkable classification accuracy of 96.7% in distinguishing between motor task and resting states, significantly outperforming competing feature selection methods such as group lasso (93.25%) and graph-based feature selection (95.76%). Ablation studies confirmed the individual contributions of both the hypergraph regularization and the temporal smoothness constraint, with the threshold-based hypergraph construction method proving superior to its k-NN counterpart. More importantly, the model demonstrated exceptional generalizability across a broad spectrum of cognitive domains. When applied to 18 distinct cognitive tasks, including working memory, language processing, and social cognition, the framework successfully identified task-specific brain regions whose activation patterns were both neurobiologically plausible and highly discriminative. For instance, the model localized working memory processes to the prefrontal cortex and language comprehension to the superior temporal gyrus, findings that are strongly corroborated by the established neuroscience literature. Furthermore, the method exhibited an ability to decode fine-grained cognitive states, such as predicting task difficulty levels within language paradigms, where the identified brain regions showed a significant correlation ($r = 0.251$ for story task, $p < 0.001$; $r = 0.278$ for math task, $p < 0.001$) with actual task difficulty and correctly captured the temporal evolution of cognitive load.

In a complementary line of work, Xi et al. [231] introduce a Hypergraph Representation of Multimodal Brain Networks (HRMBN) for classifying end-stage renal disease patients with mild cognitive impairment (ESRDaMCI). Their model integrates functional connectivity from fMRI and structural connectivity from diffusion kurtosis imaging via an attention diffusion mechanism. Node representations are learned through a diffusion process guided by an attention matrix, and bilinear pooling is used to extract connection features. A hypergraph is then constructed from these features, and its Laplacian is incorporated as a manifold regularization term alongside an ℓ_1-norm sparsity penalty. The resulting model achieved a classification accuracy of 91.09%, significantly outperforming several baseline methods, and identified discriminative brain regions in ESRDaMCI patients, many of which belong to the default mode network.

From a theoretical perspective, this hypergraph-based multitask framework offers two principal advantages. First, it effectively addresses the small-sample-size problem inherent in neuroimaging by leveraging high-order subject correlations through the hypergraph structure, which acts as a sophisticated manifold regularizer. Second, the integration of group sparsity with temporal smoothness allows the model to identify stable, temporally coherent neural signatures that are consistent across related cognitive tasks, thereby providing a more robust and interpretable feature set for downstream analysis. The success of this approach underscores the utility of hypergraphs not merely as a representational tool but as a foundational component for structured regularization in high-dimensional, temporally resolved neural decoding tasks.

5.3. Neurodegenerative diseases and aging

The advantages of moving beyond pairwise connectivity are particularly evident in the study of neurodegenerative diseases and aging, where pathophysiological processes often involve the large-scale, progressive disintegration of distributed neural systems. HOI analysis has proven uniquely sensitive to these complex changes, offering biomarkers for early diagnosis and new insights into disease mechanisms that remain invisible to conventional network models.

In Alzheimer's disease (AD), HOI metrics capture disruptions that remain invisible to conventional pairwise analysis. For instance, HOIs are disrupted in regions involved in the early pathological process, while the "classical" functional connectivity of these zones remains largely unchanged [230]. These disruptions in inter-system interactions have been shown to be independent of amyloid load, confirming the value of altered HOIs as a pathology marker distinct from

classical AD biomarkers [260]. The diagnostic power of this approach is underscored by the consistent finding that classifiers based on nonlinear higher-order features prove more effective than traditional methods extracting bivariate linear features [227]. This has spurred the development of sophisticated hypergraph-based modeling frameworks for AD diagnosis. Early work demonstrated that hyper-networks constructed via sparse linear regression models, combining brain region and subgraph features, could achieve high classification accuracy between AD patients and normal controls [226].

Subsequent dynamic hypergraph inference frameworks have further refined this, integrating multimodal data like MRI and PET to enable fine-grained discrimination not only between AD and controls but also among subtypes of mild cognitive impairment (MCI), such as converters and non-converters to AD [261]. These methods often employ a semi-supervised framework to align the constructed hypergraph structure with clinical labels, enhancing diagnostic consistency. More recently, deep learning architectures have been integrated, with hypergraph autoencoders and Generative Adversarial Networks (GANs) being used to learn deep latent embeddings and generate robust hypergraph representations from multi-view data, further improving classification performance and aiding in biomarker identification [262–264]. The field is also advancing towards more interpretable and semantically-aware models. Multi-modal diffusion-based hypergraph frameworks that incorporate dual priors, including genetic data like APOE, enhance prediction accuracy while addressing data heterogeneity by preserving semantic relationships across diverse data types [265]. Furthermore, multi-task feature selection models regularized by hypergraph p-Laplacians have been successfully applied to multimodal data, facilitating the extraction of shared discriminative features across modalities like sMRI and PET [266].

The analysis of longitudinal data using hypergraph-regularized multi-task frameworks has also shown great promise (see Fig. 22), effectively capturing disease progression patterns over time and achieving exceptionally high classification accuracies for AD and MCI [267]. The developed pipeline comprises four stages:

1. *Data Preprocessing*: Resting-state fMRI and sMRI data are drawn from the ADNI database at four time points (baseline, 6, 12, and 24 months), including 136 AD patients, 200 individuals with MCI, and 176 NC.
2. *Hypergraph Construction*: For each modality and time point, a subject-level hypergraph is constructed using KNN to encode high-order inter-subject relationships based on multimodal features.
3. *Multi-Task Feature Selection*: A joint multi-task learning model selects discriminative features across all time points, integrating (i) hypergraph Laplacian regularization to preserve high-order sample structure and (ii) fused Lasso regularization to enforce temporal smoothness between consecutive visits.
4. *Classification*: Selected fMRI and sMRI features are concatenated and classified using a multi-kernel SVM with learned linear kernel weights, enabling optimal fusion of modalities for final diagnostic grouping (AD, MCI, or NC).

The utility of HOIs is perhaps most critical at the prodromal stage of AD, namely MCI, where early detection is paramount. The application of hypergraph models to MCI represents a concerted effort to capture the subtle, distributed network abnormalities that characterize this transitional state. Initial foundational work by Jie et al. established the functional connectivity hyper-network for MCI classification using resting-state fMRI, demonstrating that modeling hyperedges connecting multiple brain regions could detect subtle disruption patterns missed by traditional pairwise methods [268].

This approach was significantly advanced through the integration of multimodal imaging. Gao et al. [269] constructed subject-level hypergraphs by integrating T1-weighted MRI, DTI, resting-state fMRI, and arterial spin labeling (ASL), using a semi-supervised learning framework that leveraged both labeled and unlabeled data to enhance classification accuracy across a cohort of 41 MCI patients and 63 controls.

This line of research was further refined by incorporating anatomical constraints. Li et al. [270] introduced anatomically weighted functional distances, building hypergraphs that respected known anatomical pathways from T1 and DTI data while modeling functional connectivity from fMRI, which improved classification performance and provided more biologically meaningful insights. A key methodological evolution came with the introduction of the functionally weighted LASSO for estimating hyper-connectivity networks, which used physiological perfusion signals from ASL to enforce sparsity and improve the interpretability of functional interactions. This method not only enhanced MCI classification but also allowed for the identification of specific hyperedges as potential biomarkers [227]. These multimodal hyper-networks consistently demonstrate much better discriminative characteristics than either conventional pairwise connectivity networks or unimodal hyper-connectivity networks [227]. This principle holds for other etiologies of MCI, such as in patients with end-stage renal disease, where a hypergraph representation of multimodal brain networks significantly outperforms state-of-the-art methods [231]. Collectively, these studies confirm that MCI is characterized by a reduction in neuronal higher-order interactions and that metrics capturing these changes are consistently more effective for discriminating between individuals with and without mild cognitive decline [223–225,228].

Beyond the Alzheimer's spectrum, HOI analysis is revealing novel aspects of other neurodegenerative conditions. In Parkinson's disease, emerging research using topological data analysis has established that high-order topological features are altered and are associated with disease severity [221]. These impairments in higher-order information exchange are particularly noted in regions such as the frontal lobe, insula, and sensorimotor areas [236]. Similarly, in multiple sclerosis, a statistical approach using multivariate cumulants has shown that spontaneous fMRI signals are organized into higher-order networks, which can successfully classify disease groups and explain behavioral variations [78].

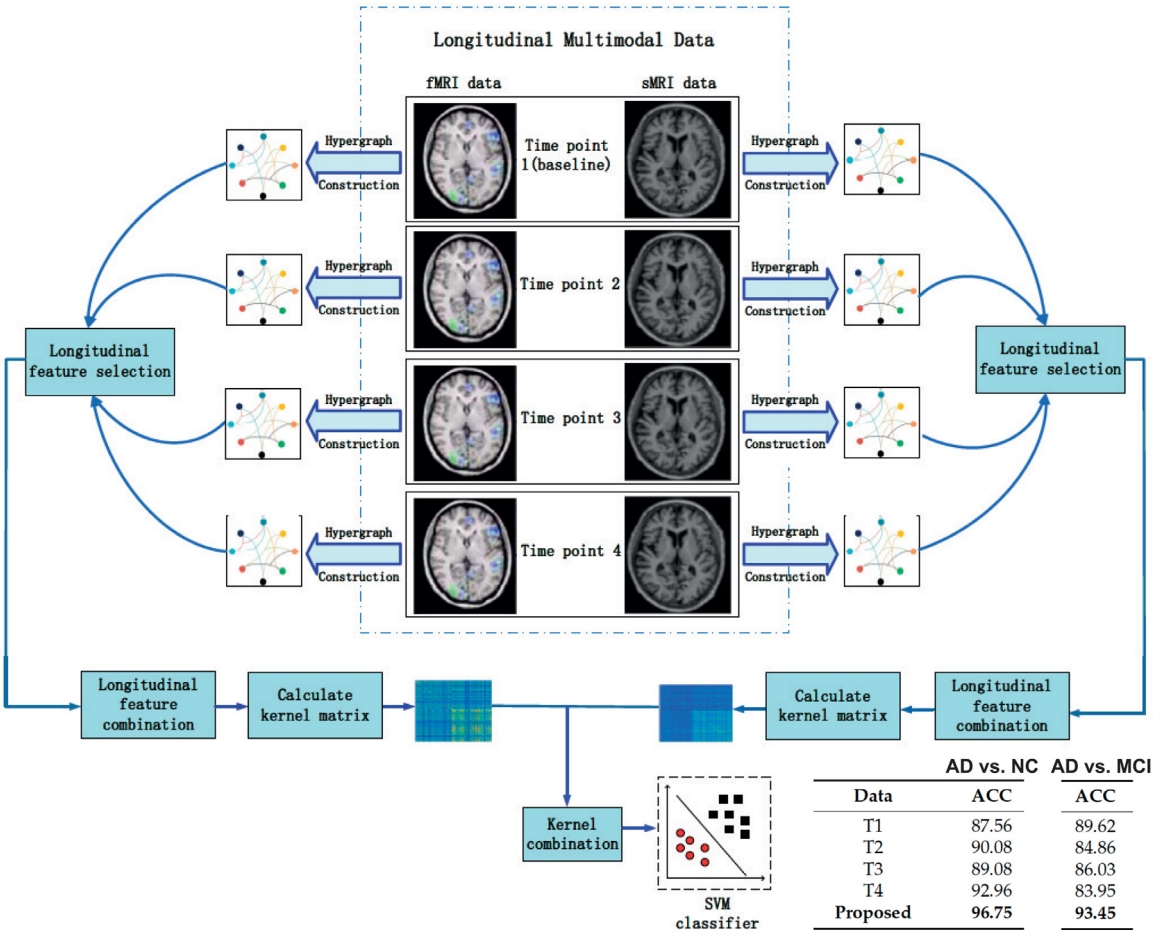

Fig. 22. Overview of the longitudinal imaging and hypergraph-based multi-task feature selection framework for AD and MCI classification [267]. The panel below compares classification performance across individual time points (T1–T4) and the proposed longitudinal integration strategy.
Source: Adapted from [267]; licensed under a Creative Commons Attribution 4.0 International license.

Finally, the study of brain aging itself appears very promising through the lens of HOIs. Initial studies suggest that the aging brain exhibits a more pronounced predominance of redundant information dependencies, particularly in prefrontal and motor areas [215]. This shift in the balance of redundant and synergistic information processing may underlie the cognitive changes associated with normal aging, providing a new framework for understanding the neurobiology of the aging brain.

In summary, the application of HOI analysis in neurodegenerative diseases and aging is providing a more nuanced, sensitive, and mechanistically informative picture of how large-scale brain networks break down. From sophisticated multimodal hypergraphs for classifying MCI to topological markers in Parkinson's disease, these approaches offer powerful tools for early diagnosis, tracking of disease progression, and understanding the fundamental principles of brain aging.

5.4. Neurodevelopmental disorders: ASD and ADHD

The study of HOIs has significantly advanced our understanding of neurodevelopmental disorders, whose complex and heterogeneous clinical profiles are increasingly recognized as emergent properties of distributed, system-level brain dysregulation rather than localized deficits. This systems-level perspective is especially relevant for Autism Spectrum Disorder (ASD) and Attention-Deficit/Hyperactivity Disorder (ADHD), where HOI-based approaches have enhanced both diagnostic precision and the identification of robust neurophysiological biomarkers.

In ASD, HOI analyses have not only corroborated the involvement of canonical regions, such as the thalamus, cerebellum, and specific association cortices, but also revealed how their multi-way functional integration is disrupted in the disorder. Wang et al. [237] employed the partial entropy decomposition (PED) framework to quantify synergistic and redundant interactions among triplets of brain regions in ASD (see Fig. 23). First, the PED algorithm is applied to all possible triplets of brain regions to quantify redundant and synergistic information sharing. Then, group-level

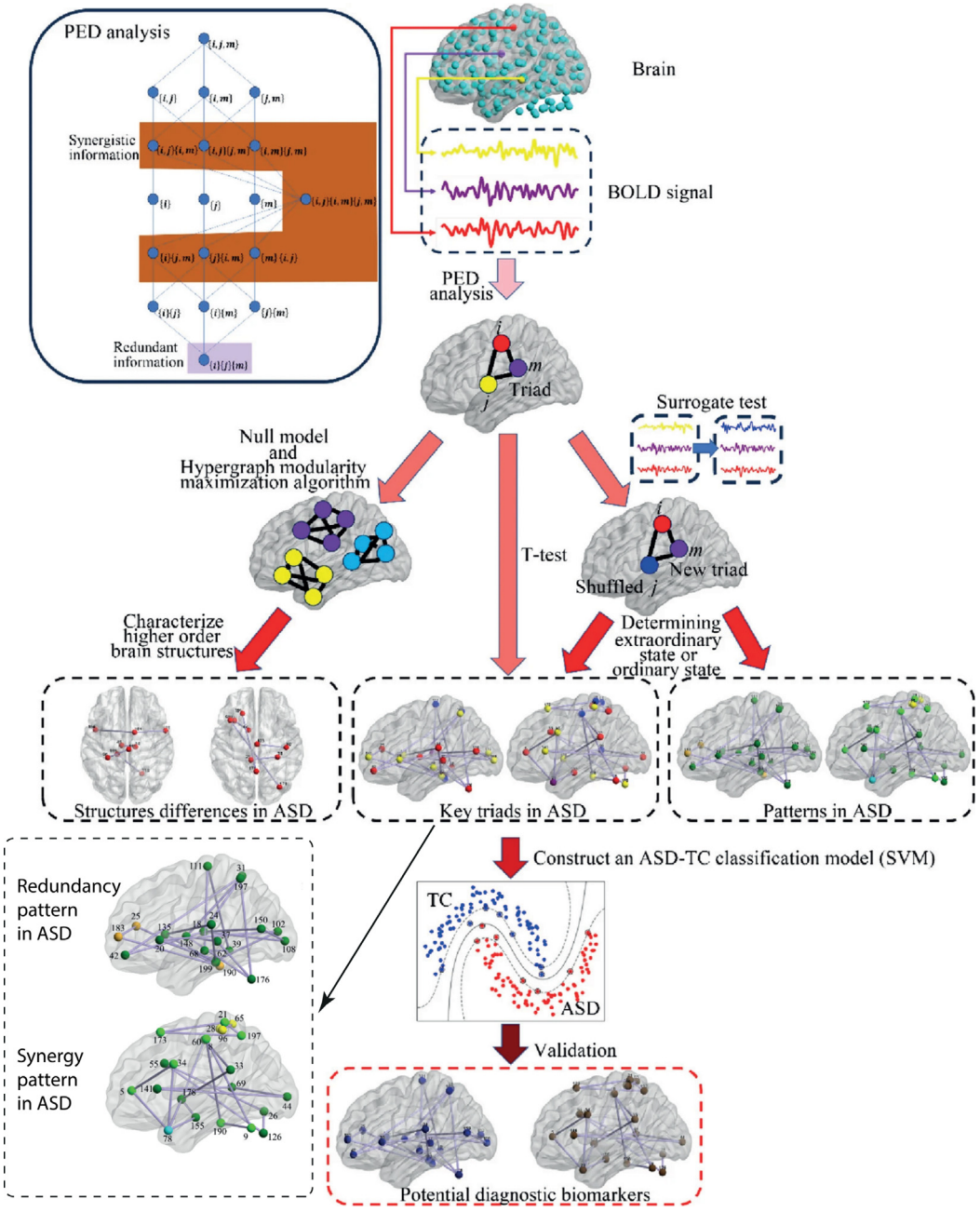

Fig. 23. Workflow for higher-order dependency analysis in ASD using PED to identify diagnostic biomarkers (key functional triads) [237].
Source: Adapted from [237].

differences in HOI measures are assessed via surrogate-based statistical testing followed by two-sample t-tests, yielding a set of discriminative triads that significantly differ between ASD and typically developing controls (TC). These triads are used to construct a hypergraph representation of higher-order functional architecture, which is then analyzed via hypergraph modularity maximization to reveal community structure and regional participation patterns. Finally, the HOI features derived from the key triads are used as input to a SVM classifier to distinguish ASD from TC participants, validating their utility as potential diagnostic biomarkers. This analysis uncovered a set of discriminative functional triads that reliably differentiate individuals with ASD from neurotypical controls. Crucially, when incorporated into a machine learning classifier, these HOI-derived features achieved high diagnostic accuracy (up to 97%), underscoring their potential as quantitative biomarkers for ASD.

A consistent finding across studies on ASD is that models extracting HOI features from fMRI data enable more accurate classification compared to those relying on pairwise metrics [67,238–242,244]. The application of hypergraph learning has been central to this progress. Early foundational work by Munsell et al. [271] demonstrated that a hypergraph framework fusing structural and functional connectomes could identify latent, discriminative relationships that outperformed traditional feature selection methods in distinguishing children with ASD from healthy controls. This capacity to model complex, high-dimensional relationships has been greatly enhanced by the development of hypergraph neural networks (HGNNs).

For instance, the FC-HAT model, an attention-enhanced hypergraph network, dynamically constructs hyperedges to isolate ASD-specific dysconnectivity patterns, achieving superior classification on a large cohort [243]. Similarly, Yang et al. [67] demonstrated that high-order functional networks constructed via hypergraphs provided superior diagnostic performance over low-order graph methods across a cohort of over 1100 subjects.

A major challenge in ASD research is multisite data heterogeneity. Hypergraph models have been specifically adapted to address this. Wang et al. [244] developed a multiview hypergraph embedding method that explicitly accounts for cross-atlas and cross-site variability, improving harmonization and classification accuracy. The flexibility of the hypergraph formalism also allows for its integration with cutting-edge deep learning architectures. Transformer-based hypergraph models have shown versatility in classifying both ASD and Alzheimer's disease, highlighting their generalizability across disparate neurological disorders [233]. Furthermore, recent models have begun to incorporate spatiotemporal dynamics, using hypergraph attention networks to learn both temporal dynamics and high-order spatial relationships, further pushing the boundaries of classification performance and mechanistic insight [39].

The utility of HOI modeling extends powerfully to Attention-Deficit/Hyperactivity Disorder (ADHD), a condition increasingly understood as arising from distributed dysregulation across networks that support attention, cognitive control, and executive function. Early hypergraph-based approaches marked a paradigm shift by moving beyond pairwise connectivity to capture the multi-region coordination deficits characteristic of ADHD. In a foundational study, Jie et al. [202] introduced functional connectivity hyper-networks (FCHNs), demonstrating that hyperedges – linking three or more brain regions – could reveal distinct dysconnectivity patterns in ADHD, particularly involving the prefrontal cortex and cingulate systems.

This framework was subsequently refined through sparse hypergraph learning, which incorporates hypergraph Laplacian regularization to identify compact, interpretable subnetworks with high discriminative power. Such models have consistently implicated alterations in the sensorimotor and dorsal attention networks as key biomarkers of ADHD pathology [252].

More recently, the field has shifted toward dynamic and individualized hypergraph representations that better reflect the heterogeneous and fluctuating nature of ADHD symptoms. The FC-HAT hypergraph attention network exemplifies this trend: by leveraging attention mechanisms to dynamically reweight hyperedges during inference, it adapts to individual neurofunctional variability and identifies critical hubs – most notably the dorsolateral prefrontal cortex – as central to ADHD-related dysregulation [243]. Extending this further, spatio-temporal hypergraph attention networks jointly model spatial topology and temporal evolution in dynamic functional connectivity, uncovering transient, unstable network states that are thought to underlie core ADHD symptoms such as lapses in attention and cognitive control [39]. These advances not only improve classification performance but also offer a pathway toward real-time, state-sensitive neuromonitoring and personalized intervention strategies.

Beyond purely data-driven approaches, there is a growing emphasis on integrating domain knowledge. Methods that incorporate prior neuroanatomical knowledge of ADHD-related regions into the hypergraph modeling process have demonstrated improved classification performance and enhanced translational relevance [272]. Furthermore, self-supervised learning frameworks that leverage hypergraphs to capture high-order semantic and topological information have shown robust performance on the multisite ADHD-200 dataset, successfully identifying key disease-associated brain regions and improving diagnostic generalization [245].

In summary, the investigation of HOIs in ASD and ADHD has moved the field from a focus on isolated connections to a systems-level understanding of network dysregulation. Hypergraph models and related HOI metrics have consistently provided a more sensitive and accurate tool for diagnosis, while simultaneously offering a powerful framework for identifying the distributed, complex neural interactions that underlie these heterogeneous neurodevelopmental conditions.

5.5. Psychiatric disorders

HOI analysis has offered a transformative framework for investigating the neural underpinnings of psychiatric disorders—conditions long recognized for their complexity and distributed brain abnormalities. Rather than reflecting localized dysfunction, disorders such as Major Depressive Disorder (MDD) and schizophrenia are now increasingly viewed as manifestations of disrupted integration across large-scale, multi-regional brain networks. HOI-based approaches have been pivotal in advancing this systems-level understanding, uncovering specific failures in network coordination and providing robust, quantifiable features for computational diagnosis.

In MDD, HOI characterization using Q-analysis – a topological method that identifies q-connected components across interaction orders – has revealed a central role for visual networks and their aberrant interactions with higher-order cognitive, limbic, and sensorimotor systems in disease pathology [65]. As illustrated in Fig. 24A,B, this is most evident at

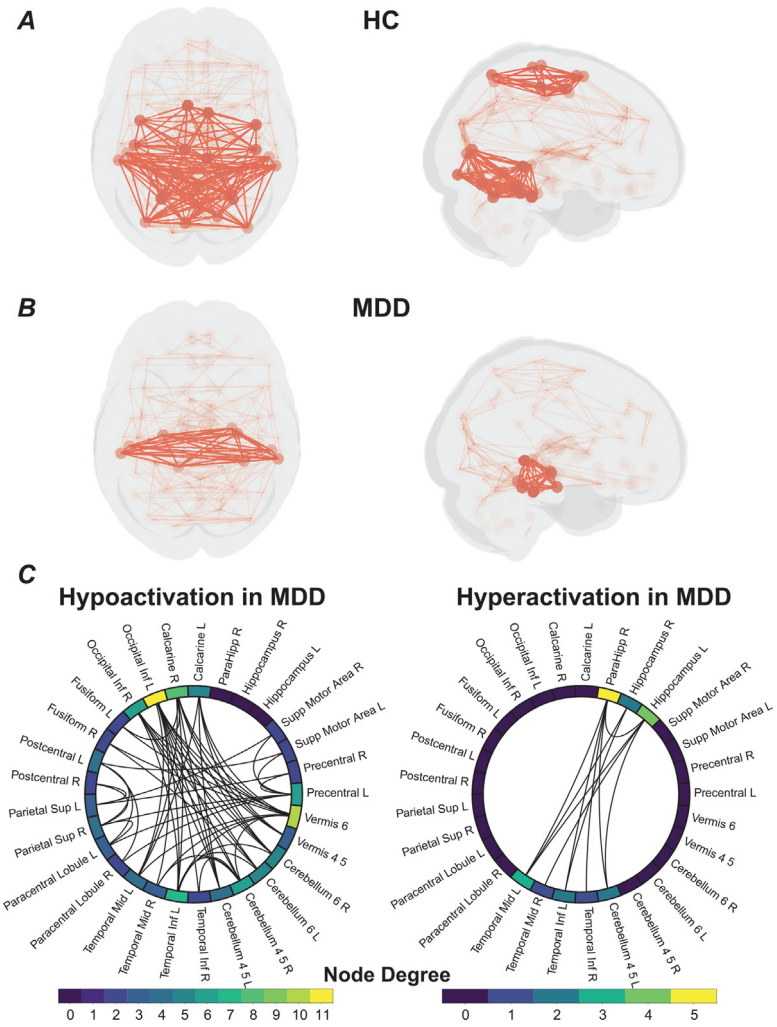

Fig. 24. Topological reorganization of high-order functional architecture in Major Depressive Disorder (MDD) revealed by Q-analysis. (*A*, *B*) q-connected components at level $q = 9$ for healthy controls (HC) and individuals with MDD, shown in superior and lateral views. Dark red subnetworks represent the q-connected components—defined as sets of cliques of order $\geq q$ that are interconnected via shared faces of dimension $r \geq q$; cliques linked only through lower-dimensional faces ($r < q$) belong to separate components. Light red networks depict the full consensus functional connectomes. At $q = 9$, the HC group exhibits three distinct high-order components integrating occipital, temporal, sensorimotor, and cerebellar regions, whereas the MDD group shows only a single component, characterized by limbic involvement and loss of occipito–parietal and sensorimotor integration. (*C*) Group differences in connectivity within the $q = 9$ components: *hypoactivated* edges (present in HC but absent in MDD) and *hyperactivated* edges (present in MDD but absent in HC). Adapted from [65]; licensed under a Creative Commons Attribution 4.0 International license.

topology level $q = 9$, where high-order functional components reflect the brain's capacity for integrated information processing. Healthy controls exhibit three distinct q-connected components that cohesively link occipital, temporal, cerebellar, and sensorimotor regions. In contrast, individuals with MDD show a marked simplification of this architecture: only a single high-order component remains, which prominently incorporates limbic structures (e.g., hippocampus, parahippocampal gyrus) but notably excludes the pre- and postcentral gyri as well as large portions of the occipital and parietal cortices. This reorganization signifies a profound loss of functional complexity and segregation in the depressed brain, highlighting how HOI methods can expose topological signatures of psychopathology that are invisible to pairwise connectivity analyses.

Further delineating these disruptions, Fig. 24C identifies the specific hypoactivated and hyperactivated connections that underpin the differences in Fig. 24A,B. The analysis reveals a hypoactivated subnetwork in MDD, comprising missing connections primarily among visual, temporal, parietal, cerebellar, and sensorimotor regions, with key disrupted hubs in the left inferior occipital gyrus and the cerebellar vermis. Conversely, a hyperactivated subnetwork was identified, featuring redundant connections that overly integrate the temporal lobe, cerebellum, hippocampus, and parahippocampal

gyrus, with the right parahippocampal gyrus emerging as a primary disrupted hub. This pattern confirms a pathological shift towards heightened limbic integration at the expense of sensory and motor network integration in MDD.

The diagnostic power of this approach is substantial. For instance, the directed hypergraph method, which explicitly models the directionality of information flow between groups of regions, has been used to create a depression state classifier that demonstrates clear superiority over models using features derived from "classical" pairwise functional connectivity [249]. This finding is reinforced by a series of studies employing various hypergraph construction techniques. Zheng et al. [246] showed that HOI features significantly improve depression classification accuracy compared to pairwise methods, also identifying novel cerebellar biomarkers.

Further refinements, particularly, the high-order line graph transformations of hypernetworks, have pushed classification accuracy for MDD to very high levels, underscoring the critical information captured by these complex models [250]. The robustness of these HOI-based biomarkers is further validated by their performance in large, multisite cohorts. The hypergraph-based semantic and topological self-supervised learning (HGST) framework demonstrated effective diagnosis of MDD on the REST-meta-MDD dataset, which includes over 1000 patients, successfully identifying key brain regions associated with the disorder [245]. Methodologically, the construction of these hyper-networks has been optimized through regularized regression techniques, with studies finding that the elastic net method achieved better classification results than LASSO-based approaches for identifying MDD [247].

Earlier information-theoretic approaches found that high-order, nonlinear interactions could distinguish schizophrenia patients from healthy controls in a way that pairwise methods could not [214]. This presaged the ability of HOI methods to detect subtle, system-wide disturbances in schizophrenia. This line of inquiry has been extended by dynamic hypergraph models, which have shown that high-order features improve schizophrenia classification and that healthy controls generally exhibit higher levels of HOI, consistent with a model of deficient functional integration in the disorder [156].

Beyond classification, hypergraph models are increasingly used for transdiagnostic and mechanistic discovery. For example, a hypergraph clustering approach has been applied to uncover transdiagnostic biotypes that cut across traditional diagnostic categories of schizophrenia and psychotic bipolar disorder, aligning with modern research frameworks that emphasize dimensional phenotypes [273]. Furthermore, the integration of multimodal data through hypergraph manifold regularization frameworks has enabled the fusion of imaging genetics data, enriching the understanding of schizophrenia by linking risk genes to functional brain anomalies [274].

The application of HOI methods is increasingly extending beyond mood and psychotic disorders to encompass other psychiatric conditions, notably anxiety disorders. Recent work employing a Subspace-Enhanced Hypergraph Neural Network (SE-HGNN) has successfully distinguished neural signatures across anxiety subtypes, including generalized anxiety disorder, panic disorder, and social anxiety, demonstrating the potential of HOI-based models as tools for differential diagnosis within the anxiety spectrum [251].

Collectively, HOI analyses across psychiatric disorders point to a unifying pathophysiological motif: disrupted integration within and between large-scale brain networks. In major depressive disorder, this manifests as aberrant over-integration of visual networks with limbic regions; in schizophrenia, as premature functional decoupling of cognitive control systems resembling accelerated network aging. By quantifying multi-region coordination beyond pairwise links, HOI metrics offer a sensitive and mechanistically grounded framework for characterizing the systems-level dysregulation that defines severe mental illness.

5.6. Other neurological disorders

In epilepsy, for instance, graph-based models incorporating HOIs offer a more accessible framework for explaining complex dynamics such as the brain's intrinsic capacity to abort seizure generation, a phenomenon linked to the synchronization stability of the epileptic brain network [275]. Similarly, in migraine, HOI analysis has revealed disrupted interactions within the thalamo-cortico-somatosensory system, potentially underpinning impaired information processing, including the central sensitization and altered pain perception characteristic of the disorder [276].

The clinical utility of network metrics is particularly evident in traumatic brain injury, where they can predict cognitive recovery and empirically explain the counterintuitive phenomenon of significant cognitive decline resulting from relatively small focal damage. Crucially, damage to brain regions with high network integration indices leads to more extensive cognitive impairments. In such predictions, the participation coefficient, which measures a node's intermodular connectivity, has emerged as a more reliable predictor of deficits across various cognitive domains than simpler metrics like node degree, underscoring the importance of a node's role in the global network architecture [277].

Perhaps the most profound applications of HOI analysis are found in the study of disorders of consciousness. Research consistently demonstrates a pronounced large-scale reorganization of key brain hubs and severe alterations in overall network architecture in comatose patients and those with impaired consciousness due to conditions like hepatic encephalopathy [149,278,279]. Data from studies on pharmacologically diminished consciousness further indicate a consistent theme of reduced large-scale integration of neuronal hubs alongside enhanced isolated, local information processing [280–282]. This breakdown of global integration, as captured by information-theoretic HOI metrics like O-information, has been directly observed in a single-case study of hepatic encephalopathy, where high-order synergistic information processing predominated during the recovery phase, capturing complexity entirely missed by pairwise methods [149].

Beyond their clinical relevance, these findings refine our fundamental understanding of the anatomical and dynamical basis of consciousness. The observed collapse of large-scale, integrated network organization in unconscious states provides empirical support for theoretical frameworks like the Global Workspace Theory and Integrated Information Theory, which posit that consciousness depends on a system's capacity for broad information distribution and high-level integration—a capacity that HOI metrics are uniquely positioned to quantify [283–285]. Thus, the study of HOIs in these neurological conditions not only advances diagnosis and prognosis but also bridges clinical observation with foundational theories of brain function.

6. Conclusion

The transition from pairwise to HOI models represents a fundamental paradigm shift in the analysis of fMRI-based functional brain networks. As this review has detailed, HOI frameworks, including hypergraphs, simplicial complexes, and advanced multivariate statistical, information-theoretic, and machine learning methods, offer a more nuanced, sensitive, and mechanistically informative view of brain organization. They move beyond the reductionist assumption that all neural interactions are dyadic, enabling the detection of emergent, synergistic dependencies among groups of brain regions that are critical for complex cognition and are often disrupted in neurological and psychiatric disorders. Empirical evidence increasingly confirms that HOI metrics provide superior discriminative power in classifying conditions such as Alzheimer's disease, autism spectrum disorder, and schizophrenia, and offer deeper insights into the brain's dynamic, integrative processes.

However, the field faces several significant methodological challenges that must be addressed to ensure rigorous and reproducible science. First among these is the problem of determining the truthfulness of identified HOIs. Many construction methods, such as the widely used clique complex approach, rely on strong a priori assumptions, for example, that every clique in a thresholded correlation graph represents a genuine multi-region interaction. This assumption ignores the possibility that such patterns may arise spuriously from aggregated pairwise effects or common inputs. Without careful validation, reported HOIs risk being statistical artifacts rather than neurobiologically meaningful phenomena. This underscores the necessity for developing and adopting verification frameworks, such as two-stage pipelines where candidate HOIs identified by one method (e.g., clique detection) are tested for irreducibility using another (e.g., LASSO, multivariate cumulants or information-theoretic synergy measures).

A second major challenge is the high computational complexity inherent in HOI analysis. Methods based on information decomposition (e.g., Partial Information Decomposition), multivariate cumulants, or exhaustive hyperedge enumeration scale combinatorially with the number of brain regions. This makes whole-brain, high-resolution HOI mapping with more than four interacting elements in HOI computationally prohibitive with current resources, particularly for dynamic or longitudinal analyses. Efficient algorithms, dimensionality reduction techniques, and scalable implementations – possibly leveraging GPU acceleration and distributed computing – are urgently needed to make these methods practical for large-scale studies.

Third, the quantitative analysis of hypergraphs remains underdeveloped. Unlike graphs, for which a rich arsenal of metrics and models exists, hypergraphs, especially heterogeneous ones with hyperedges of varying cardinalities, lack a unified, well-established analytical toolkit. Researchers often resort to simplifying transformations [250], such as line graphs, star expansions, or cluster expansions, to project hypergraphs into graph representations amenable to conventional analysis. While practical, these approximations inevitably discard or distort higher-order information. There is a clear need for new mathematical tools tailored to hypergraphs, including generalized centrality measures, robust community detection algorithms, and dynamic models that preserve the intrinsic multi-way relationships.

Beyond these core issues, other obstacles merit attention. These include the sensitivity of HOI measures to preprocessing choices and noise in fMRI data, the difficulty of interpreting high-dimensional HOI patterns in neurobiological terms, and the lack of standardized benchmarks for comparing different HOI methodologies. Furthermore, the field must grapple with the conceptual distinction between HOIs as within-subject, multi-region neural dependencies and the increasingly common repurposing of "higher-order" to describe between-subject or multi-view relationships in machine learning pipelines. Clarifying this terminology will be crucial for coherent theory-building.

Looking ahead, several promising trends are shaping the future of HOI research. Topological Data Analysis (TDA), particularly persistent homology, is emerging as a powerful framework for capturing multiscale, noise-robust HOI signatures without relying on hard thresholds. TDA provides a principled way to characterize the shape and stability of higher-order structures, offering insights into the brain's topological resilience and its alterations in disease. Machine learning and AI are being actively leveraged to discover complex, nonlinear HOIs directly from data. Graph Neural Networks (GNNs), transformers, and hypergraph neural networks can learn latent higher-order representations end-to-end, often achieving state-of-the-art performance in diagnostic classification. However, the "black-box" nature of many deep learning models necessitates parallel advances in explainable AI (XAI) to extract interpretable neurobiological insights.

Other notable directions include the integration of multimodal data (e.g., combining fMRI with DTI, EEG, or genetic information) within multilayer HOI frameworks, the development of dynamic and time-resolved HOI models to capture the brain's transient functional assemblies, and the translational application of HOI biomarkers for early diagnosis, prognosis, and treatment monitoring in clinical settings. The adoption of two-stage validation approaches, the creation of open-source software libraries dedicated to HOI analysis, and the establishment of large, publicly available benchmark datasets will further accelerate methodological progress and ensure reproducibility.

In summary, the study of higher-order interactions in fMRI-based brain networks is a rapidly evolving frontier that holds great promise for unraveling the complexities of neural computation and its disruption in disease. While significant challenges remain, particularly concerning validation, scalability, and analytical tooling, the convergence of mathematical innovation, computational advances, and neuroscientific inquiry is paving the way for a more holistic understanding of the brain as a genuine complex system. As methodologies mature and interdisciplinary collaborations deepen, HOI-based approaches are poised to become an indispensable component of modern network neuroscience, ultimately bridging the gap between local neural activity and the emergent dynamics of cognition, behavior, and consciousness.

CRediT authorship contribution statement

Semen A. Kurkin: Writing – review & editing, Writing – original draft, Visualization, Validation, Methodology, Investigation, Formal analysis, Data curation, Conceptualization. **Alexander N. Pisarchik:** Writing – review & editing, Writing – original draft, Methodology, Investigation, Formal analysis, Data curation, Conceptualization. **Larisa A. Mayorova:** Writing – review & editing, Writing – original draft, Validation, Methodology, Investigation, Formal analysis, Data curation. **Alexander E. Hramov:** Writing – review & editing, Writing – original draft, Visualization, Validation, Supervision, Resources, Project administration, Methodology, Investigation, Funding acquisition, Formal analysis, Data curation, Conceptualization.

Declaration of competing interest

The authors declare that they have no conflict of interest.

Acknowledgments

This work was supported by the Russian Science Foundation, Russia, grant No. 23-71-30010.

Appendix

Table A.5
The most relevant studies on the application of the higher-order interactions (HOIs) concept to fMRI-derived functional networks. Unless otherwise specified, most studies use resting-state fMRI.

Study	Application domain	Study design	HOIs assessing method	Primary findings
		Information-Theoretic Approaches		
Plis et al. 2014 [214]	Schizo-phrenia	Cross-sectional, Case-control, Task-based	Hypergraph, Information-Theoretic: Multi-information	High-order, nonlinear interactions distinguish schizophrenia; not detected by pairwise methods
Gatica et al. 2021 [215]	Healthy Aging	Cross-sectional, Lifespan (10-80 years)	High-order redundant and synergistic maps, Information-Theoretic: O-Information	Older subjects exhibit higher redundancy across all interaction orders; identified a "redundancy core" in prefrontal and motor cortices; suggests shift in integration-segregation balance with age
Herzog et al. 2022 [222]	Behavioral variant Frontotemporal Dementia (bvFTD), Alzheimer's Disease (AD)	Cross-sectional, Case-control, Multimodal	Hypergraph, Information-Theoretic: Dual Total Correlation	HOI more accurate than pairwise; hypo/hyperconnectivity; compensatory processes in hubs; robust classification
Sparacino et al. 2023 [149]	Hepatic Encephalopathy	Single-case, pre/post intervention	Hypergraph, Information-Theoretic: O-information	High-order synergies predominate in recovery; HOIs capture complexity missed by pairwise
Varley et al. 2023 [31]	Healthy Adults	Cross-sectional, Discovery-focused	Hypergraph, Information-Theoretic: Partial Entropy Decomposition (PED)	PED reveals widespread higher-order synergies in fMRI data invisible to pairwise functional connectivity (FC). FC networks primarily reflect redundant information. Synergistic communities are more variable across subjects and dynamic over time.
Wang et al. 2024 [237]	ASD	Cross-sectional, Case-control, ML classification	Information-Theoretic: Partial Entropy Decomposition (PED), Hypergraph Modularity Maximization	PED captures triad-level redundancy/synergy; surrogate tests reveal extraordinary brain region states; key triads differentiate ASD (85%–97% accuracy); hypergraphs show looser thalamic link in ASD
Ray et al. 2025 [236]	Parkinson's Disease with Hyposmia	Cross-sectional, Case-control	High-order redundant and synergistic maps, Information-Theoretic: O-Information	PD patients (especially with hyposmia) show reduced synergy and redundancy vs. HC; synergy reduction in frontal, insula, and sensory-motor regions correlates with odor identification; HOI features aid classification (91% accuracy)
		Statistical Approaches		
Zhang et al. 2016 [223]	MCI	Cross-sectional, Case-control	Hypergraph, Statistical: Correlation's Correlation/eFC	HOI improves sensitivity by 25%; reveals new links; complementary to functional connectivity
Chen et al. 2016 [224]	MCI	Cross-sectional, Case-control, ML classification	Hypergraph, Statistical: Correlation's Correlation/eFC and Clustering	HOI improves area under the curve (AUC) to 0.93; captures complex interactions; clustering reveals local patterns

(*continued on next page*)

Table A.5 (*continued*).

Study	Application domain	Study design	HOIs assessing method	Primary findings
Zhang et al. 2017b [216]	Healthy Adults	Test-retest reliability of different HOI metrics, healthy adults	Dynamic Hypergraph, Statistical: Correlation's Correlation/eFC	HOI metrics reliable; more so for weak between-network connections; dynamics-based high-order functional connectivity models complex interactions
Zhang et al. 2017c [225]	MCI, AD	Cross-sectional, Case-control, ML classification	Dynamic Hypergraph, Statistical: Correlation's Correlation/eFC	High-order functional connectivity networks more discriminative; improves early MCI classification
Gu et al. 2017 [217]	Healthy youth, Developmental Changes	Cross-sectional	Hypergraph, Statistical: Correlation's Correlation/eFC and Clustering	Cluster hyperedges show a strong resemblance to previously-described functional modules of the brain (e.g., visual, default mode, salience). The greatest developmental effects occur in networked hyperedges within the functional core
Zhou et al. 2018 [228]	MCI	Cross-sectional, Case-control, ML classification	Hypergraph, Statistical: Matrix Variate Normal Distribution (MVND)	Fusion of low/high-order functional connectivity improves MCI classification; low-order more discriminative
Zhao et al. 2018 [238]	Autism Spectrum Disorder (ASD)	Cross-sectional, Case-control, ML classification	Hypergraph, Statistical: Correlation's Correlation or edge functional connectivity (eFC)	High-order features complement low-order; best ASD accuracy (81%) with both
Zheng et al. 2019 [246]	Major Depressive Disorder (MDD)	Cross-sectional, Case-control, ML classification	Hypergraph, Statistical: Clustering and Correlation's Correlation/eFC	HOI features improve depression classification (82.5% vs. 67.5%); novel cerebellar biomarkers
Niu et al. 2019 [218]	Normal function (tasks)	Cross-sectional, Task-based	Hypergraph, Statistical, Model-based approaches	HOI strength weak in tasks; pairwise interactions dominate; HOIs not central at macroscopic level
Zhao et al. 2020 [239]	ASD	Cross-sectional, Case-control, ML classification	Dynamic Hypergraph, Statistical: Correlation's Correlation/eFC	HOIs provide complementary info; best ASD accuracy (83%) with multi-level features
Khatri and Kwon, 2022 [229]	AD, MCI	Cross-sectional, Case-control, ML classification	Dynamic Hypergraph, Statistical: Correlation's Correlation/eFC	All-band HOIs yield 94.1% accuracy for AD; temporal regions key
Pan et al. 2022 [156]	Schizo-phrenia	Cross-sectional, Case-control, ML classification	Hypergraph, Statistical: Clustering and Correlation's Correlation/eFC	High-order features improve schizophrenia classification (81.8%); healthy controls have higher HOI
Zhao et al. 2022 [240]	ASD	Cross-sectional, Case-control, ML classification	Hypergraph, Statistical: Matrix Variate Normal Distribution, Hierarchical Sub-Network Method	Improved classification accuracy
Arbabyazd et al. 2023 [230]	AD, amnestic MCI	Cross-sectional, Case-control	Dynamic Hypergraph, Statistical: Correlation's Correlation/eFC	HOIs not redundant with pairwise; HOIs strengths reduced in AD; unique dynamic functional connectivity disordering
Yang et al. 2023 [67]	ASD	Cross-sectional, Case-control, ML classification	Hypergraph, Statistical: Averaging Multiple Related ROIs Connected by Hyperedges	Low-order and high-order networks have certain complementarity and combining them effectively can improve classification accuracy
Wang et al. 2023 [234]	Early Mild Cognitive Impairment (EMCI)	Cross-sectional, Case-control, Multimodal (MRI, rs-fMRI, DTI), ML classification	Hypergraph, Statistical: Correlation's Correlation/eFC	Proposed framework achieved 91.4% classification accuracy, outperforming existing methods. High-order network provides sensitivity, low-order network provides robustness; fusion yields superior discriminative power
Zhang et al. 2023 [235]	AD, MCI (Early MCI, Late MCI)	Cross-sectional, Case-control, Multimodal (MRI, rs-fMRI, DTI), ML classification	Statistical, Model-based: Edge-Centric Effective Connection Network (EECN), Improved Conditional Granger Causality on Edge Time Series	Achieved high accuracy (e.g., 91.5% for Controls vs. EMCI, 98.3% for Controls vs. AD). EECN reveals progressive loss of causal influence between connections as disease advances
Santoro et al. 2024 [33]	Healthy Adults (Tasks, Rest), Individual Differences	Cross-sectional, Task-based	Simplicial Complex, Statistical: Instantaneous Higher-Order Co-fluctuations; Topological Data Analysis: Persistent Homology	Local HOIs (violating triangles, homological scaffold) outperform pairwise methods in task decoding, brain fingerprinting, and brain-behavior association; global HOIs show no advantage
Hindriks et al. 2024 [78]	Normal, Multiple Sclerosis	Cross-sectional, Case-control	Hypergraph, Statistical: Multivariate Cumulant	Spontaneous fMRI signals organized into higher-order networks; cumulants classify disease groups, explain behavior
		ML-based Approaches		
Jie et al. 2016 [202]	AD, MCI, ADHD	Cross-sectional, Case-control, ML classification	Hypergraph, ML-based: Sparse Representation	Hyper-networks outperform pairwise; higher-order features improve classification and biomarker discovery
Guo et al. 2017 [226]	AD	Cross-sectional, Case-control, ML classification	Hypergraph, ML-based: Sparse Linear Regression Model	HOIs improve AD classification (91.6%); identifies abnormal regions
Guo et al. 2018 [247]	MDD	Cross-sectional, Case-control, ML classification	Hypergraph, ML-based: LASSO/Group LASSO/Elastic Net	The elastic net method achieved better classification results than the LASSO methods
Li et al. 2019 [227]	MCI	Cross-sectional, Case-control, Multimodal (fMRI, Arterial Spin Labeling (ASL)), ML classification	Hypergraph, ML-based: functionally-weighted LASSO	Multimodal hyper-networks demonstrated much better discriminative characteristics (accuracy 86.9%) than either the conventional pairwise connectivity networks or the unimodal hyper-connectivity networks
Xiao et al. 2019 [219]	Learning Ability (WRAT Score)	Cross-sectional, Multi-paradigm	Hypergraph, ML-based: Sparse Representation + Hypergraph Learning (Adaptive Hyperedge Weighting)	Proposed weighted hypergraph method outperformed traditional graphs and unweighted hypergraphs; multi-hypergraph fusion further improved classification; identified HOI-relevant frontal and temporal regions associated with learning ability

(*continued on next page*)

Table A.5 (*continued*).

Study	Application domain	Study design	HOIs assessing method	Primary findings
Zhao et al. 2021 [241]	ASD	Cross-sectional, Case-control, ML classification	Hypergraph, ML-based: Cluster-based Multi-view High-order Functional Connectivity Network	Multi-view HOIs improve ASD diagnosis (86.2%); phase mismatch addressed
Hao et al. 2022 [242]	ASD	Cross-sectional, Case-control, ML classification	ML-based: Cluster-based Hypergraph (k-Nearest Neighbors Scheme), Deep-Broad Learning	Hypergraph features outperform pairwise; 71.8% accuracy; identifies ASD-related regions
Li et al. 2022 [248]	MDD	Cross-sectional, Case-control, ML classification	Hypergraph, ML-based: Sparse Group LASSO	Dynamic HOIs improve MDD classification (92.2%); identifies discriminative regions
Ji et al. 2022 [243]	ADHD, ASD	Cross-sectional, Case-control, ML classification	ML-based: Hypergraph attention network for functional brain network classification (FC-HAT)	Hypergraph neural networks can extract high-order structures from brain networks. FC-HAT achieves superior results in classifying cerebral diseases (e.g., ADHD and ASD) and reveals the associated biomarkers
Xi et al. 2022 [231]	End-Stage Renal Disease with MCI	Cross-sectional, Case-control, Multimodal (Diffusion Kurtosis Imaging (DKI), fMRI), ML classification	Hypergraph	The proposed hypergraph representation of multimodal brain networks significantly outperforms several state-of-the-art multimodal methods, achieving an accuracy rate of 91%
Liu et al. 2023 [232]	MCI, ASD	Cross-sectional, Case-control, ML classification	ML-based: Sparse Linear Regression Model, Spatio-temporal Weighted (STW) Hypergraph, Multi-template Data, STW Multi-Hypergraph Convolutional Network (STW-MHGCN)	Spatio-temporal HOIs superior for MCI/ASD classification; deep fusion of templates
Wang et al. 2023 [220]	Healthy youth, Developmental Changes, Learning Ability	Cross-sectional, Task-based, ML classification	ML-based: Dynamic weighted hypergraph neural network (dwHGCN)	Dynamic weighted hypergraph convolutional network identifies active decision-related HOIs, improves classification. Potential hub regions are identified related to brain developments and learning ability during adolescence
Liu et al. 2024 [249]	MDD	Cross-sectional, Case-control, ML classification	Hypergraph, ML-based: Sparse Regression Algorithm with the Temporal Lag Effect, Directed Hypergraph Convolutional Network (DHGCN)	Directional HOIs outperform undirected and pairwise; directionality crucial for MDD identification
Guo et al. 2024a [250]	MDD	Cross-sectional, Case-control, ML classification	Hypergraph, ML-based: LASSO, High-order Line Graph	High-order line graph outperforms traditional hypernetworks; accuracy 92.4% for MDD
Wang et al. 2024 [244]	ASD	Cross-sectional, Case-control, Multisite ML	ML-based: Cluster-based Hypergraph (k-Nearest Neighbors Scheme), Multiview Hyperedge-Aware Hypergraph Convolutional Network (HGCN)	Hypergraphs outperform simple graphs; multi-atlas integration improves ASD diagnosis
Han et al. 2024 [233]	ASD, AD, MCI	Cross-sectional, Case-control, Multimodal, ML classification	ML-based: Hypergraph Transformer (HGTrans), KNN-based Hypergraph Construction, Cross-Attention Transformer	Multimodal hypergraph fusion of fMRI & DTI; outperforms single-modality & graph methods; achieves 79.9% accuracy (ABIDE-NYU), 74.9% (ABIDE-TCD), 74.0% (ADNI); cross-attention integrates structural & functional HOIs
Teng et al. 2024 [75]	AD, Cognitive Tasks	Cross-sectional, Case-control, Task-based	Hypergraph, ML-based, Model-based: Fuzzy Cognitive Maps with Hypergraph Laplacian Regularization (High-Order Functional Connectivity Networks With Temporal Information, THFCN)	Proposed THFCN embeds temporal and high-order features into FCNs; achieves 12% higher accuracy than non-temporal hypergraph methods; identifies discriminative ROIs and directed information flow
Hu et al. 2025 [39]	ADHD, ASD	Cross-sectional, Case-control, ML classification	ML-based: Hypergraph Attention-based Spatio-Temporal Aggregation	The proposed ML method learns sparse and informative HOIs among brain regions from fMRI data, achieving superior disease classification performance and identifying meaningful HOI patterns relevant to brain disorders
Han et al. 2025 [245]	ADHD, MDD	Cross-sectional, Case-control, ML classification	ML-based: Sparse Representation, HyperGraph Semantic and Topological self-supervised learning (HGST)	HGST with semantic-aware (masked node reconstruction) and topology-aware (contrastive learning) modules; achieves 70.0% accuracy (ADHD), 64.3% (MDD); identifies disease-related regions (e.g., precuneus in MDD)
Tang et al. 2025 [251]	Anxiety Disorders (AnD)	Cross-sectional, Case-control, Multimodal (fMRI/sMRI)	Hypergraph, ML-based: Subspace-enhanced Hypergraph Neural Network (seHGNN) with learnable incidence matrix	Achieves high AnD classification accuracy (94.1% with ensemble learning); identifies discriminative AnD biomarkers in the limbic system (e.g., right anterior cingulate, hippocampus); subspace enhancement adaptively reinforces hyperedge influence for improved feature extraction
Approaches Based on Simplicial Complexes Identification				
Petri et al. 2014 [77]	Altered States of Consciousness (Psilocybin vs. Placebo)	Placebo-control, Within-subject	Simplicial Complex, Topological Data Analysis: Persistent Homology, Homological Scaffolds	Psilocybin reduces stability of mesoscopic cycles but increases persistence of specific scaffold edges, indicating disrupted normal organization with emergent strong, cross-modular connections
Kurkin et al. 2024 [65]	MDD	Cross-sectional, Case-control	Simplicial Complex, Topological Data Analysis: Q-analysis	MDD: lower topology, more isolated edges, higher substantia nigra integration, reduced topological diversity and complexity
Ling et al. 2025 [221]	Normal, Parkinson's	Cross-sectional, Case-control	Simplicial Complex, Topological Data Analysis	High-order topological features altered in Parkinson's; associated with disease severity

References

[1] N. Wiener, Cybernetics or Control and Communication in the Animal and the Machine, MIT Press, 2019.
[2] W.G. Walter, The contingent negative variation: an electro-cortical sign of sensori-motor reflex association in man, Prog. Brain Res. 22 (1968) 364–377.
[3] M.A. Brazier, The electrical activity of the nervous system: Electrical signals are the neurophysiologist's clue to coding in the nervous system, Science 146 (3650) (1964) 1423–1428.
[4] G. Dumermuth, P. Huber, B. Kleiner, T. Gasser, Numerical analysis of electroencephalographic data, IEEE Trans. Audio Electroacoust. 18 (4) (1970) 404–411.
[5] G. Dumermuth, L. Molinari, Spectral analysis of the EEG: some fundamentals revisited and some open problems, Neuropsychobiology 17 (1–2) (1987) 85–99.
[6] B. Biswal, F. Zerrin Yetkin, V.M. Haughton, J.S. Hyde, Functional connectivity in the motor cortex of resting human brain using echo-planar MRI, Magn. Reson. Med. 34 (4) (1995) 537–541.
[7] K.J. Friston, C.D. Frith, P.F. Liddle, R.S. Frackowiak, Functional connectivity: the principal-component analysis of large (PET) data sets, J. Cereb. Blood Flow Metab. 13 (1) (1993) 5–14.
[8] E. Bullmore, O. Sporns, Complex brain networks: graph theoretical analysis of structural and functional systems, Nature Rev. Neurosci. 10 (3) (2009) 186–198.
[9] O. Sporns, G. Tononi, R. Kötter, The human connectome: a structural description of the human brain, PLoS Comput. Biol. 1 (4) (2005) e42.
[10] D.J. Watts, S.H. Strogatz, Collective dynamics of 'small-world' networks, Nature 393 (6684) (1998) 440–442.
[11] D.S. Bassett, E. Bullmore, Small-world brain networks, Neuroscientist 12 (6) (2006) 512–523.
[12] M.P. Van Den Heuvel, O. Sporns, Rich-club organization of the human connectome, J. Neurosci. 31 (44) (2011) 15775–15786.
[13] D.S. Bassett, N.F. Wymbs, M.A. Porter, P.J. Mucha, J.M. Carlson, S.T. Grafton, Dynamic reconfiguration of human brain networks during learning, Proc. Natl. Acad. Sci. 108 (18) (2011) 7641–7646.
[14] A.E. Hramov, N.S. Frolov, V.A. Maksimenko, S.A. Kurkin, V.B. Kazantsev, A.N. Pisarchik, Functional networks of the brain: from connectivity restoration to dynamic integration, Phys.-Usp. 64 (6) (2021) 584.
[15] Y. Du, S. Fang, X. He, V.D. Calhoun, A survey of brain functional network extraction methods using fmri data, Trends Neurosci. (2024).
[16] G. Marrelec, A. Krainik, H. Duffau, M. Pélégrini-Issac, S. Lehéricy, J. Doyon, H. Benali, Partial correlation for functional brain interactivity investigation in functional MRI, Neuroimage 32 (1) (2006) 228–237.
[17] C.W. Granger, Investigating causal relations by econometric models and cross-spectral methods, Econ.: J. Econ. Soc. (1969) 424–438.
[18] A.K. Seth, A.B. Barrett, L. Barnett, Granger causality analysis in neuroscience and neuroimaging, J. Neurosci. 35 (8) (2015) 3293–3297.
[19] W. Escalante Puente de la Vega, A.N. Pisarchik, Effective brain connectivity analysis during endogenous selective attention based on granger causality, Appl. Sci. 16 (2026) 101.
[20] M. Niedostatek, A. Baptista, J. Yamamoto, J. Kurths, R. Sanchez Garcia, B.D. MacArthur, G. Bianconi, Mining higher-order triadic interactions, Nat. Commun. (2025).
[21] F. Battiston, G. Cencetti, I. Iacopini, V. Latora, M. Lucas, A. Patania, J.-G. Young, G. Petri, Networks beyond pairwise interactions: Structure and dynamics, Phys. Rep. 874 (2020) 1–92.
[22] F. Battiston, E. Amico, A. Barrat, G. Bianconi, G. Ferraz de Arruda, B. Franceschiello, I. Iacopini, S. Kéfi, V. Latora, Y. Moreno, et al., The physics of higher-order interactions in complex systems, Nat. Phys. 17 (10) (2021) 1093–1098.
[23] A.P. Millán, H. Sun, L. Giambagli, R. Muolo, T. Carletti, J.J. Torres, F. Radicchi, J. Kurths, G. Bianconi, Topology shapes dynamics of higher-order networks, Nat. Phys. (2025) 1–9.
[24] J.M. Beggs, D. Plenz, Neuronal avalanches in neocortical circuits, J. Neurosci. 23 (35) (2003) 11167–11177.
[25] S. Boccaletti, P. De Lellis, C. Del Genio, K. Alfaro-Bittner, R. Criado, S. Jalan, M. Romance, The structure and dynamics of networks with higher order interactions, Phys. Rep. 1018 (2023) 1–64.
[26] G. Bianconi, Higher-Order Networks, Cambridge University Press, 2021.
[27] Y. Zhao, S. Maletić, Simplicial Complexes in Complex Systems: In Search for Alternatives, World Scientific, 2021.
[28] C. Giusti, R. Ghrist, D.S. Bassett, Two's company, three (or more) is a simplex: Algebraic-topological tools for understanding higher-order structure in neural data, J. Comput. Neurosci. 41 (2016) 1–14.
[29] F.V. Farahani, W. Karwowski, N.R. Lighthall, Application of graph theory for identifying connectivity patterns in human brain networks: A systematic review, Front. Neurosci. 13 (2019) 585.
[30] J. Wang, X. Zuo, Y. He, Graph-based network analysis of resting-state functional MRI, Front. Syst. Neurosci. 4 (2010) 1419.
[31] T.F. Varley, M. Pope, M. Grazia, Joshua, O. Sporns, Partial entropy decomposition reveals higher-order information structures in human brain activity, Proc. Natl. Acad. Sci. 120 (30) (2023) e2300888120.
[32] A.I. Luppi, P.A. Mediano, F.E. Rosas, N. Holland, T.D. Fryer, J.T. O'Brien, J.B. Rowe, D.K. Menon, D. Bor, E.A. Stamatakis, A synergistic core for human brain evolution and cognition, Nature Neurosci. 25 (6) (2022) 771–782.
[33] A. Santoro, F. Battiston, M. Lucas, G. Petri, E. Amico, Higher-order connectomics of human brain function reveals local topological signatures of task decoding, individual identification, and behavior, Nat. Commun. 15 (1) (2024) 10244.
[34] T. Robiglio, L. Di Gaetano, A. Altieri, G. Petri, F. Battiston, Higher-order ising model on hypergraphs, 2024, arXiv preprint arXiv:2411.19618.
[35] M.R.R. Tabar, F. Nikakhtar, L. Parkavousi, A. Akhshi, U. Feudel, K. Lehnertz, Revealing higher-order interactions in high-dimensional complex systems: A data-driven approach, Phys. Rev. X 14 (1) (2024) 011050.
[36] D.S. Bassett, O. Sporns, Network neuroscience, Nature Neurosci. 20 (3) (2017) 353–364.
[37] E.G.Z. Centeno, G. Moreni, C. Vriend, L. Douw, F.A.N. Santos, A hands-on tutorial on network and topological neuroscience, Brain Struct. Funct. 227 (3) (2022) 741–762.
[38] M.K. Chung, A.B. El-Yaagoubi, A. Qiu, H. Ombao, From density to void: Why brain networks fail to reveal complex higher-order structures, 2025, arXiv preprint arXiv:2503.14700.
[39] W. Hu, X. Su, G. Li, Y. Pan, A. Lin, Learning high-order relationships with hypergraph attention-based spatio-temporal aggregation for brain disease analysis, 2025, arXiv preprint arXiv:2505.12068.
[40] J. Niu, Y. Du, Applications of hypergraph-based methods in classifying and subtyping psychiatric disorders: a survey, Radiol. Sci. 2 (01) (2023) 83–95.
[41] Y. Ji, Y. Zhang, H. Shi, Z. Jiao, S.-H. Wang, C. Wang, Constructing dynamic brain functional networks via hyper-graph manifold regularization for mild cognitive impairment classification, Front. Neurosci. 15 (2021) 669345.
[42] I. Amburg, N. Veldt, A. Benson, Clustering in graphs and hypergraphs with categorical edge labels, in: Proceedings of the Web Conference 2020, 2020, pp. 706–717.
[43] Z. Feng, M. Qiao, H. Cheng, Modularity-based hypergraph clustering: Random hypergraph model, hyperedge-cluster relation, and computation, Proc. the ACM Manag. Data 1 (3) (2023) 1–25.

[44] A.N. Pisarchik, N. Peña Serrano, W. Escalante Puente de la Vega, R. Jaimes-Reátegui, Hypergraph analysis of functional brain connectivity during figurative attention, Appl. Sci. 15 (7) (2025) 3833.
[45] P. Pranav, R. Van de Weygaert, G. Vegter, B.J. Jones, R.J. Adler, J. Feldbrugge, C. Park, T. Buchert, M. Kerber, Topology and geometry of Gaussian random fields I: on betti numbers, Euler characteristic, and Minkowski functionals, Mon. Not. R. Astron. Soc. 485 (3) (2019) 4167–4208.
[46] Edelsbrunner, Letscher, Zomorodian, Topological persistence and simplification, Discrete Comput. Geom. 28 (2002) 511–533.
[47] A. Patania, F. Vaccarino, G. Petri, Topological analysis of data, EPJ Data Sci. 6 (1) (2017) 1–6.
[48] A. Zomorodian, G. Carlsson, Computing persistent homology, in: Proceedings of the 20th Annual Symposium on Computational Geometry, 2004, pp. 347–356.
[49] M. Feng, M.A. Porter, Persistent homology of geospatial data: A case study with voting, SIAM Rev. 63 (1) (2021) 67–99.
[50] R. Ghrist, Barcodes: The persistent topology of data, Bull. Am. Math. Soc. 45 (1) (2008) 61–75.
[51] A. Hatcher, Algebraic Topology, Cambridge University Press, 2002.
[52] F.R. Chung, The Laplacian of a hypergraph, Expand. Graphs 10 (1992) 21–36.
[53] L. Lu, X. Peng, High-order random walks and generalized laplacians on hypergraphs, Internet Math. 9 (1) (2013) 3–32.
[54] J. Rodriguez, Laplacian eigenvalues and partition problems in hypergraphs, Appl. Math. Lett. 22 (6) (2009) 916–921.
[55] T.-H.H. Chan, Z. Liang, Generalizing the hypergraph laplacian via a diffusion process with mediators, Theoret. Comput. Sci. 806 (2020) 416–428.
[56] A. Louis, Hypergraph Markov operators, eigenvalues and approximation algorithms, in: Proceedings of the Forty-Seventh Annual ACM Symposium on Theory of Computing, 2015, pp. 713–722.
[57] F. Abdelnour, H.U. Voss, A. Raj, Network diffusion accurately models the relationship between structural and functional brain connectivity networks, Neuroimage 90 (2014) 335–347.
[58] S.G. Surampudi, S. Naik, R.B. Surampudi, V.K. Jirsa, A. Sharma, D. Roy, Multiple kernel learning model for relating structural and functional connectivity in the brain, Sci. Rep. 8 (1) (2018) 3265.
[59] S.G. Surampudi, J. Misra, G. Deco, R.S. Bapi, A. Sharma, D. Roy, Resting state dynamics meets anatomical structure: Temporal multiple kernel learning (tMKL) model, NeuroImage 184 (2019) 609–620.
[60] D.V. Anand, M.K. Chung, Hodge Laplacian of brain networks, IEEE Trans. Med. Imaging 42 (5) (2023) 1563–1573.
[61] R.H. Atkin, Mathematical Structure in Human Affairs, Heinemann Educational, London, 1974.
[62] R. Atkin, The methodology of Q-analysis: How to study corporations by using concepts of connectivity, Manag. Decis. 18 (7) (1980) 380–390.
[63] N. Smirnov, S. Kurkin, A. Hramov, A topological graph kernel based on Q-analysis of clique complexes, Eur. Phys. J. Spec. Top. (2025) 1–9.
[64] M. Andjelković, B. Tadić, R. Melnik, The topology of higher-order complexes associated with brain hubs in human connectomes, Sci. Rep. 10 (1) (2020) 17320.
[65] S.A. Kurkin, N.M. Smirnov, R. Paunova, S. Kandilarova, D. Stoyanov, L. Mayorova, A.E. Hramov, Beyond pairwise interactions: higher-order Q-analysis of fMRI-based brain functional networks in patients with major depressive disorder, IEEE Access (2024).
[66] N. Smirnov, S. Kurkin, A. Hramov, A Q-analysis package for higher-order interactions analysis in python and its application in network physiology, Front. Netw. Physiol. 5 (1) (2025) 1691159.
[67] J. Yang, F. Wang, Z. Li, Z. Yang, X. Dong, Q. Han, Constructing high-order functional networks based on hypergraph for diagnosis of autism spectrum disorders, Front. Neurosci. 17 (2023) 1257982.
[68] R.M. Hutchison, T. Womelsdorf, E.A. Allen, P.A. Bandettini, V.D. Calhoun, M. Corbetta, S. Della Penna, J.H. Duyn, G.H. Glover, J. Gonzalez-Castillo, et al., Dynamic functional connectivity: Promise, issues, and interpretations, Neuroimage 80 (2013) 360–378.
[69] B. Cao, Y. Guo, F. Xia, L. Li, Z. Ren, M. Lu, J. Wang, R. Huang, Dynamic reconfiguration of brain functional networks in world class gymnasts: a resting-state functional MRI study, Brain Commun. 7 (2) (2025) fcaf083.
[70] T.O. Laumann, A.Z. Snyder, C. Gratton, Challenges in the measurement and interpretation of dynamic functional connectivity, Imaging Neurosci. 2 (2024) 1–19.
[71] A. Behrouz, F. Hashemi, Learning temporal higher-order patterns to detect anomalous brain activity, in: Machine Learning for Health (ML4H), PMLR, 2023, pp. 39–51.
[72] J.M. Buldú, M.A. Porter, Frequency-based brain networks: From a multiplex framework to a full multilayer description, Netw. Neurosci. 2 (4) (2018) 418–441.
[73] Y. Huang, Y. Li, Y. Yuan, X. Zhang, W. Yan, T. Li, Y. Niu, M. Xu, T. Yan, X. Li, et al., Beta-informativeness-diffusion multilayer graph embedding for brain network analysis, Front. Neurosci. 18 (2024) 1303741.
[74] M. De Domenico, Multilayer modeling and analysis of human brain networks, Giga Sci. 6 (5) (2017) gix004.
[75] Y. Teng, K. Wu, J. Liu, Y. Li, X. Teng, Constructing high-order functional connectivity networks with temporal information from fMRI data, IEEE Trans. Med. Imaging (2024).
[76] A.E. Sizemore, C. Giusti, A. Kahn, J.M. Vettel, R.F. Betzel, D.S. Bassett, Cliques and cavities in the human connectome, J. Comput. Neurosci. 44 (2018) 115–145.
[77] G. Petri, P. Expert, F. Turkheimer, R. Carhart-Harris, D. Nutt, P.J. Hellyer, F. Vaccarino, Homological scaffolds of brain functional networks, J. R. Soc. Interface 11 (101) (2014) 20140873.
[78] R. Hindriks, T.A. Broeders, M.M. Schoonheim, L. Douw, F. Santos, W. van Wieringen, P.K. Tewarie, Higher-order functional connectivity analysis of resting-state functional magnetic resonance imaging data using multivariate cumulants, Hum. Brain Mapp. 45 (5) (2024) e26663.
[79] M. Yuan, W. Jia, X. Luo, J. Ye, P. Zhu, J. Li, MHSA: A multi-scale hypergraph network for mild cognitive impairment detection via synchronous and attentive fusion, in: 2024 IEEE International Conference on Bioinformatics and Biomedicine, BIBM, IEEE, 2024, pp. 2808–2815.
[80] S. Ogawa, T.-M. Lee, A.R. Kay, D.W. Tank, Brain magnetic resonance imaging with contrast dependent on blood oxygenation, Proc. Natl. Acad. Sci. 87 (24) (1990) 9868–9872.
[81] S. Ogawa, D.W. Tank, R. Menon, J.M. Ellermann, S.G. Kim, H. Merkle, K. Ugurbil, Intrinsic signal changes accompanying sensory stimulation: Functional brain mapping with magnetic resonance imaging, Proc. Natl. Acad. Sci. 89 (13) (1992) 5951–5955.
[82] K.K. Kwong, J.W. Belliveau, D.A. Chesler, I.E. Goldberg, R.M. Weisskoff, B.P. Poncelet, D.N. Kennedy, B.E. Hoppel, M.S. Cohen, R. Turner, Dynamic magnetic resonance imaging of human brain activity during primary sensory stimulation, Proc. Natl. Acad. Sci. 89 (12) (1992) 5675–5679.
[83] R. Buxton, Interpreting oxygenation-based neuroimaging signals: the importance and the challenge of understanding brain oxygen metabolism, Front. Neuroenergetics 2 (2010) 1648.
[84] K.R. Thulborn, J.C. Waterton, P.M. Matthews, G.K. Radda, Oxygenation dependence of the transverse relaxation time of water protons in whole blood at high field, Biochim. et Biophys. Acta (BBA)-General Subj. 714 (2) (1982) 265–270.
[85] R.B. Buxton, The physics of functional magnetic resonance imaging (fMRI), Rep. Progr. Phys. 76 (9) (2013) 096601.
[86] P.T. Fox, M.E. Raichle, Focal physiological uncoupling of cerebral blood flow and oxidative metabolism during somatosensory stimulation in human subjects, Proc. Natl. Acad. Sci. 83 (4) (1986) 1140–1144.
[87] G.A. Dienel, Brain glucose metabolism: Integration of energetics with function, Physiol. Rev. (2018).
[88] G.A. Dienel, L. Hertz, Glucose and lactate metabolism during brain activation, J. Neurosci. Res. 66 (5) (2001) 824–838.
[89] A.A. Phillips, F.H. Chan, M.M.Z. Zheng, A.V. Krassioukov, P.N. Ainslie, Neurovascular coupling in humans: physiology, methodological advances and clinical implications, J. Cereb. Blood Flow Metab. 36 (4) (2016) 647–664.

[90] E.M. Hillman, Coupling mechanism and significance of the BOLD signal: A status report, Annu. Rev. Neurosci. 37 (1) (2014) 161–181.
[91] N. Bazargani, D. Attwell, Astrocyte calcium signaling: the third wave, Nature Neurosci. 19 (2) (2016) 182–189.
[92] V. Muoio, P. Persson, M. Sendeski, The neurovascular unit–concept review, Acta Physiol. 210 (4) (2014) 790–798.
[93] L. Yang, W. Zhao, Y. Kan, C. Ren, X. Ji, From mechanisms to medicine: Neurovascular coupling in the diagnosis and treatment of cerebrovascular disorders: a narrative review, Cells 14 (1) (2024) 16.
[94] D. Zhang, J. Ruan, S. Peng, J. Li, X. Hu, Y. Zhang, T. Zhang, Y. Ge, Z. Zhu, X. Xiao, et al., Synaptic-like transmission between neural axons and arteriolar smooth muscle cells drives cerebral neurovascular coupling, Nature Neurosci. 27 (2) (2024) 232–248.
[95] I.M. Inocencio, N. Kaur, N.T. Tran, F.Y. Wong, Cerebral haemodynamic response to somatosensory stimulation in preterm lambs is enhanced following sildenafil and inhaled nitric oxide administration, Front. Physiol. 14 (2023) 1101647.
[96] D. Attwell, A.M. Buchan, S. Charpak, M. Lauritzen, B.A. MacVicar, E.A. Newman, Glial and neuronal control of brain blood flow, Nature 468 (7321) (2010) 232–243.
[97] S.P. Marrelli, Mechanisms of endothelial $P2Y_1$-and $P2Y_2$-mediated vasodilatation involve differential $[Ca2+]+i$ responses, Am. J. Physiology—Heart Circ. Physiol. 281 (4) (2001) H1759–H1766.
[98] S.E. Wölfle, D.J. Chaston, K. Goto, S.L. Sandow, F.R. Edwards, C.E. Hill, Non-linear relationship between hyperpolarisation and relaxation enables long distance propagation of vasodilatation, J. Physiol. 589 (10) (2011) 2607–2623.
[99] C. De Wit, T.M. Griffith, Connexins and gap junctions in the EDHF phenomenon and conducted vasomotor responses, Pflügers Archiv-European J. Physiol. 459 (6) (2010) 897–914.
[100] J.D. Ball, E. Hills, A. Altaf, P. Ramesh, M. Green, F.B. Surti, J.S. Minhas, T.G. Robinson, B. Bond, A. Lester, et al., Neurovascular coupling methods in healthy individuals using transcranial doppler ultrasonography: A systematic review and consensus agreement, J. Cereb. Blood Flow Metab. 44 (12) (2024) 1409–1429.
[101] R.B. Panerai, M. Eyre, J.F. Potter, Multivariate modeling of cognitive-motor stimulation on neurovascular coupling: transcranial Doppler used to characterize myogenic and metabolic influences, Am. J. Physiology-Regulatory, Integr. Comp. Physiol. 303 (4) (2012) R395–R407.
[102] T. Csipo, P. Mukli, A. Lipecz, S. Tarantini, D. Bahadli, O. Abdulhussein, C. Owens, T. Kiss, P. Balasubramanian, Á. Nyúl-Tóth, et al., Assessment of age-related decline of neurovascular coupling responses by functional near-infrared spectroscopy (fNIRS) in humans, Geroscience 41 (5) (2019) 495–509.
[103] S. Amemiya, H. Takao, O. Abe, Resting-state fMRI: Emerging concepts for future clinical application, J. Magn. Reson. Imaging 59 (4) (2024) 1135–1148.
[104] J. Klohs, W.C. Chen, R. Araki, Advanced preclinical functional magnetic resonance imaging of the brain, Npj Imaging 3 (1) (2025) 27.
[105] R. Stickland, M. Allen, L. Magazzini, K.D. Singh, R.G. Wise, V. Tomassini, Neurovascular coupling during visual stimulation in multiple sclerosis: a MEG-fMRI study, Neuroscience 403 (2019) 54–69.
[106] Y. Li, Y. Liu, Z. Zhang, T. Wan, H. Liu, Deep learning for enhancing high-resolution BOLD-fMRI: A narrative review of super-resolution, segmentation, and registration methods, Neurosurg. Subspecialties 1 (2025) 92–102.
[107] V. Kuperman, Magnetic Resonance Imaging: Physical Principles and Applications, Elsevier, 2000.
[108] M.A. Lindquist, T.D. Wager, Principles of functional magnetic resonance imaging, in: Handbook of Neuroimaging Data Analysis, London: CRC Press, 2014, pp. 139–174.
[109] R.B. Buxton, E.C. Wong, L.R. Frank, Dynamics of blood flow and oxygenation changes during brain activation: The balloon model, Magn. Reson. Med. 39 (6) (1998) 855–864.
[110] N.K. Logothetis, J. Pauls, M. Augath, T. Trinath, A. Oeltermann, Neurophysiological investigation of the basis of the fMRI signal, Nature 412 (6843) (2001) 150–157.
[111] G.M. Boynton, S.A. Engel, G.H. Glover, D.J. Heeger, Linear systems analysis of functional magnetic resonance imaging in human V1, J. Neurosci. 16 (13) (1996) 4207–4221.
[112] A. Devor, A.K. Dunn, M.L. Andermann, I. Ulbert, D.A. Boas, A.M. Dale, Coupling of total hemoglobin concentration, oxygenation, and neural activity in rat somatosensory cortex, Neuron 39 (2) (2003) 353–359.
[113] K.J. Friston, A. Mechelli, R. Turner, C.J. Price, Nonlinear responses in fMRI: the balloon model, Volterra kernels, and other hemodynamics, NeuroImage 12 (4) (2000) 466–477.
[114] C. Martin, Y. Zheng, N.R. Sibson, J.E.W. Mayhew, J. Berwick, Complex spatiotemporal haemodynamic response following sensory stimulation in the awake rat, NeuroImage 66 (2013) 1–8.
[115] B. Yesilyurt, K. Uğurbil, K. Uludağ, Dynamics and nonlinearities of the BOLD response at very short stimulus durations, Magn. Reson. Imaging 26 (7) (2008) 853–862.
[116] A.J. Kennerley, S. Harris, M. Bruyns-Haylett, L. Boorman, Y. Zheng, J. Berwick, M. Jones, Early and late stimulus-evoked cortical hemodynamic responses provide insight into the neurogenic nature of neurovascular coupling, J. Cereb. Blood Flow Metab. 32 (3) (2012) 468–480.
[117] M.M.B. Cardoso, Y.B. Sirotin, B. Lima, E. Glushenkova, A. Das, The neuroimaging signal is a linear sum of neurally distinct stimulus- and task-related components, Nature Neurosci. 15 (9) (2012) 1298–1306.
[118] K.J. Friston, S. Williams, R. Howard, R.S. Frackowiak, R. Turner, Movement-related effects in fMRI time-series, Magn. Reson. Med. 35 (3) (1996) 346–355.
[119] M. Jenkinson, P. Bannister, M. Brady, S. Smith, Improved optimization for the robust and accurate linear registration and motion correction of brain images, Neuroimage 17 (2) (2002) 825–841.
[120] J.D. Power, K.A. Barnes, A.Z. Snyder, B.L. Schlaggar, S.E. Petersen, Spurious but systematic correlations in functional connectivity MRI networks arise from subject motion, Neuroimage 59 (3) (2012) 2142–2154.
[121] O. Esteban, C.J. Markiewicz, R.W. Blair, C.A. Moodie, A.I. Isik, A. Erramuzpe, J.D. Kent, M. Goncalves, E. DuPre, M. Snyder, et al., Fmriprep: a robust preprocessing pipeline for functional MRI, Nature Methods 16 (1) (2019) 111–116.
[122] M.A. Lindquist, S. Geuter, T.D. Wager, B.S. Caffo, Modular preprocessing pipelines can reintroduce artifacts into fmri data, Hum. Brain Mapp. 40 (8) (2019) 2358–2376.
[123] A.C. Evans, D.L. Collins, S. Mills, E.D. Brown, R.L. Kelly, T.M. Peters, 3D statistical neuroanatomical models from 305 MRI volumes, in: 1993 IEEE Conference Record Nuclear Science Symposium and Medical Imaging Conference, IEEE, 1993, pp. 1813–1817.
[124] P.J. Talairach, P. Tournoux, Co-planar Stereotaxic Atlas of the Human Brain, Thieme, New York, 1988.
[125] A.R. Laird, J.L. Robinson, K.M. McMillan, D. Tordesillas-Gutiérrez, S.T. Moran, S.M. Gonzales, K.L. Ray, C. Franklin, D.C. Glahn, P.T. Fox, et al., Comparison of the disparity between talairach and MNI coordinates in functional neuroimaging data: validation of the lancaster transform, Neuroimage 51 (2) (2010) 677–683.
[126] J. Ashburner, A fast diffeomorphic image registration algorithm, Neuroimage 38 (1) (2007) 95–113.
[127] K.J. Worsley, A.C. Evans, S. Marrett, P. Neelin, A three-dimensional statistical analysis for CBF activation studies in human brain, J. Cereb. Blood Flow Metab. 12 (6) (1992) 900–918.
[128] K. Friston, O. Josephs, E. Zarahn, A. Holmes, S. Rouquette, J.-B. Poline, To smooth or not to smooth?: Bias and efficiency in fMRI time-series analysis, Neuroimage 12 (2) (2000) 196–208.

[129] V.S. Khorev, S.A. Kurkin, G. Zlateva, R. Paunova, S. Kandilarova, M. Maes, D. Stoyanov, A.E. Hramov, Disruptions in segregation mechanisms in fMRI-based brain functional network predict the major depressive disorder condition, Chaos Solitons Fractals 188 (2024) 115566.
[130] R. Pauli, A. Bowring, R. Reynolds, G. Chen, T.E. Nichols, C. Maumet, Exploring fMRI results space: 31 variants of an fMRI analysis in AFNI, FSL, and SPM, Front. Neuroinformatics 10 (2016) 24.
[131] W.D. Penny, K.J. Friston, J.T. Ashburner, S.J. Kiebel, T.E. Nichols, Statistical Parametric Mapping: the Analysis of Functional Brain Images, Elsevier, 2011.
[132] M. Jenkinson, C.F. Beckmann, T.E. Behrens, M.W. Woolrich, S.M. Smith, Fsl, Neuroimage 62 (2) (2012) 782–790.
[133] R.W. Cox, AFNI: software for analysis and visualization of functional magnetic resonance neuroimages, Comput. Biomed. Res. 29 (3) (1996) 162–173.
[134] A. Nieto-Castanon, Handbook of Functional Connectivity Magnetic Resonance Imaging Methods in CONN, Hilbert Press, 2020.
[135] J.B. Teves, J. Gonzalez-Castillo, M. Holness, M. Spurney, P.A. Bandettini, D.A. Handwerker, The art and science of using quality control to understand and improve fMRI data, Front. Neurosci. 17 (2023) 1100544.
[136] W. Lu, K. Dong, D. Cui, Q. Jiao, J. Qiu, Quality assurance of human functional magnetic resonance imaging: A literature review, Quant. Imaging Med. Surg. 9 (6) (2019) 1147.
[137] T.D. Satterthwaite, D.H. Wolf, K. Ruparel, G. Erus, M.A. Elliott, S.B. Eickhoff, E.D. Gennatas, C. Jackson, K. Prabhakaran, A. Smith, et al., Heterogeneous impact of motion on fundamental patterns of developmental changes in functional connectivity during youth, Neuroimage 83 (2013) 45–57.
[138] A. Geissler, A. Gartus, T. Foki, A.R. Tahamtan, R. Beisteiner, M. Barth, Contrast-to-noise ratio (CNR) as a quality parameter in fMRI, J. Magn. Reson. Imaging: An Off. J. Int. Soc. Magn. Reson. Med. 25 (6) (2007) 1263–1270.
[139] M. Welvaert, Y. Rosseel, On the definition of signal-to-noise ratio and contrast-to-noise ratio for fMRI data, PloS One 8 (11) (2013) e77089.
[140] E.T. Rolls, C.-C. Huang, C.-P. Lin, J. Feng, M. Joliot, Automated anatomical labelling atlas 3, Neuroimage 206 (2020) 116189.
[141] N. Makris, R. Rushmore, J. Kaiser, M. Albaugh, M. Kubicki, Y. Rathi, F. Zhang, L.J. O'Donnell, E. Yeterian, V.S. Caviness, et al., A proposed human structural brain connectivity matrix in the center for morphometric analysis harvard-oxford atlas framework: a historical perspective and future direction for enhancing the precision of human structural connectivity with a novel neuroanatomical typology, Dev. Neurosci. 45 (4) (2023) 161–180.
[142] R.C. Craddock, G.A. James, P.E. Holtzheimer III, X.P. Hu, H.S. Mayberg, A whole brain fMRI atlas generated via spatially constrained spectral clustering, Hum. Brain Mapp. 33 (8) (2012) 1914–1928.
[143] K. Pearson, VII. Note on regression and inheritance in the case of two parents, Proc. R. Soc. Lond. 58 (347–352) (1895) 240–242.
[144] L. Roell, S. Wunderlich, D. Roell, F. Raabe, E. Wagner, Z. Shi, A. Schmitt, P. Falkai, S. Stoecklein, D. Keeser, How to measure functional connectivity using resting-state fmri? A comprehensive empirical exploration of different connectivity metrics, NeuroImage 312 (2025) 121195.
[145] J. Hlinka, M. Paluš, M. Vejmelka, D. Mantini, M. Corbetta, Functional connectivity in resting-state fMRI: is linear correlation sufficient? Neuroimage 54 (3) (2011) 2218–2225.
[146] D. Liu, C. Yan, J. Ren, L. Yao, V.J. Kiviniemi, Y. Zang, Using coherence to measure regional homogeneity of resting-state fmri signal, Front. Syst. Neurosci. 4 (2010) 1366.
[147] Z. Wang, A. Alahmadi, D. Zhu, T. Li, Brain functional connectivity analysis using mutual information, in: 2015 IEEE Global Conference on Signal and Information Processing, GlobalSIP, IEEE, 2015, pp. 542–546.
[148] G. Chiarion, L. Sparacino, Y. Antonacci, L. Faes, L. Mesin, Connectivity analysis in EEG data: a tutorial review of the state of the art and emerging trends, Bioengineering 10 (3) (2023) 372.
[149] L. Sparacino, L. Faes, G. Mijatović, G. Parla, V. Lo Re, R. Miraglia, J. de Ville de Goyet, G. Sparacia, Statistical approaches to identify pairwise and high-order brain functional connectivity signatures on a single-subject basis, Life 13 (10) (2023) 2075.
[150] P.L. Williams, R.D. Beer, Nonnegative decomposition of multivariate information, 2010, arXiv preprint arXiv:1004.2515.
[151] J. Schwarz, F. Zistler, A. Usheva, A. Fix, S. Zinn, J. Zimmermann, F. Knolle, G. Schneider, R. Nuttall, Investigating dynamic brain functional redundancy as a mechanism of cognitive reserve, Front. Aging Neurosci. 17 (2025) 1535657.
[152] A. Zalesky, A. Fornito, E.T. Bullmore, Network-based statistic: identifying differences in brain networks, Neuroimage 53 (4) (2010) 1197–1207.
[153] N.Z. Bielczyk, A. Llera, J.K. Buitelaar, J.C. Glennon, C.F. Beckmann, Increasing robustness of pairwise methods for effective connectivity in magnetic resonance imaging by using fractional moment series of bold signal distributions, Netw. Neurosci. 3 (4) (2019) 1009–1037.
[154] J. Faskowitz, F.Z. Esfahlani, Y. Jo, O. Sporns, R.F. Betzel, Edge-centric functional network representations of human cerebral cortex reveal overlapping system-level architecture, Nature Neurosci. 23 (12) (2020) 1644–1654.
[155] A. Santoro, F. Battiston, G. Petri, E. Amico, Higher-order organization of multivariate time series, Nat. Phys. 19 (2) (2023) 221–229.
[156] C. Pan, H. Yu, X. Fei, X. Zheng, R. Yu, Temporal-spatial dynamic functional connectivity analysis in schizophrenia classification, Front. Neurosci. 16 (2022) 965937.
[157] J.H. Ward Jr., Hierarchical grouping to optimize an objective function, J. Amer. Statist. Assoc. 58 (301) (1963) 236–244.
[158] E. Simonotto, H. Whalley, S. Lawrie, L. Murray, D. Mcgonigle, A.J. Storkey, Learning structural equation models for fMRI, Adv. Neural Inf. Process. Syst. 19 (2006).
[159] J. Guàrdia-Olmos, M. Peró-Cebollero, E. Gudayol-Ferré, Meta-analysis of the structural equation models' parameters for the estimation of brain connectivity with fMRI, Front. Behav. Neurosci. 12 (2018) 19.
[160] X. Chen, Z.J. Wang, M.J. McKeown, A sparse unified structural equation modeling approach for brain connectivity analysis, in: Proc. Int. Conf. Biomed. Bioinformat. Eng, 2009.
[161] B.P. Rogers, S.B. Katwal, V.L. Morgan, C.L. Asplund, J.C. Gore, Functional MRI and multivariate autoregressive models, Magn. Reson. Imaging 28 (8) (2010) 1058–1065.
[162] L. Harrison, W.D. Penny, K. Friston, Multivariate autoregressive modeling of fMRI time series, Neuroimage 19 (4) (2003) 1477–1491.
[163] G. Deshpande, S. LaConte, G.A. James, S. Peltier, X. Hu, Multivariate granger causality analysis of fMRI data, Hum. Brain Mapp. 30 (4) (2009) 1361–1373.
[164] K. Baba, R. Shibata, M. Sibuya, Partial correlation and conditional correlation as measures of conditional independence, Aust. N. Z. J. Stat. 46 (4) (2004) 657–664.
[165] A. Roebroeck, E. Formisano, R. Goebel, Mapping directed influence over the brain using granger causality and fMRI, Neuroimage 25 (1) (2005) 230–242.
[166] L.A. Baccalá, K. Sameshima, Partial directed coherence: a new concept in neural structure determination, Biol. Cybernet. 84 (6) (2001) 463–474.
[167] B. Schelter, J. Timmer, M. Eichler, Assessing the strength of directed influences among neural signals using renormalized partial directed coherence, J. Neurosci. Methods 179 (1) (2009) 121–130.
[168] M. Kamiński, M. Ding, W.A. Truccolo, S.L. Bressler, Evaluating causal relations in neural systems: Granger causality, directed transfer function and statistical assessment of significance, Biol. Cybernet. 85 (2) (2001) 145–157.
[169] A. Korzeniewska, M. Mańczak, M. Kamiński, K.J. Blinowska, S. Kasicki, Determination of information flow direction among brain structures by a modified directed transfer function (dDTF) method, J. Neurosci. Methods 125 (1–2) (2003) 195–207.

[170] S. Erla, L. Faes, E. Tranquillini, D. Orrico, G. Nollo, et al., Multivariate autoregressive model with instantaneous effects to improve brain connectivity estimation, Int. J. Bioelectromagn. 11 (2) (2009) 74–79.
[171] W. Mader, D. Feess, D. Saur, R. Lange, V. Glauche, C. Weiller, J. Timmer, B. Schelter, Investigating multivariate systems using directed partial correlation, Int. J. Bioelectromagn. 12 (1) (2001) 21–25.
[172] L. Novelli, A. Razi, A mathematical perspective on edge-centric brain functional connectivity, Nat. Commun. 13 (1) (2022) 2693.
[173] M. Ursino, G. Ricci, E. Magosso, Transfer entropy as a measure of brain connectivity: a critical analysis with the help of neural mass models, Front. Comput. Neurosci. 14 (2020) 45.
[174] B. Zheng, Using Transfer Entropy to Understand Information Flow and Connectivity in Neural Networks, University of Chicago, 2022.
[175] S. Ito, M.E. Hansen, R. Heiland, A. Lumsdaine, A.M. Litke, J.M. Beggs, Extending transfer entropy improves identification of effective connectivity in a spiking cortical network model, PloS One 6 (11) (2011) e27431.
[176] S. Watanabe, Information theoretical analysis of multivariate correlation, IBM J. Res. Dev. 4 (1) (1960) 66–82.
[177] M. Wibral, V. Priesemann, J.W. Kay, J.T. Lizier, W.A. Phillips, Partial information decomposition as a unified approach to the specification of neural goal functions, Brain Cogn. 112 (2017) 25–38.
[178] I. Gat, N. Tishby, Synergy and redundancy among brain cells of behaving monkeys, Adv. Neural Inf. Process. Syst. 11 (1998).
[179] L. Faes, L. Sparacino, G. Mijatovic, Y. Antonacci, L. Ricci, D. Marinazzo, S. Stramaglia, Partial information rate decomposition, 2025, arXiv preprint arXiv:2502.04550.
[180] R.A. Ince, The partial entropy decomposition: Decomposing multivariate entropy and mutual information via pointwise common surprisal, 2017, arXiv preprint arXiv:1702.01591.
[181] S.P. Sherrill, N.M. Timme, J.M. Beggs, E.L. Newman, Partial information decomposition reveals that synergistic neural integration is greater downstream of recurrent information flow in organotypic cortical cultures, PLoS Comput. Biol. 17 (7) (2021) e1009196.
[182] N. Bertschinger, J. Rauh, E. Olbrich, J. Jost, N. Ay, Quantifying unique information, Entropy 16 (4) (2014) 2161–2183.
[183] A.B. Barrett, Exploration of synergistic and redundant information sharing in static and dynamical Gaussian systems, Phys. Rev. E 91 (5) (2015) 052802.
[184] P. Venkatesh, C. Bennett, S. Gale, T. Ramirez, G. Heller, S. Durand, S. Olsen, S. Mihalas, Gaussian partial information decomposition: Bias correction and application to high-dimensional data, Adv. Neural Inf. Process. Syst. 36 (2023) 74602–74635.
[185] C. Goswami, A. Merkley, Analytically deriving partial information decomposition for affine systems of stable and convolution-closed distributions, Adv. Neural Inf. Process. Syst. 37 (2024) 86749–86835.
[186] T. Kumar, S. Vaidyanathan, H. Ananthapadmanabhan, S. Parthasarathy, B. Ravindran, A new measure of modularity in hypergraphs: Theoretical insights and implications for effective clustering, in: International Conference on Complex Networks and their Applications, Springer, 2019, pp. 286–297.
[187] B.T. Yeo, F.M. Krienen, J. Sepulcre, M.R. Sabuncu, D. Lashkari, M. Hollinshead, J.L. Roffman, J.W. Smoller, L. Zöllei, J.R. Polimeni, et al., The organization of the human cerebral cortex estimated by intrinsic functional connectivity, J. Neurophysiol. (2011).
[188] F.E. Rosas, P.A. Mediano, M. Gastpar, H.J. Jensen, Quantifying high-order interdependencies via multivariate extensions of the mutual information, Phys. Rev. E 100 (3) (2019) 032305.
[189] T. Sun, Linear dependence structure of the entropy space, Inf. Control 29 (4) (1975) 337–368.
[190] T. Scagliarini, L. Sparacino, L. Faes, D. Marinazzo, S. Stramaglia, Gradients of O-information highlight synergy and redundancy in physiological applications, Front. Netw. Physiol. 3 (2024) 1335808.
[191] J.L. Puchalla, E. Schneidman, R.A. Harris, M.J. Berry, Redundancy in the population code of the retina, Neuron 46 (3) (2005) 493–504.
[192] P.E. Latham, S. Nirenberg, Synergy, redundancy, and independence in population codes, revisited, J. Neurosci. 25 (21) (2005) 5195–5206.
[193] S. Panzeri, M. Moroni, H. Safaai, C.D. Harvey, The structures and functions of correlations in neural population codes, Nature Rev. Neurosci. 23 (9) (2022) 551–567.
[194] M. Pope, T.F. Varley, M.G. Puxeddu, J. Faskowitz, O. Sporns, Time-varying synergy/redundancy dominance in the human cerebral cortex, J. Phys.: Complex. 6 (1) (2025) 015015.
[195] J. Theiler, S. Eubank, A. Longtin, B. Galdrikian, J.D. Farmer, Testing for nonlinearity in time series: The method of surrogate data, Phys. D 58 (1–4) (1992) 77–94.
[196] T. Schreiber, A. Schmitz, Improved surrogate data for nonlinearity tests, Phys. Rev. Lett. 77 (4) (1996) 635.
[197] B. Efron, Bootstrap methods: Another look at the jackknife, in: Breakthroughs in Statistics: Methodology and Distribution, Springer, 1992, pp. 569–593.
[198] D.N. Politis, The impact of bootstrap methods on time series analysis, Statist. Sci. (2003) 219–230.
[199] J.-P. Kreiss, E. Paparoditis, Bootstrap methods for dependent data: A review, J. Korean Statist. Soc. 40 (4) (2011) 357–378.
[200] D. Zhu, X. Li, X. Jiang, H. Chen, D. Shen, T. Liu, Exploring high-order functional interactions via structurally-weighted lasso models, in: International Conference on Information Processing in Medical Imaging, Springer, 2013, pp. 13–24.
[201] R. Jain, W. Xu, HDSI: High dimensional selection with interactions algorithm on feature selection and testing, PLoS One 16 (2) (2021) e0246159.
[202] B. Jie, C.-Y. Wee, D. Shen, D. Zhang, Hyper-connectivity of functional networks for brain disease diagnosis, Med. Image Anal. 32 (2016) 84–100.
[203] R. Tibshirani, Regression shrinkage and selection via the lasso, J. R. Stat. Soc. Ser. B Stat. Methodol. 58 (1) (1996) 267–288.
[204] Y. Li, C. Sun, P. Li, Y. Zhao, G.K. Mensah, Y. Xu, H. Guo, J. Chen, Hypernetwork construction and feature fusion analysis based on sparse group lasso method on fMRI dataset, Front. Neurosci. 14 (2020) 60.
[205] L. Meier, S. Van De Geer, P. Bühlmann, The group lasso for logistic regression, J. R. Stat. Soc. Ser. B 70 (1) (2008) 53–71.
[206] B.H. Vieira, M. Schöttner, V.D. Calhoun, C.E.G. Salmon, Beyond functional connectivity: deep learning applied to resting-state fMRI time series in the prediction of 58 human traits in the HCP, BioRxiv: Prepr. Serv. Biology (2024).
[207] R.J. Meszlényi, K. Buza, Z. Vidnyánszky, Resting state fMRI functional connectivity-based classification using a convolutional neural network architecture, Front. Neuroinformatics 11 (2017) 61.
[208] B. Hebling Vieira, J. Dubois, V.D. Calhoun, C.E. Garrido Salmon, A deep learning based approach identifies regions more relevant than resting-state networks to the prediction of general intelligence from resting-state fMRI, Hum. Brain Mapp. 42 (18) (2021) 5873–5887.
[209] H. Mohammadi, W. Karwowski, Graph neural networks in brain connectivity studies: Methods, challenges, and future directions, Brain Sci. 15 (1) (2024) 17.
[210] X. Luo, J. Wu, J. Yang, S. Xue, A. Beheshti, Q.Z. Sheng, D. McAlpine, P. Sowman, A. Giral, P.S. Yu, Graph neural networks for brain graph learning: A survey, 2024, arXiv preprint arXiv:2406.02594.
[211] T. Screven, A. Necz, J. Smucny, I. Davidson, Using graph convolutional networks to address fMRI small data problems, 2025, arXiv preprint arXiv:2502.17489.
[212] H.A. Bedel, I. Sivgin, O. Dalmaz, S.U. Dar, T. Çukur, BolT: Fused window transformers for fMRI time series analysis, Med. Image Anal. 88 (2023) 102841.
[213] N. Asadi, I.R. Olson, Z. Obradovic, A transformer model for learning spatiotemporal contextual representation in fMRI data, Netw. Neurosci. 7 (1) (2023) 22–47.

[214] S.M. Plis, J. Sui, T. Lane, S. Roy, V.P. Clark, V.K. Potluru, R.J. Huster, A. Michael, S.R. Sponheim, M.P. Weisend, et al., High-order interactions observed in multi-task intrinsic networks are dominant indicators of aberrant brain function in schizophrenia, NeuroImage 102 (2014) 35–48.
[215] M. Gatica, R. Cofré, P.A. Mediano, F.E. Rosas, P. Orio, I. Diez, S.P. Swinnen, J.M. Cortes, High-order interdependencies in the aging brain, Brain Connect. 11 (9) (2021) 734–744.
[216] H. Zhang, X. Chen, Y. Zhang, D. Shen, Test-retest reliability of "high-order" functional connectivity in young healthy adults, Front. Neurosci. 11 (2017) 439.
[217] S. Gu, M. Yang, J.D. Medaglia, R.C. Gur, R.E. Gur, T.D. Satterthwaite, D.S. Bassett, Functional hypergraph uncovers novel covariant structures over neurodevelopment, Hum. Brain Mapp. 38 (8) (2017) 3823–3835.
[218] W. Niu, X. Huang, K. Xu, T. Jiang, S. Yu, Pairwise interactions among brain regions organize large-scale functional connectivity during execution of various tasks, Neuroscience 412 (2019) 190–206.
[219] L. Xiao, J. Wang, P.H. Kassani, Y. Zhang, Y. Bai, J.M. Stephen, T.W. Wilson, V.D. Calhoun, Y.-P. Wang, Multi-hypergraph learning-based brain functional connectivity analysis in fMRI data, IEEE Trans. Med. Imaging 39 (5) (2019) 1746–1758.
[220] J. Wang, H. Li, G. Qu, K.M. Cecil, J.R. Dillman, N.A. Parikh, L. He, Dynamic weighted hypergraph convolutional network for brain functional connectome analysis, Med. Image Anal. 87 (2023) 102828.
[221] Q. Ling, A. Liu, Y. Li, T. Mi, P. Chan, B.T. Yeo, X. Chen, High-order graphical topology analysis of brain functional connectivity networks using fMRI, IEEE Trans. Neural Syst. Rehabil. Eng. (2025).
[222] R. Herzog, F.E. Rosas, R. Whelan, S. Fittipaldi, H. Santamaria-Garcia, J. Cruzat, A. Birba, S. Moguilner, E. Tagliazucchi, P. Prado, et al., Genuine high-order interactions in brain networks and neurodegeneration, Neurobiol. Dis. 175 (2022) 105918.
[223] H. Zhang, X. Chen, F. Shi, G. Li, M. Kim, P. Giannakopoulos, S. Haller, D. Shen, Topographical information-based high-order functional connectivity and its application in abnormality detection for mild cognitive impairment, J. Alzheimer's Dis. 54 (3) (2016) 1095–1112.
[224] X. Chen, H. Zhang, Y. Gao, C.-Y. Wee, G. Li, D. Shen, A.D.N. Initiative, High-order resting-state functional connectivity network for mci classification, Hum. Brain Mapp. 37 (9) (2016) 3282–3296.
[225] Y. Zhang, H. Zhang, X. Chen, S.-W. Lee, D. Shen, Hybrid high-order functional connectivity networks using resting-state functional MRI for mild cognitive impairment diagnosis, Sci. Rep. 7 (1) (2017) 6530.
[226] H. Guo, F. Zhang, J. Chen, Y. Xu, J. Xiang, Machine learning classification combining multiple features of a hyper-network of fMRI data in Alzheimer's disease, Front. Neurosci. 11 (2017) 615.
[227] Y. Li, J. Liu, X. Gao, B. Jie, M. Kim, P.-T. Yap, C.-Y. Wee, D. Shen, Multimodal hyper-connectivity of functional networks using functionally-weighted LASSO for MCI classification, Med. Image Anal. 52 (2019) 80–96.
[228] Y. Zhou, L. Qiao, W. Li, L. Zhang, D. Shen, Simultaneous estimation of low-and high-order functional connectivity for identifying mild cognitive impairment, Front. Neuroinformatics 12 (2018) 3.
[229] U. Khatri, G.-R. Kwon, Classification of alzheimer's disease and mild-cognitive impairment base on high-order dynamic functional connectivity at different frequency band, Mathematics 10 (5) (2022) 805.
[230] L. Arbabyazd, S. Petkoski, M. Breakspear, A. Solodkin, D. Battaglia, V. Jirsa, State-switching and high-order spatiotemporal organization of dynamic functional connectivity are disrupted by alzheimer's disease, Netw. Neurosci. 7 (4) (2023) 1420–1451.
[231] Z. Xi, T. Liu, H. Shi, Z. Jiao, Hypergraph representation of multimodal brain networks for patients with end-stage renal disease associated with mild cognitive impairment, Math. Biosci. Eng. 20 (2) (2023) 1882–1902.
[232] J. Liu, W. Cui, Y. Chen, Y. Ma, Q. Dong, R. Cai, Y. Li, B. Hu, Deep fusion of multi-template using spatio-temporal weighted multi-hypergraph convolutional networks for brain disease analysis, IEEE Trans. Med. Imaging 43 (2) (2023) 860–873.
[233] X. Han, J. Feng, H. Xu, S. Du, J. Li, A hypergraph transformer method for brain disease diagnosis, Front. Med. 11 (2024) 1496573.
[234] W. Wang, S. Zhang, Z. Wang, X. Luo, P. Luan, A. Hramov, J. Kurths, C. He, J. Li, Diagnosis of early mild cognitive impairment based on associated high-order functional connection network generated by multimodal MRI, IEEE Trans. Cogn. Dev. Syst. 16 (2) (2023) 618–627.
[235] S. Zhang, H. Zhao, W. Wang, Z. Wang, X. Luo, A. Hramov, J. Kurths, Edge-centric effective connection network based on muti-modal MRI for the diagnosis of Alzheimer's disease, Neurocomputing 552 (2023) 126512.
[236] S. Ray, N. Kalsi, H. Boecker, N. Upadhyay, R. Panda, Altered dynamic functional connectivity and reduced higher order information interaction in Parkinson's patients with hyposmia, NPJ Syst. Biology Appl. 11 (1) (2025) 93.
[237] H. Wang, Y. Liu, Y. Ding, Identifying diagnostic biomarkers for autism spectrum disorder from higher-order interactions using the PED algorithm, Neuroinformatics 22 (3) (2024) 285–296.
[238] F. Zhao, H. Zhang, I. Rekik, Z. An, D. Shen, Diagnosis of autism spectrum disorders using multi-level high-order functional networks derived from resting-state functional MRI, Front. Hum. Neurosci. 12 (2018) 184.
[239] F. Zhao, Z. Chen, I. Rekik, S.-W. Lee, D. Shen, Diagnosis of autism spectrum disorder using central-moment features from low-and high-order dynamic resting-state functional connectivity networks, Front. Neurosci. 14 (2020) 258.
[240] F. Zhao, Z. Han, D. Cheng, N. Mao, X. Chen, Y. Li, D. Fan, P. Liu, Hierarchical synchronization estimation of low-and high-order functional connectivity based on sub-network division for the diagnosis of autism spectrum disorder, Front. Neurosci. 15 (2022) 810431.
[241] F. Zhao, X. Zhang, K.-H. Thung, N. Mao, S.-W. Lee, D. Shen, Constructing multi-view high-order functional connectivity networks for diagnosis of autism spectrum disorder, IEEE Trans. Biomed. Eng. 69 (3) (2021) 1237–1250.
[242] X. Hao, Q. An, J. Li, H. Min, Y. Guo, M. Yu, J. Qin, Exploring high-order correlations with deep-broad learning for autism spectrum disorder diagnosis, Front. Neurosci. 16 (2022) 1046268.
[243] J. Ji, Y. Ren, M. Lei, FC–HAT: Hypergraph attention network for functional brain network classification, Inform. Sci. 608 (2022) 1301–1316.
[244] W. Wang, L. Xiao, G. Qu, V.D. Calhoun, Y.-P. Wang, X. Sun, Multiview hyperedge-aware hypergraph embedding learning for multisite, multiatlas fMRI based functional connectivity network analysis, Med. Image Anal. 94 (2024) 103144.
[245] X. Han, M. Lei, J. Li, Hypergraph-based semantic and topological self-supervised learning for brain disease diagnosis, Pattern Recognit. (2025) 111921.
[246] Y. Zheng, X. Chen, D. Li, Y. Liu, X. Tan, Y. Liang, H. Zhang, S. Qiu, D. Shen, Treatment-naive first episode depression classification based on high-order brain functional network, J. Affect. Disord. 256 (2019) 33–41.
[247] H. Guo, Y. Li, Y. Xu, Y. Jin, J. Xiang, J. Chen, Resting-state brain functional hyper-network construction based on elastic net and group lasso methods, Front. Neuroinformatics 12 (2018) 25.
[248] Y. Li, Q. Li, T. Li, Z. Zhou, Y. Xu, Y. Yang, J. Chen, H. Guo, Construction and multiple feature classification based on a high-order functional hypernetwork on fMRI data, Front. Neurosci. 16 (2022) 848363.
[249] J. Liu, W. Yang, Y. Ma, Q. Dong, Y. Li, B. Hu, D. Consortium, et al., Effective hyper-connectivity network construction and learning: Application to major depressive disorder identification, Comput. Biol. Med. 171 (2024) 108069.
[250] H. Guo, X. Huang, C. Wang, H. Wang, X. Bai, Y. Li, High-order line graphs of fMRI data in major depressive disorder, Med. Phys. 51 (8) (2024) 5535–5549.
[251] Y. Tang, J. Ding, Y. Chen, Y. Gao, A. Jiang, C. Wang, Anxiety disorder identification with biomarker detection through subspace-enhanced hypergraph neural network, Neural Netw. 187 (2025) 107293.

[252] C. Zu, Y. Gao, B. Munsell, M. Kim, Z. Peng, J.R. Cohen, D. Zhang, G. Wu, Identifying disease-related subnetwork connectome biomarkers by sparse hypergraph learning, Brain Imaging Behav. 13 (4) (2019) 879–892.
[253] S. Parisot, S.I. Ktena, E. Ferrante, M. Lee, R. Guerrero, B. Glocker, D. Rueckert, Disease prediction using graph convolutional networks: application to autism spectrum disorder and Alzheimer's disease, Med. Image Anal. 48 (2018) 117–130.
[254] J. Liu, G. Tan, W. Lan, J. Wang, Identification of early mild cognitive impairment using multi-modal data and graph convolutional networks, BMC Bioinformatics 21 (Suppl 6) (2020) 123.
[255] E.N. Pitsik, V.A. Maximenko, S.A. Kurkin, A.P. Sergeev, D. Stoyanov, R. Paunova, S. Kandilarova, D. Simeonova, A.E. Hramov, The topology of fMRI-based networks defines the performance of a graph neural network for the classification of patients with major depressive disorder, Chaos Solitons Fractals 167 (2023) 113041.
[256] Y. Feng, H. You, Z. Zhang, R. Ji, Y. Gao, Hypergraph neural networks, in: Proceedings of the AAAI Conference on Artificial Intelligence, vol. 33, (01) 2019, pp. 3558–3565.
[257] S. Bai, F. Zhang, P.H. Torr, Hypergraph convolution and hypergraph attention, Pattern Recognit. 110 (2021) 107637.
[258] J.D. Power, A.L. Cohen, S.M. Nelson, G.S. Wig, K.A. Barnes, J.A. Church, A.C. Vogel, T.O. Laumann, F.M. Miezin, B.L. Schlaggar, et al., Functional network organization of the human brain, Neuron 72 (4) (2011) 665–678.
[259] Y. Qu, K. Fu, L. Wang, Y. Zhang, H. Wu, Q. Liu, Hypergraph-based multitask feature selection with temporally constrained group sparsity learning on fMRI, Mathematics 12 (11) (2024) 1733.
[260] Z. Zhang, M.Y. Chan, L. Han, C.A. Carreno, E. Winter-Nelson, G.S. Wig, A.D.N.I. (ADNI, et al., Dissociable effects of alzheimer's disease-related cognitive dysfunction and aging on functional brain network segregation, J. Neurosci. 43 (46) (2023) 7879–7892.
[261] Y. Zhu, X. Zhu, M. Kim, J. Yan, D. Kaufer, G. Wu, Dynamic hyper-graph inference framework for computer-assisted diagnosis of neurodegenerative diseases, IEEE Trans. Med. Imaging 38 (2) (2018) 608–616.
[262] A. Banka, I. Buzi, I. Rekik, Multi-view brain hyperconnectome autoencoder for brain state classification, in: International Workshop on Predictive Intelligence in Medicine, Springer, 2020, pp. 101–110.
[263] J. Pan, B. Lei, Y. Shen, Y. Liu, Z. Feng, S. Wang, Characterization multimodal connectivity of brain network by hypergraph GAN for alzheimer's disease analysis, in: Chinese Conference on Pattern Recognition and Computer Vision, PRCV, Springer, 2021, pp. 467–478.
[264] X.-A. Bi, Y. Wang, S. Luo, K. Chen, Z. Xing, L. Xu, Hypergraph structural information aggregation generative adversarial networks for diagnosis and pathogenetic factors identification of Alzheimer's disease with imaging genetic data, IEEE Trans. Neural Networks Learn. Syst. 35 (6) (2022) 7420–7434.
[265] A.I. Aviles-Rivero, C. Runkel, N. Papadakis, Z. Kourtzi, C.-B. Schönlieb, Multi-modal hypergraph diffusion network with dual prior for Alzheimer classification, in: International Conference on Medical Image Computing and Computer-Assisted Intervention, Springer, 2022, pp. 717–727.
[266] Y. Ban, H. Lao, B. Li, W. Su, X. Zhang, Diagnosis of alzheimer's disease using hypergraph p-Laplacian regularized multi-task feature learning, J. Biomed. Inform. 140 (2023) 104326.
[267] S. Wang, H. Zhang, W. Kong, Multimodal classification of alzheimer's disease using longitudinal data analysis and hypergraph regularized multi-task feature selection, Bioengineering 12 (4) (2025) 388.
[268] B. Jie, D. Shen, D. Zhang, Brain connectivity hyper-network for MCI classification, in: International Conference on Medical Image Computing and Computer-Assisted Intervention, Springer, 2014, pp. 724–732.
[269] Y. Gao, C.-Y. Wee, M. Kim, P. Giannakopoulos, M.-L. Montandon, S. Haller, D. Shen, MCI identification by joint learning on multiple MRI data, in: International Conference on Medical Image Computing and Computer-Assisted Intervention, Springer, 2015, pp. 78–85.
[270] Y. Li, X. Gao, B. Jie, P.-T. Yap, M.-j. Kim, C.-Y. Wee, D. Shen, Multimodal hyper-connectivity networks for MCI classification, in: International Conference on Medical Image Computing and Computer-Assisted Intervention, Springer, 2017, pp. 433–441.
[271] B.C. Munsell, G. Wu, Y. Gao, N. Desisto, M. Styner, Identifying relationships in functional and structural connectome data using a hypergraph learning method, in: International Conference on Medical Image Computing and Computer-Assisted Intervention, Springer, 2016, pp. 9–17.
[272] C. Cao, H. Fu, G. Li, M. Wang, X. Gao, ADHD diagnosis guided by functional brain networks combined with domain knowledge, Comput. Biol. Med. 177 (2024) 108611.
[273] Y. Du, J. Niu, V.D. Calhoun, A new hypergraph clustering method for exploring transdiagnostic biotypes in mental illnesses: application to schizophrenia and psychotic bipolar disorder, in: 2021 IEEE 18th International Symposium on Biomedical Imaging, ISBI, IEEE, 2021, pp. 971–974.
[274] Y. Zhang, H. Zhang, L. Xiao, Y. Bai, V.D. Calhoun, Y.-P. Wang, Multi-modal imaging genetics data fusion via a hypergraph-based manifold regularization: Application to schizophrenia study, IEEE Trans. Med. Imaging 41 (9) (2022) 2263–2272.
[275] Z. Li, C. Wang, M. Li, B. Han, X. Zhang, X. Zhou, Synchronization stability of epileptic brain network with higher-order interactions, Chaos: An Interdiscip. J. Nonlinear Sci. 35 (1) (2025).
[276] W. Dai, E. Qiu, X. Lin, S. Zhang, M. Zhang, X. Han, Z. Jia, H. Su, X. Bian, X. Zang, et al., Abnormal thalamo–cortical interactions in overlapping communities of migraine: An edge functional connectivity study, Ann. Neurol. 94 (6) (2023) 1168–1181.
[277] D.E. Warren, J.D. Power, J. Bruss, N.L. Denburg, E.J. Waldron, H. Sun, S.E. Petersen, D. Tranel, Network measures predict neuropsychological outcome after brain injury, Proc. Natl. Acad. Sci. 111 (39) (2014) 14247–14252.
[278] S. Achard, C. Delon-Martin, P.E. Vértes, F. Renard, M. Schenck, F. Schneider, C. Heinrich, S. Kremer, E.T. Bullmore, Hubs of brain functional networks are radically reorganized in comatose patients, Proc. Natl. Acad. Sci. 109 (50) (2012) 20608–20613.
[279] T. Jao, M. Schroeter, C.-L. Chen, Y.-F. Cheng, C.-Y.Z. Lo, K.-H. Chou, A.X. Patel, W.-C. Lin, C.-P. Lin, E.T. Bullmore, Functional brain network changes associated with clinical and biochemical measures of the severity of hepatic encephalopathy, Neuroimage 122 (2015) 332–344.
[280] M.T. Alkire, Loss of effective connectivity during general anesthesia, Int. Anesthesiol. Clin. 46 (3) (2008) 55–73.
[281] M.S. Schröter, V.I. Spoormaker, A. Schorer, A. Wohlschläger, M. Czisch, E.F. Kochs, C. Zimmer, B. Hemmer, G. Schneider, D. Jordan, et al., Spatiotemporal reconfiguration of large-scale brain functional networks during propofol-induced loss of consciousness, J. Neurosci. 32 (37) (2012) 12832–12840.
[282] J. Schrouff, V. Perlbarg, M. Boly, G. Marrelec, P. Boveroux, A. Vanhaudenhuyse, M.-A. Bruno, S. Laureys, C. Phillips, M. Pélégrini-Issac, et al., Brain functional integration decreases during propofol-induced loss of consciousness, Neuroimage 57 (1) (2011) 198–205.
[283] B.J. Baars, The conscious access hypothesis: origins and recent evidence, Trends Cogn. Sci. 6 (1) (2002) 47–52.
[284] S. Dehaene, J.-P. Changeux, Experimental and theoretical approaches to conscious processing, Neuron 70 (2) (2011) 200–227.
[285] G. Tononi, Consciousness as integrated information: a provisional manifesto, Biological Bull. 215 (3) (2008) 216–242.